Politecnico di Milano

Dipartimento di Matematica F. Brioschi

Dottorato in Modelli e Metodi Matematici per l'Ingegneria - XXIV Ciclo

---

Characterization of delayed after-depolarization in extended FitzHugh-Nagumo models

Chiara Lelli

matr. 738625

Advisor: Prof. Paolo Biscari
Dipartimento di Matematica "F. Brioschi",
Politecnico di Milano, Italy

Ph.D. Coordinator: Prof. Paolo Biscari

Academic year 2011-2012

---

ai miei genitori

"Le risposte non vengono ogniqualvolta sono necessarie,
come del resto succede spesse volte che il rimanere
semplicemente ad aspettarle sia l'unica risposta possibile."
J. Saramago *Cecità*

Contents

List of Figures

List of Tables

Introduction

One of the most common causes of mortality in the highly-civilized world is the heart failure that brings to a sudden death [1]. Several factors may induce a cardiac arrest, like coronary artery disease, damaged cardiac tissue, irregularity in the heart anatomy or alterations in the electric signal that regulates the heartbeat. In some cases, during the postmortem examination, the cause of the death can be recognized, but in other cases, as for arrhythmia, physical damages are not visible so that it is more difficult to understand the real phenomenon underlying the heart failure [2].

In this framework, the detailed study of the cardiac arrhythmias phenomenology together with the understanding of how an irregular propagation of the electric impulse can affect the heart functioning , become a fundamental subject of research. Indeed the comprehension of these phenomena may help for the prevention and the prediction of sudden cardiac death.

Generally speaking, arrhythmias can be classified as triggered and reentrant [3]. The first type includes all the irregular events due to a series of electrical impulses which are initiated in an abnormal way, while the second class refers to an irregular potential wave that, before dying out completely, excites again the cardiac cells compromising the evolution of the membrane potential (action potential).

Triggered arrhythmias are principally induced by an after-depolarization of the membrane that brings the value of the potential to a critical threshold associated with the initiation of the action potential. The after-depolarizations can occur either during the repolarization phase of the cardiac action potential (early after-depolarization or EADs) or at the final stage before the potential permanently approaches its resting value (delayed after-depolarizations or DADs). In both cases, if the membrane depolarization exceeds the activation threshold an abnormal impulse follows the main one giving rise to a secondary excitation wave that may lead to an extrasystole.

In this work we only focus on DADs. The afterpotentials involved in DADs may be generated when the cell is overloaded with calcium ions, the overloading being due to both positive currents that flow towards the in-

tracellular environment and internal mechanisms that cause calcium release above a critical threshold. The resulting depolarization can reach the potential threshold required to trigger a secondary electrical wave, and, if it propagates along the cardiac fibers, extra-contractions of the heart are induced.

In this Thesis we develop a study that aims at characterizing the delayed after-depolarization phenomenon through existing models that describe the propagation of the action potential in the cardiac membrane. The mathematical ingredient of these models is represented by a two-variable dynamical system, generally nonlinear, involving some constitutive parameters that contain information on the physiological properties of the tissue. A solution to the dynamical system simulates the evolution of a cardiac action potential, that starts with the initial electrical stimulation and ends up when the potential recovers the relaxed configuration.

The original idea that is supported throughout the Thesis is to associate the DAD event with special trajectories of the dynamical system, characterized by a secondary important oscillation (spike) of the membrane potential occurring after the main upstroke. The spike models the depolarization of the membrane and its amplitude determines the occurrence of a supra-threshold phenomenon that may yield triggered arrhythmia.

The particular solutions introduced in the Thesis are identified by critical values of the model parameters, these values being computed here by numerical simulations. Actually the emergence of anomalies in the electric signal may be ascribed to alterations in the normal features of the cardiac membrane, such as its conductance or its excitation properties.

The two-variable dynamical systems we deal with are derived by the FitzHugh-Nagumo model [4, 5, 6], which simulates an action potential propagating along the neuronal membrane. Owing to its flexibility and its universal charcter, this model can be simply fitted to contexts other than neuronal, like the cardiac framework.

More particularly, by providing the dynamical system with suitable corrections that interpret the mechanisms underlying the heart functioning, we can bring the model toward an accurate description of the cardiac action potential and consequently we can simulate in a more realistic way the occurrence of after-depolarizations. Obviously the improvement of the description yields some complexities in the solutions to the motion equations, and the characterization of the spike-solutions becomes more complicated.

In chapter 1 we presented a briefly description of the heart structure, that is the main composition of the cardiac muscle and the role of the different constituents and we analyzed the ionic mechanisms, occurring across the membrane, that generate the electric impulse which is then propagated

by the heart conduction system. In the same chapter we provided a more detailed investigation of the action potential evolution, in order to introduce the readers to the main subject of the Thesis.

Chapter 2 deals with the specific analysis of the after-depolarizations. We have summarized the physiological explanations of the phenomenon recovered in the literature and we have examined the cellular interactions that cause the spreading of the depolarization wave an then the generation of the arrhythmia.

In chapters 3 and 4 we developed the main research of the Thesis. Precisely, chapter 3 contains the analysis of the FitzHugh-Nagumo-type models that we used to derive our description. A deep analytical examination is performed, in terms of phase plane analysis and equilibrium configurations, and we present also a discussion about the improvements introduced in the models to approach a real representation of the cardiac dynamics. On the contrary, in chapter 4 we defined and investigated the spike-solutions and the critical values of the constitutive parameters that characterize their occurrence. We deeply discuss also the choice of the spike amplitude because it is a crucial issue of the study. Indeed the comparison between this value and the depolarization threshold that activates the excitation wave determines the modeling of sub-threshold or supra-threshold depolarization, the last phenomena being the triggering event for the extrasystole.

Therefore, we examine also the conditions under which a supra-threshold episode generates a potential wave that propagates through the membrane, meaning that we provide the model with a predictive tool of DAD-triggered aftercontractions.

Chapter 1

The Heart

1.1 Introduction

The heart is a muscular organ that rhythmically contracts to coerce blood spreading into the body of a living creature with a circulatory system. The beating of the heart is controlled by the autonomic nervous system and an internal control center (pacemaker) called the sinoatrial node.

Mammals have a double circulatory system. Indeed their heart is divided into two halves that work separately and feed different parts of the body. One side of the heart pumps blood to the lungs and back to the heart. The other side of the heart pumps blood to all other parts of the body and back to the heart.

The human heart is contained in the chest, and in particular it is located between the two lungs. Its shape is similar to that of an inverted cone with the tip pointing down. Although its size varies with the person's weight, age, sex, and state of health, to have an idea of its dimensions we can say that a human heart has the size of a person's closed fist. The heart volume is about 20 cm^3 in the childhood, reaching 150/160 cm^3 in a middle-aged person.

The aim of this chapter is to present a brief introduction to the anatomy of the human heart, in order to provide the reader with all the elements that will be useful for the topic of this Thesis. Obviously for a deeper analysis on the functioning of the cardiac muscle, the reader should refer to an appropriate literature (e.g. [7, 8, 9]).

1.2 Heart anatomy and cardiac tissue composition

1.2.1 The cardiac cavities

The heart is divided into a left and a right half through a longitudinal partition. Each cavity is transversely separated into two chambers, one at the top called atrium, and one at the bottom, called ventricle (Fig. 1.1).

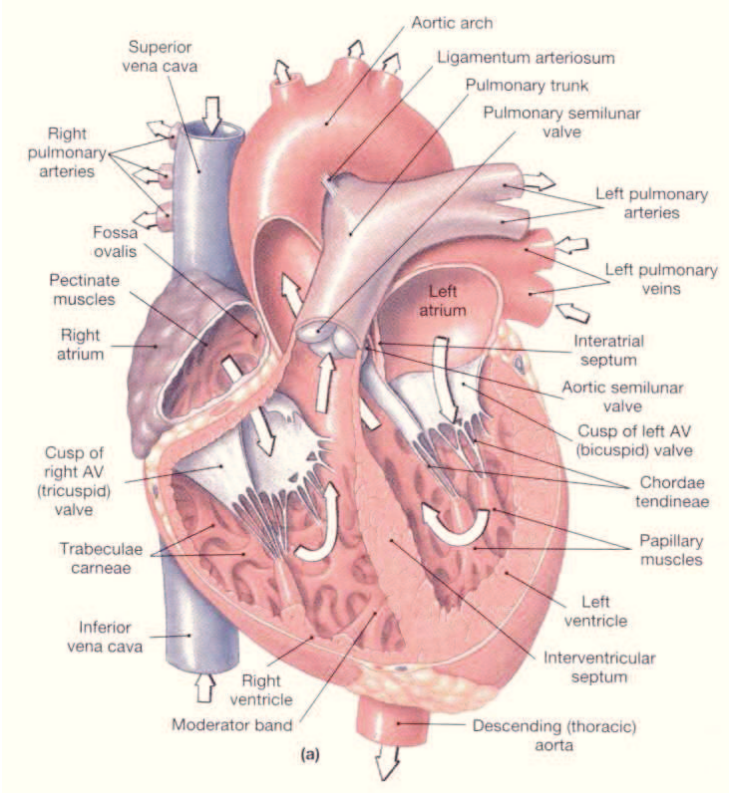

Figure 1.1: Structure of the heart (from www.edoctoronline.com/medical-atlas.asp).

The blood flow is regulated by four valves: two valves separate the atria from the ventricles, the other two regulate the outflow from the right ventricle through the pulmonary artery and from the left ventricle through the aorta.

The valve between the left atrium and ventricle is called *bicuspid* or *mitral valve*, such a name deriving from its shape similar to a bishop's mitre, since it has two flaps like the typical bishop headgear. On the contrary the valve separating the right atrium from the corresponding ventricle has three cusps, and it is called *tricuspid valve*.

The atria are thin-walled cavities which main property is to have the capacity to contain the blood received from the veins. The right atrium collects blood coming from the two venae cavae, the major veins bringing back deoxygenated blood from the head, body, and limbs. The left atrium receives blood coming from the lungs by means of the four pulmonary veins.

On the other hand the ventricles collect blood from the atria and pump it feeding the circulatory system.

More particularly, the right ventricle drives the blood received from the right atrium to the main pulmonary artery while the left ventricle feeds all the arteries of the body. Due to their function of spreading the blood into the entire body, the ventricular cavities have stouter walls than the atria. The left ventricle walls, in particular, are thicker than those of the other chambers, as their contraction should generate sufficient blood pressure to propel the blood into the arteries.

The left ventricle is able to pump to a peak pressure of 17 kPa in a regular heartbeat, while the right ventricle develops a maximum pressure of 4 kPa.

1.2.2 The cardiac wall

The cardiac wall is made of three coatings: the external one, *pericardium*, the intermediate one, *myocardium* and the internal one, *endocardium* (Fig. 1.2).

The pericardium is the serous membrane that encloses the heart. It consists of two layers: an internal serous layer and an external fibrous layer. The *serous pericardium* is in turn composed by two coatings: a parietal pericardium and a visceral pericardium. The parietal pericardium is integrated within the fibrous pericardium such that it is difficult to distinguish from each other, while the visceral pericardium is fused with the epicardium, that represents the external stratum of the cardiac wall. Between the two coatings of the serous pericardium the pericardial cavity is located. It is filled with a serous fluid which allows the heart to beat in a frictionless way.

The *fibrous pericardium* is the outer layer of the pericardium and it principally defends the heart against excessive dilations eventually caused by an increasing in the blood volume.

The endocardium is a thin membrane that covers the internal surface of the cardiac cavities. It is made of three layers, the *endotelium* (composed by large polygon cells), the *proper tonaca* and the *subendocardial stratum*, and

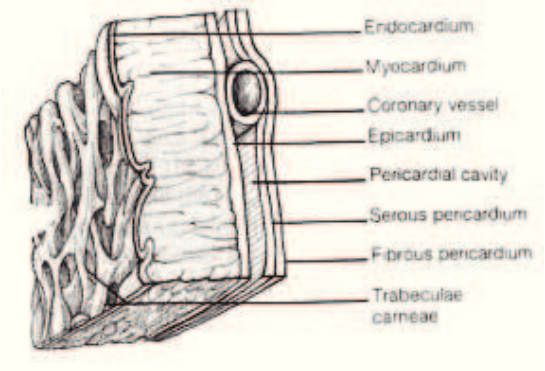

Figure 1.2: Internal structure of the cardiac wall (from http://nursegeorge.com/ecg1.html).

contains various blood vessels, some muscle bundles, and a portion of the system of conduction of the heart.

The myocardium is the cardiac contractile stratum as it is composed by the muscular fibers characterized by cross striations, that is the alternation of thick and thin filaments. In the myocardial stratum we can distinguish three

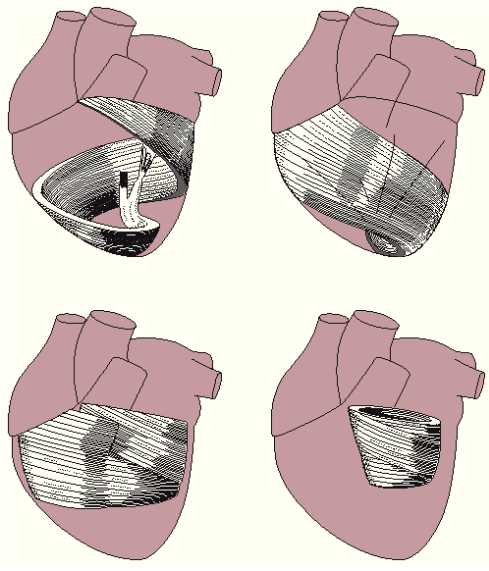

Figure 1.3: Orientation of cardiac muscle fibers (from [10]).

muscle bundle belonging to: (1) atria, (2) ventricles, (3) atrial-ventricular

node of His.

1. The right and the left atria are connected by the *Bachmann's bundle*, or *anterior interatrial bundle*, that is a wide group of muscle accountable for the initiation of the electrical signal in the left atrium.

2. The ventricular bundles of the myocardium are U-shaped, the U convexity being directed towards the tip of the heart (Fig. 1.3). They can be subdivided in four parts: a left and a right hand bundle, with a spiral shape, that together constitute an external layer that encloses both the ventricles; an internal muscle bunch enveloping the ventricles, and finally a fourth group of fibers that arranges around the left ventricle only.

3. The only connection between the atrial and ventricular myocardium is the *atrial-ventricular bundle of His*. For the most part, the atrial-ventricular node is made of particular muscle spindle-shaped cells, that play a fundamental role in the transmission of the electric signal (see section 1.5).

From the microscopic point of view, the myocardium consists of fibers called *myocytes*. These cells are linked one to another through particular connections called *gap junctions*. They provide for an electric and mechanic coupling, allowing the ions passage (as described below) and consequently the transfer of the contractile tension (Fig. 1.4).

The myocardial muscles merged through the gap junctions form filamentous structures named *cardiac fibres*. The cardiac fibres are themselves grouped, with connective tissue acting as lubricating fluid containing a rich capillary network.

Two proteins carry out the main activities of the myocyte: the mitochondria and the sarcomere. The mitochondria are the cellular power sources and occupy about one-third of the volume of the myocyte. Thanks to the abundant presence of the mitochondria, the cardiac muscle ability to extract oxygen from the blood is definitely larger than that of other tissues. The sarcomere is the contractile unit of the myocardium and its activation is due to an electrical stimulus.

1.3 The myocyte conduction system

The regulation system of the ionic flux in cardiomyocytes is mainly located in the sarcolemma, the cytoplasmic membrane that covers the cardiac cells (see Fig. 1.4). It is developed in a large network made of tubuli (T tubuli)

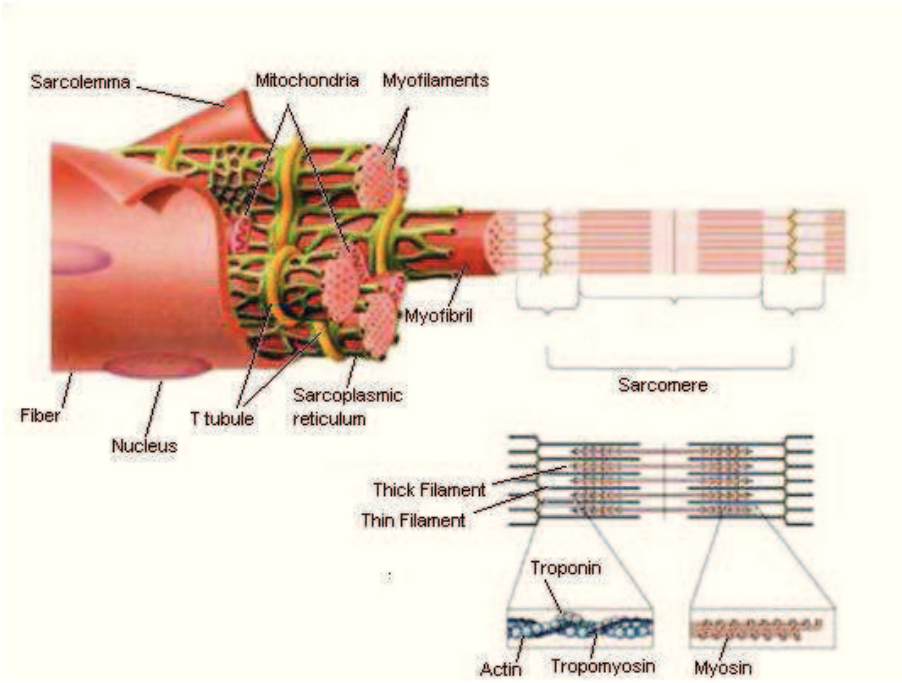

Figure 1.4: Myocardial components (from http://magisnef.wordpress.com/2007/04/02/fisiologia-muscular-componentes-del-musculo).

that spread in deep from the extracellular environment. They allow for the diffusion of the depolarization in all the cellular regions.

The sarcolemma contains many channels, exchangers and pumps responsible for the ionic homeostasis of the cells. One of the most important membrane proteins is the Na^+-K^+ pump, also called Na^+-K^+-ATPase (see Fig. 1.5), that produces a net outward current through the ejection of three Na^+ ions for two K^+ ions.

Moreover the Na^+-Ca^{2+} exchanger is a bidirectional channel that enables one Ca^{2+} ion to go out in exchange for three Na^+ ions which enter the intracellular space. The activity of the exchanger represents the predominant mechanism responsible for Ca^{2+} efflux from the myocyte.

Other significant proteins crossing the lipid stratum of the sarcolemma are the ionic channels, that enable ions transfer both inward and outward. Ion channels are classified on the basis of the specific ionic flux of which they allow the transit: in the following we will mainly deal with Na^+, K^+ and Ca^{2+} channels.

Each ion channel is also characterized by the gating mechanism (the pro-

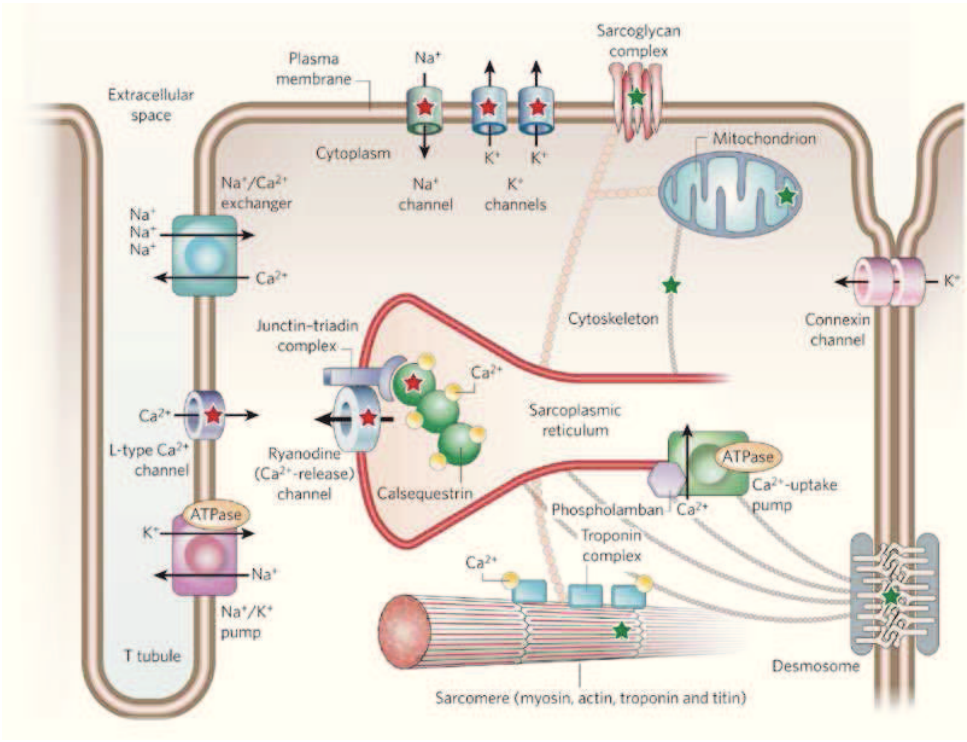

Figure 1.5: Microscopic structure of a myocyte (from [11]).

cess that causes the opening and closing of the channel): voltage dependent, ligand-dependent and mechano-sensitive gating.

The voltage-dependent ion channels activity depends on changes in the membrane potential, while ligand-dependent channels conductance is related to reactions involving chemical components. The stretch-activated channels can transform a mechanical input into an electrical property because their sensitivity to the ions passage changes with the stretch magnitude.

Usually, in modeling the electrical properties of cardiac cell membrane, ion channels are represented by an equivalent resistor. However, most ion channels are regulated by a nonlinear current-voltage low, as the current magnitude depends on the direction of ionic flux (into or out of the cells), the electrochemical potential being equal. This characteristic is called rectification and it is an important property of K^+ channels.

Each myocyte is made of parallel bundles of myofilaments, called myofibrils, that contain the principal elements for the development of the contractile function: the actin and the myosin. The myofibrils are part of a more complex system, named *sarcoplasmic reticulum*, composed by a tubu-

lar structure that carries out an important role in the control of intracellular ion motion. Indeed this area is a wide storage for the calcium ions, that during the contraction-relaxation cycle are eventually released or absorbed. The sarcoplasmic reticulum calcium release yields the amount of Ca^{2+} required for the activation of the contractile proteins [12, 13].

1.4 The cardiac cycle

The cardiac cycle is defined as the chain of events occurring during one complete heartbeat. It is made of three phases: *systole*, *diastole*, and *complete rest*. Each cycle lasts 0.8 seconds while the complete rest phase between one cycle and the other lasts 0.4 seconds. This sequence is repeated 70/80 times a minute under resting conditions.

The cycle begins when blood, that is low in oxygen, fills the right atrium through the superior and inferior vena cavae. When the right atrium is completely filled, it contracts and the tricuspid valve opens so that blood is pumped into the right ventricle (atrial systole).

When the right ventricle is full with blood the ventricular myocardium contracts (ventricular systole): the organization of the fibers induces a decrease in the ventricular cavities volume and consequently the blood pressure grows up. The pressure force determines the closure of the tricuspid valve, so that the backward flow of blood is not allowed, and the blood flux reaches the pulmonary artery.

Blood rich of oxygen returns from the lungs to the left atrium through the pulmonary veins; once it is filled, the left atrium reduces its volume and the blood is pumped into the left ventricle. This occurs at the same time of the right atrial systole.

After the mitral valve is closed, the left ventricle contracts and the aortic valve between the ventricle and the aorta opens so that oxygen-rich blood flows out into the aorta.

The closure of the atrial-ventricular valves in the systole induces vibrations in the heart walls and causes the first and loudest heart beat sound, while their closure during diastolic phase is responsible for the second, lower heart beat.

1.5 The heart conduction system

Cardiac cells develop two functions: they have a contractile ability and they are excitable. These two features are linked each other, since the activation

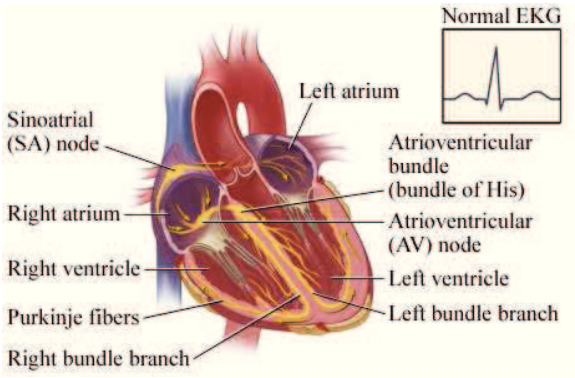

Figure 1.6: The heart conduction system (from http://www.webmd.com/heart/conduction-system-of-the-heart).

of the mechanical function is provided by an electrical signal that propagates in the tissue, the propagation being allowed by the excitable property of the cells.

The electric stimulus is generated in the *sinoatrial node* located on the right atrium below the superior vena cava (Fig. 1.6) and from here reaches the *atrial-ventricular node*, which is situated in the layer of the interatrial septum near the tricuspid valve.

The atrial-ventricular node expands through the interventricular septum and becomes part of the His bundle. Then the bundle of His branches into a left and right ramification, that conduct stimulus to the right and left ventricle respectively.

The sinoatrial node is the stimulation source of the heart because it is responsible of the generation of the electric impulse determining the heart-beat. For this reason its cells are called *pacemaker cells*. It rhythmically emits a stimulus that depolarizes the adjacent muscle, propagates in the myocardium of both atria making them contract and then reaches the atrial-ventricular node. When the atria depolarization is completed the electric impulse spreads in the His bundle and in its two branches.

As soon as the electric impulse reaches the ventricular myocardium, it contracts.

1.5.1 The cardiac action potential

When an excitable cell is activated, the membrane potential of that cell evolves according to a process called *action potential*.

All the cells of the heart conduction tissue are able to autonomously generate series of action potential, but the sino-atrial node cells own a greater capacity simply because the frequency of their spontaneous electric shocks is higher. They give rise to the action potential with a 70 volt/minute capacity, while the capacity of atrial-ventricular node cells is about 30 millivolt/minute.

The different phases of the action potential are associated with the motion of positive and negative charges, and principally with the channels conductance to calcium, potassium and sodium ions.

Calcium is the main resource for the contractile activity, while potassium and sodium are involved the myocardium relaxation.

The excitable cells are characterized by a negatively-charged intracellular region and a positive extracellular area. The specific placement of this charges gives rise to a potential difference that, in the equilibrium state, is about -90 mV. This is the so called *membrane potential at rest*.

The pacemaker cells that start the impulse do not own a relaxing potential because they undergo a continuous transfer of ionic charges, while the cells that really contract (*working myocytes*), giving rise to the heartbeat, are characterized by a relaxed configuration, described above.

In the following we summarize the five phases of the action potential [14, 9].

Phase 4 *Resting membrane potential and diastolic depolarization.* In the rest state the membrane is quite permeable to K^+ and the potential value is near to the potassium Nernst potential. The leading actors of this phase are the *inward rectifier K^+ channels* [15], that privilege the inward flow of K^+ ions.

Atrial and ventricular cells have a stable membrane potential between two action potentials (that is, during the diastolic phase).

Conversely, in other cells (SA node, His-Purkinje) the rest membrane potential slowly depolarizes during the diastole, thus giving rise to the so called *diastolic depolarization*. Sometimes the depolarization may reach the threshold for cell activation so that a spontaneous action potential is triggered.

When the cell is depolarized by other external forces, the inward rectifier K^+ channels close and the membrane potential can change.

Phase 0 *Upstroke or rapid depolarization* (1-3 ms). An appropriate depolarizing stimulus induces the opening of stimulus-dependent Na^+ channels, so that sodium ions flows into the cell and the membrane undergoes a local depolarization.

If the local depolarization reaches a physiological value generating the electrical activation (*potential threshold*), voltage-dependent Na^+ channels (so called because their conductance changes depending on variations in potential difference) open, thus generating an inward flow of Na^+ ions. As a consequence the membrane internal environment becomes positively charged and the action potential starts.

The onset of the action potential does not depend on the stimulus amplitude. More precisely, if the depolarizing impulse exceeds the activation threshold the cell undergoes the potential upstroke, while the action potential fails if the stimulus does not achieve the threshold. This phenomenon is called *all or none response*.

In the atrial and ventricular cells the upstroke is caused by the voltage-dependent Na^+ channels opening, while in the SA and AV node the depolarization is linked to the activity of the voltage-dependent Ca^{2+} channels. In these cells the upstroke is slower.

While internal $[Na^+]$ and positive intracellular charge increase, the strength of the Na^+ flux decreases until the membrane potential reaches the sodium Nernst potential so that sodium channels are inactivated.

Phase 1 *Early rapid repolarization* (6-15 ms). In correspondence of the inactivation of the fast Na^+ channels, the K^+ channels open and a slow current moves K^+ ions towards the extracellular environment. This transient outward current is the phenomenon underlying the small downward deviation in the action potential (Fig. 1.7).

Phase 2 *Plateau* (200-400 ms). During this phase the membrane conductance to most of the ions decreases and the most significant activity is the balance between a weak inward calcium current and a low flux of K^+ through the potassium channels. Consequently the membrane potential is not affected by large changes, as evidenced by the horizontal trace in Fig. 1.7.

Phase 3 *Final rapid repolarization* (100-150 ms). The slow inward Ca^{2+} and Na^+ currents involved in the previous phase fade away while the *delayed rectifier K^+ channels* open and K^+ ions move gradually to the extracellular space. Consequently a positive charge on the external surface is recovered and the cellular resting conditions are achieved.

During an action potential the susceptibility of the cells changes, because some phases in particular require precise excitability conditions. Two characteristics of the cell sensitivity are commonly selected.

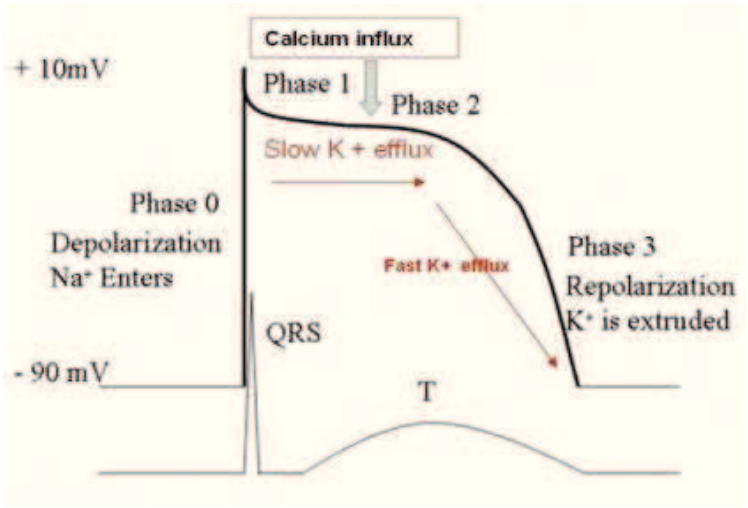

Figure 1.7: Basic cardiac action potential (from http://drsvenkatesan.wordpress.com/2009/08/26, modified from www.ocw.tufts.edu).

- *Absolute refractory period.* It corresponds to the plateau phase and lasts until the potential reaches -40 mV. During this phase the cell is completely insensitive to the impulses, whatever their intensity. This is an essential characteristic of the cardiac muscle because it prevents a propagation of a secondary impulse while the heart is still in the systolic phase. Owing to the refractory period the ventricle can be entirely filled by blood and it develops the highest tension before performing another contraction.

- *Relative refractory period.* This phase follows the previous phase. During the repolarization the outward potassium flux brings the membrane potential closer to the K^+ equilibrium potential. It may occur that the membrane potential becomes slightly more negative than the usual resting potential. Then, and until the potassium conductance returns to the resting value, a greater stimulus is needed to reach the threshold for a secondary action potential. The achievement of the K^+ Nernst potential marks the end of the relative refractory period.

Chapter 2

The Delayed After-Depolarization

2.1 Introduction

The after-depolarization (or after potential) is a depolarization of the membrane potential that follows an action potential and influences its future evolution. During an after-depolarization the potential difference across the heart membrane increases (meaning that it evolves towards more positive values), and if the depolarization achieves the potential activation threshold, it can induce a spontaneous action potential. If this secondary upstroke, which is called spontaneous because it is not triggered by an external stimulus but is induced by an intrinsic mechanism, propagates in the cardiac membrane, it may generate after-contractions of the cardiac tissue that consequently give rise to arrhythmias that are said to be triggered.

There exist two types of after-depolarizations: the early after-depolarization and the delayed after-depolarization. The first one occurs during the repolarization phase of the action potential (phases 2 and 3 described in the previous chapter), while the delayed after-depolarization happens after the completion of the repolarization phase before the potential stabilizes about its steady value (Fig. 2.1).

Early after-depolarizations (EADs) mainly occur if the action potential duration extends into a critical value. Indeed, in this situation, L-type Ca^{2+} channels (low threshold type calcium channels), that normally open during the plateau phase, can be again stimulated so that they open again and lead to an inward depolarizing current while the membrane is still depolarized. The long action potential duration has been observed in some individuals with a genetic arrhythmic syndromes. The best known example is the long

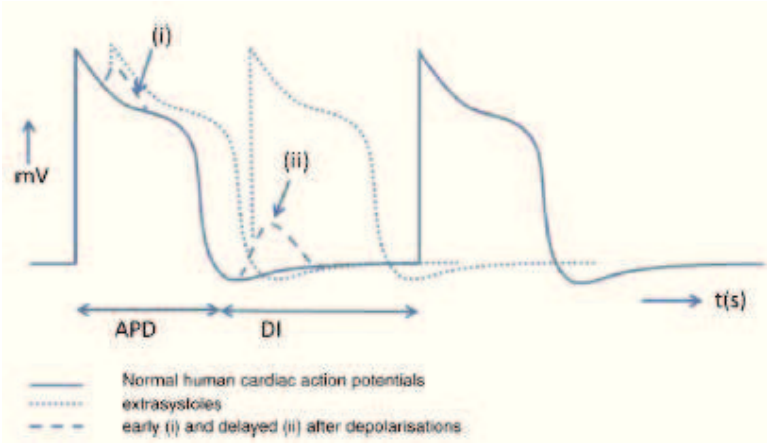

Figure 2.1: Early after-depolarization and delayed after-depolarization occurring during the cardiac action potential [3].

Q-T syndrome that causes a long Q-T interval on the electrocardiogram (the Q-T interval is the time elapsing between the beginning of the Q wave and the T wave completion during the electrical event).

On the other hand the delayed after-depolarization (DAD) is generally related to enhanced Ca^{2+} outflow from the sarcoplasmic reticulum through the ryanodine receptor channel (see Fig. 1.5). The calcium concentration within the cytosolic area increases and consequently the Na^{+}-Ca^{2+} exchanger expels one Ca^{2+} ion in exchange for three Na^{+} ions causing a net intake of positive charges in the intracellular environment that contributes to a membrane depolarization.

The release of calcium from the sarcoplasmic reticulum can be activated both by an external process, called Ca^{2+}-induced Ca^{2+} release (CICR), or by an internal mechanisms that bring the concentration of calcium ions above a critical threshold that triggers a spontaneous calcium release. CICR is a characteristic of the ryanodine-sensitive Ca^{2+} stores, and is caused by an increase in calcium concentration at the intracellular cytoplasmic surface that induces an increase in Ca^{2+} efflux from the calcium compartment [16, 13, 12].

2.2 Quantitative results from the literature

Although performing quantitative studies on the dependence between Ca^{2+} release from sarcoplasmic reticulum and DAD amplitude is a complex goal, some authors have tried to delineate experimentally this relationship by artificially triggering the DAD phenomenon.

In the following we mention the three main results from Schlotthauer and Bers [17], Luo-Rudy [16] and Xie et al. [18]. In the first article the authors work with caffeine-induced sarcoplasmic reticulum Ca^{2+} release to generate DADs with different concentration of calcium. The calcium load in the sarcoplasmic reticulum is varied by changing the frequency of the action potentials. For each test, after the last induced action potential, they inject a certain amount of caffeine in order to immediately induce Ca^{2+} efflux and DAD. The results they found are depicted in Fig. 2.2: stimulation from 1 to 3 Hz brings to subthreshold DAD, while at 4 Hz a suprathreshold depolarization is achieved so that a spontaneous action potential is induced.

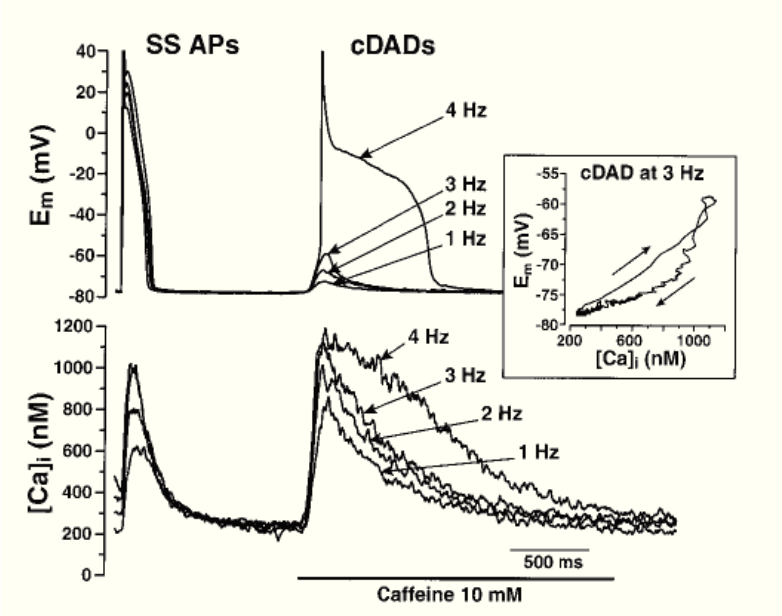

Figure 2.2: Dependence of delayed after-depolarization from the calcium concentration generated by Ca^{2+} release from sarcoplasmic reticulum. The two graphs show the last steady state action potentials followed by the caffeine-induced DADs and the Ca^{2+} transient for different values of the action potential frequency respectively (from [17]).

Figure 2.2 also evidences that the activation threshold for a spontaneous action potential is about 65 mV (see also [18]), which is more or less 1/8 of the amplitude of the steady state action potential. This is only a qualitative result but it will guide us in the mathematical modeling of after-depolarization. Indeed, the membrane potential threshold is a critical parameter for the model that marks out the outcome of cardiac triggered arrhythmias.

Some different simulations have been made by Luo and Rudy. They performed experiments on the spontaneous Ca^{2+} release from the sarcoplasmic reticulum in order to understand the ionic currents that largely influence the DAD generation. In addition to the current developed by the Na^{+}-Ca^{2+} exchanger, they consider another contribution due to the so called non specific Ca^{2+}-activated channel. This ionic current is the sum of the sodium and potassium currents through the nonspecific Ca^{2+}-activated channel. They found that if the intracellular concentration of calcium attains a physiological value, the depolarization is mainly due to the current through the Na^{+}-Ca^{2+} exchanger, while in Ca^{2+} overload conditions both the contributions are of fundamental importance.

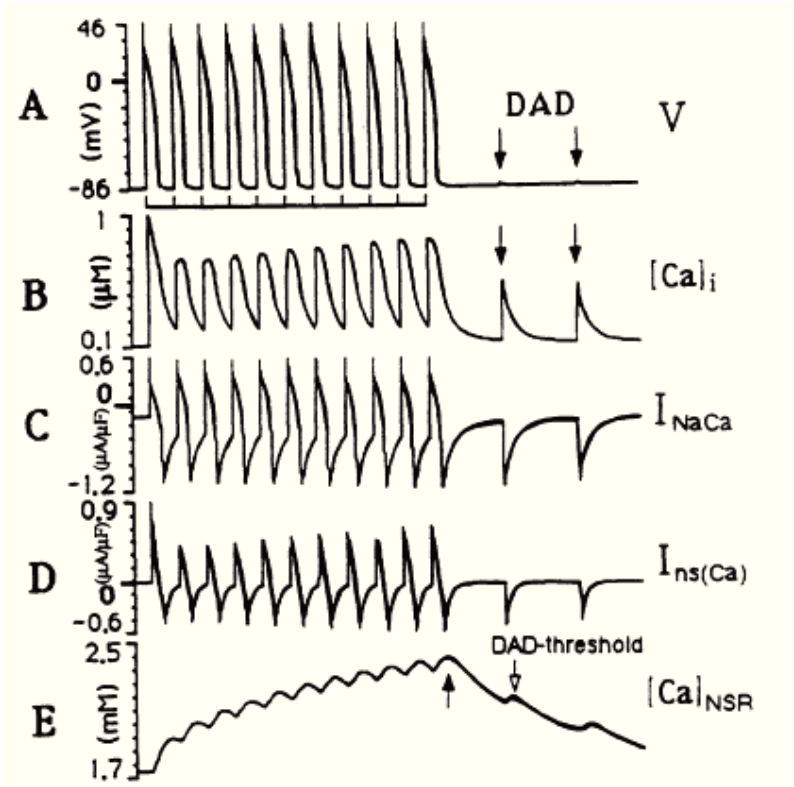

Figure 2.3: Contributions to DAD generation in the Luo-Rudy model (from [16]).

Figure 2.3 shows the results of the experiments made in normal conditions of intracellular calcium. When the induced series of electric cycles ends, a spontaneous Ca^{2+} release is observed followed by an increase in the intracellular calcium concentration (panel B). Then the two currents described

above are activated (panels C and D) so that they depolarize the cell and yield DAD phenomenon shown in panel A. In picture E we can read the minimum concentration of calcium in the sarcoplasmic reticulum that could generate spontaneous Ca^{2+} release.

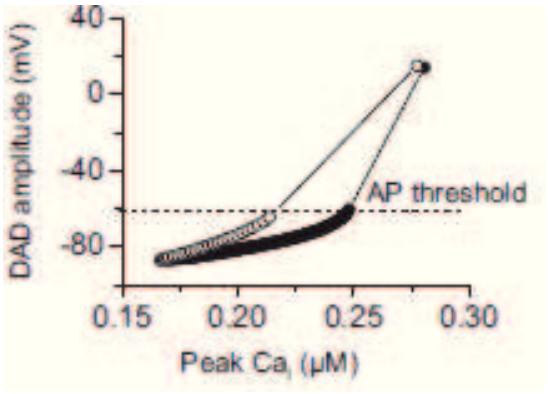

Figure 2.4: Relationship between DAD amplitude and the amount of sarcoplasmic reticulum Ca^{2+} release in a single myocyte (from [18]). Open circles and solid circles refer to a different time for the release (respectively $\tau = 10$ ms and $\tau = 50$ ms).

In Fig. 2.4 we report the quantitative results from [18]. In that experiment, Xie et al. fixed the threshold depolarization to -62.9 mV, and investigated the dependence of the DAD amplitude from the rate of sarcoplasmic reticulum Ca^{2+} release in a single myocyte. The graph shows that if the time constant for the calcium outflow is increased from 10 ms (solid marks) to 50 ms (empty marks), the measure of total Ca^{2+} efflux necessary to trigger an action potential grows up.

2.3 DADs and cardiac arrhythmias

We can classify three types of cardiac arrhythmias according to the physiological processes underlying the abnormal functioning of the heart [19]. The most common type of arrhythmia is the reentry activity caused by alterations in the spreading of the electric pulse along the tissue mainly due to the mutual influence between neighboring cells and the non homogeneous texture of the myocardium.

On the other hand mechanisms involving the cellular background induce automaticity and triggered activity. The first phenomenon concerns the cardiac cells ability to generate a spontaneous action potential by means of an autonomous diastolic suprathreshold depolarization occurring after the action potential. All the cardiomyocytes can perform this ability but in a healthy tissue only pacemaker cells carry out this function.

Triggered activity is related to the after-depolarization and is observed when the depolarization achieves the potential threshold and yields a triggered action potential.

The triggering event for EADs is commonly ascribed to a critical duration of the repolarization, and for this reason the resulting arrhytmia is more likely to occur when the cell is excited with a slow series of impulses. Consequently EAD-induced triggered activity is associated with bradycardia or pauses.

By contrast, the appearance of DADs is usually related to rapid heart stimulations, so they generally can induce tachycardias.

As we have already said before, the irregularities in the heartbeat caused by DADs occur under conditions that increase the intracellular calcium concentration. One example is the digitalis-induced triggered activity occurring when the patient undergoes high dosage of cardiac glycosides (digitalis) used in the case of congestive heart failure and heart rhythm problems. Digitalis medicines acts by increasing the force of the heartbeat since they enhance the calcium load in the cardiac cells so that the muscle fibers experience a stronger contraction.

Digitalis-induced DADs are generally detected in Purkinje fibers, while in the ventricular myocardium they are readily generated in cells and tissue from the M region. This region is located between the endocardial and epicardial layers of the heart tissue and the specific property of the M cells is to have a prolonged action potential [20, 21]. Therefore, since a long duration of the action potential allows a great influx of Ca^{2+} ions, the calcium concentration inside the cells increase and a DAD can occur more easily.

The mechanism for which a DAD can yield aftercontractions of the heart tissue is the so called source-sink mismatch between adjacent cells [18].

Indeed, if a single myocyte undergoes a DAD phenomenon (the source of depolarizing current), the change of its membrane potential establishes an electrical discrepancy with the neighboring cells, which are still repolarized (the sink). Consequently a potential wave spreads from the tissue near the single myocyte with the aim to reduce the voltage difference.

If the density of this electrical wave is sufficient to bring the neighboring myocytes to their activation threshold, a spontaneous action potential propagates in the tissue.

In [18], Xie et al. showed some interesting experimental results. They

performed simulations in a one, two and three dimensional tissue where a certain amount of cells is designed to experience a suprathreshold DAD (*susceptible myocytes*). Then they estimate how many contiguous myocytes, that simultaneously exhibit a DAD, are required to activate a spontaneous action potential that propagates in the tissue.

Their findings for the 1D case are visible in Fig. 2.5. They placed in the central region of the fiber the myocytes generating DADs of amplitude 24.6 mV, that is 0.2 mV above the threshold, and they found that a number of 80 *susceptible myocytes* are required to propagate a DAD wave in the tissue. Then by increasing the total release of calcium from the sarcoplasmic reticulum, the DAD magnitude enhances further above the potential limit for a triggered action potential (see Fig. 2.4), while the number of required cells for an action potential decreases substantially (see Fig. 2.6).

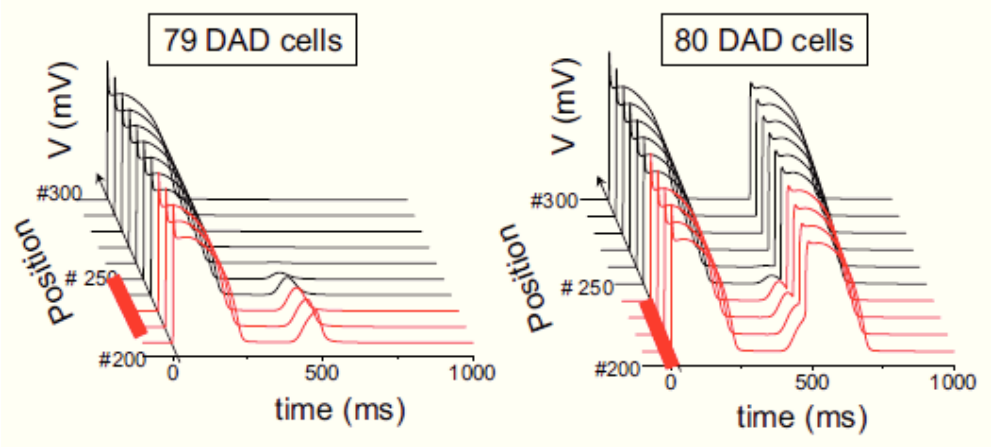

Figure 2.5: Action potential along a 1D fiber. The red lines identify the DADs-susceptible cells: the left panel reproduces the simulation with 79 excited myocytes while the right graph takes account for 80 cells so that a propagation of the triggered action potential is reproduced (from [18]).

The experiments on 2D or 3D tissues show that the number of *susceptible myocytes* necessary to generate an extra-action potential increases exponentially. This means that for tissues with a simple texture, that therefore can be associated with a one-dimensional structure (for instance Purkinje fibers), the occurrence of DAD phenomena is more likely since for the excitation of the whole fiber it is sufficient that a limited portion of myocytes experiences a DAD. On the contrary, in more complex networks, the DAD phenomenon is rather rare. The authors of [18] explain this result by stating that the propagation of the depolarizing stimulus is substantially influenced by the

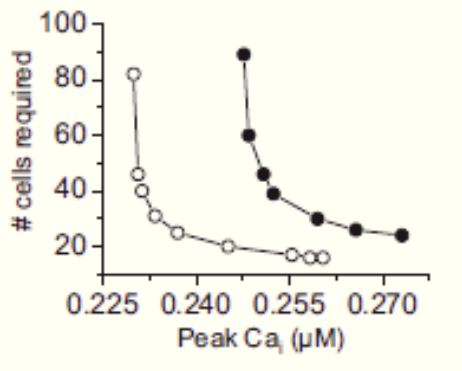

Figure 2.6: Number of adjacent DAD-stimulating myocytes required for the propagation of a triggered action potential versus the total amount of calcium released for different release time constant (open circles $\tau = 10$ ms, solid circles $\tau = 50$ ms) (from [18]).

curvature factor of the surface between the *susceptible myocytes* and the neighboring repolarized cells. In particular in two and three-dimensional lattices the contact surface between the cells extends in several directions and then the DAD source must develop a stronger signal to excited the neighboring cells.

Chapter 3

Mathematical models for the cardiac action potential

In the last decades several models reproducing the electrophysiology of the cardiac tissue are studied. They differ substantially for the mathematical complexity of the equations and the level of detail with which they represent the underlying biology [22]. In order to understand the advantages or disadvantages of studying one of these models, they can be divided in three main categories [23, 24]: the simplified two-variable models, and the first and second generation cardiac cells model.

The two-variable models are characterized by a phenomenological approach through which the cardiac electric event is described by accounting only for the excitation and the recovery phenomena. Despite their simplicity, these models exhibit a remarkable ability to reproduce basic properties of the dynamics of the cardiac tissue. Indeed the parameters and the functions involved in the equations can often be fitted to quantitatively reproduce the features that, from time to time, the model should highlight. Related to this category are the FitzHugh-Nagumo type models, including the FitzHugh-Nagumo model [4] and all its modified representations (for instance the Aliev and Panfilov model [25]).

On the other hand, the first generation models are based on experimental information acquired from voltage clamp and patch clamp studies about the voltage and time dependence of ion channel conductance. They describe the individual ionic currents that cross the cell membrane and model the kinetics of the resulting ionic flow. All these systems derive from the Hodgkin-Huxley model [26, 27] of the squid giant axon and improve its basic physiological representation by adding a detailed description of membrane channels, exchanger and pumps. Some examples are provided by Noble [28], who adapted the Hodgkin-Huxley model to the cardiac Purkinje cells, Beeler and Reuter

[29] who added a simplified description of the intracellular calcium concentration, and the Luo-Rudy model [30] which describes six distinct membrane currents. In the second generation models the number of the unknowns is increased by adding detailed characterizations of intracellular concentrations of sodium, potassium and calcium ions [31, 16]. Consequently they require a noteworthy computational effort.

3.1 The FitzHugh-Nagumo model

The FitzHugh-Nagumo model is a two-variable dynamical system that simulates the propagation of the electrical signal along the nerve membrane. It is deduced from the Hodgkin-Huxley model, indeed it essentially arises as a compact reformulation of the Hodgkin-Huxley equations. For this reason it does not involve an exhaustive description of the ionic flows through the membrane, but it provides a flexible model and allows a straightforward mathematical analysis.

Before going into details of the FitzHugh-Nagumo dynamical system, in the following we briefly report the main features of the Hodgkin-Huxley research.

3.1.1 The Hodgkin-Huxley model

The Hodgkin-Huxley dynamical system is based on the basic observation that the cell membrane can be modeled as an electrical circuit [32]. As a matter of fact, since the cell membrane acts as charge separator, it can be represented as a capacitor. Consequently, the equivalent electric representation of a specific channel can be viewed as a resistor (not necessarily ohmic) in parallel with the capacitor, so that the complete system is the circuit depicted in Fig. 3.1.

By imposing the balance between the currents at node A, the equation associated with the circuit in Fig. 3.1(a) is

$$i_{c_{\mathrm{m}}} + i_{\mathrm{ion}} + i_{\mathrm{appl}} = 0,$$

where $i_{c_{\mathrm{m}}}$ denotes the capacitor current density, i_{ion} is the sum of the contributions of all the ionic currents and i_{appl} is an externally applied current density. By specifying the expression for $i_{c_{\mathrm{m}}}$, we get

$$c_{\mathrm{m}} \frac{\mathrm{d}V_{\mathrm{m}}}{\mathrm{d}t} + i_{\mathrm{ion}} = -i_{\mathrm{appl}}, \tag{3.1}$$

where c_{m} is the membrane capacitance per unit area (Table 3.1) and V_{m} is the difference between the internal and the external membrane potential

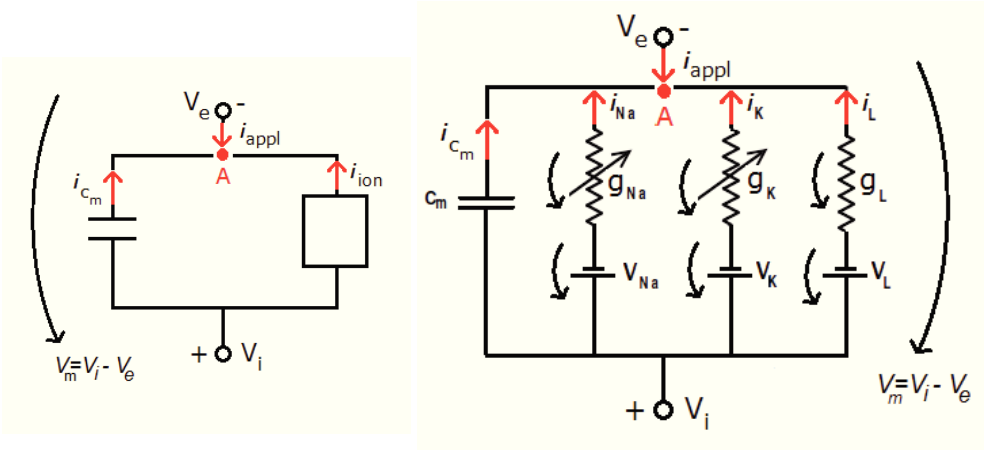

(a) (b)

Figure 3.1: Electrical circuit model of the cell membrane.

($V_{\mathrm{m}} = V_i - V_e$). A common way of computing i_{ion} is to consider the ionic current density as a linear function of the potential [32]. Then, for each ionic flux, we get the relation

$$i_{\mathrm{i}} = g_{\mathrm{i}}(V_{\mathrm{m}} - V_{\mathrm{i}}), \tag{3.2}$$

where g_{i} is the membrane conductance (per unit area) of passage of the specific ion and V_s is the Nernst potential (that is the equilibrium potential difference across the membrane).

By taking account of (3.2), and by considering that the principal ionic currents are due to K^+ and Na^+ ions, equation (3.1) becomes

$$c_{\mathrm{m}}\frac{\mathrm{d}V_{\mathrm{m}}}{\mathrm{d}t} = -g_{\mathrm{Na}}(V_{\mathrm{m}} - V_{\mathrm{Na}}) - g_{\mathrm{K}}(V_{\mathrm{m}} - V_{\mathrm{K}}) - g_{\mathrm{L}}(V_{\mathrm{m}} - V_{\mathrm{L}}) - i_{\mathrm{appl}}, \tag{3.3}$$

where the term $g_{\mathrm{L}}(V_{\mathrm{m}} - V_{\mathrm{L}})$ accounts for other ionic currents (for instance the Cl^- flux) that are combined together into a current called the leakage current.

For practical purposes Hodgkin and Huxley replaced the variable V_{m} with $v = V_{\mathrm{m}} - V_{\mathrm{eq}}$ and V_{i} ($i = \mathrm{Na}, \mathrm{K}, \mathrm{L}$) with $v_i = V_{\mathrm{i}} - V_{\mathrm{eq}}$, where V_{eq} is the absolute value of the membrane resting potential (namely the potential difference between the inner and outer regions of the cell membrane when the cell is not conducting an impulse). Then (3.3) becomes

$$c_{\mathrm{m}}\frac{\mathrm{d}v}{\mathrm{d}t} = -g_{\mathrm{Na}}(v - v_{\mathrm{Na}}) - g_{\mathrm{K}}(v - v_{\mathrm{K}}) - g_{\mathrm{L}}(v - v_{\mathrm{L}}) - i_{\mathrm{appl}}.$$

The two scientists modeled the conductances of the ionic channels by performing voltage clamp experiments on the giant axon of the squid. Voltage

clamping is an experimental method that uses electrodes to alter the membrane potential allowing to test membrane conductance of ions at specific membrane potentials. It is also possible to measure the equilibrium potential of the membrane to certain ions.

On the basis of the experimental results, they hypothesized that the ionic conductances could be written as some power of a variable satisfying a first-order differential equation. Therefore they deduce the following relations:

$$\begin{aligned} g_{\mathrm{K}} &= \bar{g}_{\mathrm{K}} n^4 \\ \frac{\mathrm{d}n}{\mathrm{d}t} &= \alpha_n(v)(1-n) - \beta_n(v)n \end{aligned}$$

for the potassium conductance, n being the potassium activation variable. Similarly for the sodium conductance:

$$\begin{aligned} g_{\mathrm{Na}} &= \bar{g}_{\mathrm{Na}} m^3 h \\ \frac{\mathrm{d}w}{\mathrm{d}t} &= \alpha_w(v)(1-w) - \beta_w(v)w \qquad w = m, h \end{aligned}$$

where m is the sodium activation variable and h the sodium inactivation variable. The empirical functions $\alpha_n(v)$, $\beta_n(v)$, $\alpha_w(v)$ and $\beta_w(v)$ have been adjusted by Hodgkin and Huxley to fit the data of the giant axon of the squid.

The differential equations describing the evolution of the variables n, m and h (that are called *gating variables*) characterize how ionic channels open and close in response to voltage [32]. If one assumes that the channel can exist in either a closed or an open state, and that the rate of change from one state to another is dependent on the voltage, there must be two functions establishing the rate of conversion from the close state to the open state ($\alpha(v)$) and viceversa ($\beta(v)$).

Therefore, if c denotes the fraction of channels in the open state and consequently $(1-c)$ the fraction of closed channels, the differential equation for the evolution of c is

$$\frac{\mathrm{d}c}{\mathrm{d}t} = \alpha(v)(1-c) - \beta(v)c.$$

In summary, the Hodgkin-Huxley motion equations are:

$$\begin{aligned}
c_{\mathrm{m}}\frac{\mathrm{d}v}{\mathrm{d}t} &= -\bar{g}_{\mathrm{Na}}m^3h(v-v_{\mathrm{Na}}) - \bar{g}_{\mathrm{K}}n^4(v-v_{\mathrm{K}}) - \bar{g}_{\mathrm{L}}(v-v_{\mathrm{L}}) - i_{\mathrm{appl}} \\
\frac{\mathrm{d}n}{\mathrm{d}t} &= \alpha_n(v)(1-n) - \beta_n(v)n \\
\frac{\mathrm{d}m}{\mathrm{d}t} &= \alpha_m(v)(1-m) - \beta_m(v)m \\
\frac{\mathrm{d}h}{\mathrm{d}t} &= \alpha_h(v)(1-h) - \beta_h(v)h.
\end{aligned}$$

3.1.2 The FitzHugh simplification

In 1960 FitzHugh [5] proposed a reduced system by contracting the Hodgkin-Huxley equations to a two-variable model. He noted that for brief time intervals, the variables h and n change very little while v and m vary considerably. This means that the sodium channels activation and the membrane potential have a fast dynamics, while the sodium channels inactivation and the potassium channels change very slowly. Therefore FitzHugh concluded that the behavior of v and m could be studied by setting h and n constant and equal to their resting values, and solving the fast dynamical system:

$$\begin{aligned}
c_{\mathrm{m}}\frac{\mathrm{d}v}{\mathrm{d}t} &= -\bar{g}_{\mathrm{K}}n_0^4(v-v_{\mathrm{K}}) - \bar{g}_{\mathrm{Na}}m^3h_0(v-v_{\mathrm{Na}}) - \bar{g}_{\mathrm{L}}(v-v_{\mathrm{L}}) - i_{\mathrm{appl}} \\
\frac{\mathrm{d}m}{\mathrm{d}t} &= \alpha_m(1-m) - \beta_m m
\end{aligned} \tag{3.4}$$

where n_0 and h_0 are the equilibrium values of the slow variables.

In the following we show a brief analysis in the phase plane of (3.4) where α_m and β_m are replaced with the expression provided by Hodgkin and Huxley [27, 32],

$$\alpha_m = 0.1\frac{25-v}{\exp\left(\frac{25-v}{10}\right)-1} \tag{3.5}$$

$$\beta_m = 4\exp\left(-\frac{v}{18}\right) \tag{3.6}$$

and the assigned values of the parameters are shown in Table 3.1. In this study we will assume $i_{\mathrm{appl}} = 0$.

Firstly, we notice that in the limit $v \to 25^{\pm}$, α_m tends to 0.1, so that α_m may easily be defined to be strictly positive for all v. Analogously $\beta_m > 0$ $\forall v$.

The m and v nullclines intersect in three points, corresponding to three steady states of the fast equations (Fig. 3.2). It can be shown that two of

Table 3.1: Values of the parameters in (3.4) [32].

c_{m}	1 μF/cm^2	$\bar{g}_{\mathrm{L}}$	0.3 mS/cm^2
$\bar{g}_{\mathrm{K}}$	36 mS/cm^2	v_{L}	10.6 mV
v_{K}	-12 mV	n_0	0.3176
$\bar{g}_{\mathrm{Na}}$	120 mS/cm^2	h_0	0.596
v_{Na}	115 mV		

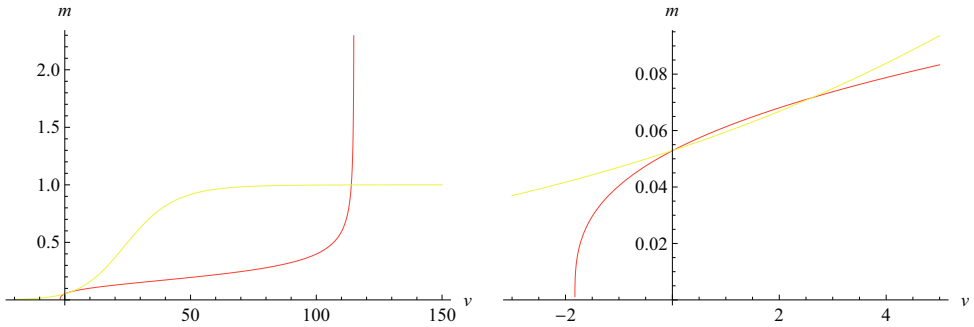

Figure 3.2: (a) Representation of the m-nullcline (yellow line), the v-nullcline (red line) and the equilibrium points of dynamical system (3.4). (b) An enlargement of the region near the origin.

these three points are stable steady states of the fast subsystem, while one is a saddle point. For this reason we will call the three steady states v_r , v_s, and v_e, that is respectively resting, saddle, and excited states (Fig. 3.3).

We now prove the stability of the equilibrium points by linearizing the system through the indirect Liapunov method. If the general form of a nonlinear dynamic system is

$$\dot{\mathbf{x}} = \mathbf{f}(\mathbf{x}(t)) \tag{3.7}$$

and if $\bar{\mathbf{x}}$ is an equilibrium point, we can approximate $\mathbf{f}$ in the neighborhood of this point, $\mathbf{x} = \bar{\mathbf{x}} + \mathbf{y}$, by means of a Taylor expansion

$$\mathbf{f}(\bar{\mathbf{x}} + \mathbf{y}) = \mathbf{f}(\bar{\mathbf{x}}) + \mathbf{F}\mathbf{y} + o(|\mathbf{y}|)$$

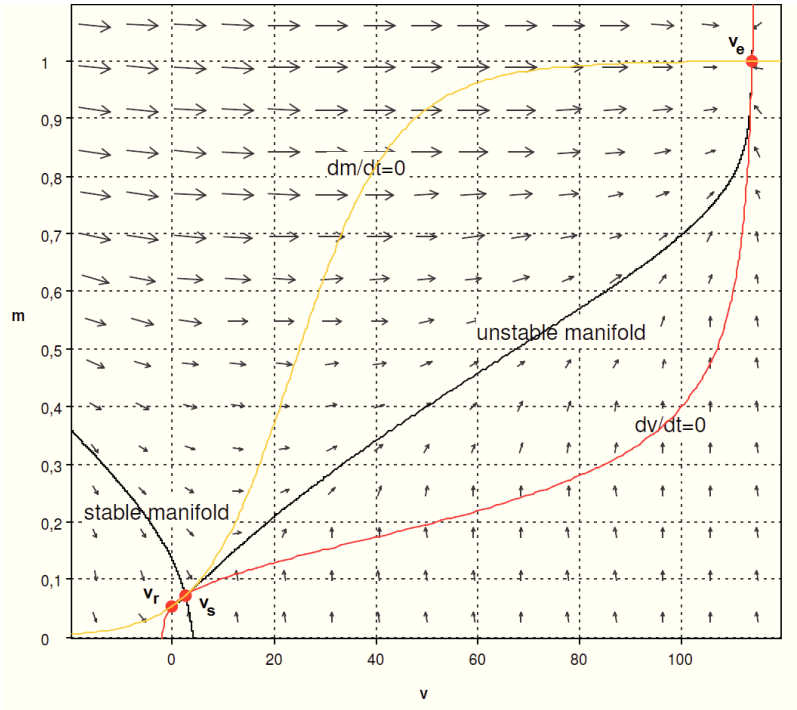

Figure 3.3: The phase portrait associated to the dynamical system (3.4): representation of the nullclines, the vector field, the three equilibrium points and the stable and unstable manifolds corresponding to the saddle point v_s.

where $\mathbf{F}$ is the Jacobian matrix of the vector $\mathbf{f}$ computed at point $\bar{\mathbf{x}}$

$$\mathbf{F} = \begin{bmatrix} \frac{\partial f_1}{\partial x_1} & \frac{\partial f_1}{\partial x_2} & \cdots & \frac{\partial f_1}{\partial x_n} \\ \frac{\partial f_2}{\partial x_1} & \frac{\partial f_2}{\partial x_2} & \cdots & \frac{\partial f_2}{\partial x_n} \\ \vdots & & & \\ \frac{\partial f_n}{\partial x_1} & \frac{\partial f_n}{\partial x_2} & \cdots & \frac{\partial f_n}{\partial x_n} \end{bmatrix}_{x=\bar{x}}.$$

Since $\mathbf{f}(\bar{\mathbf{x}}) = 0$, the linearized system (3.7) is reduced to

$$\dot{\mathbf{y}} = \mathbf{F}\mathbf{y}.$$

Now, let $(\bar{v}, \bar{m})$ be an equilibrium point of (3.4). The Jacobian matrix has the following form

$$\mathbf{F} = \begin{bmatrix} \frac{-\bar{g}_{\mathrm{K}} n_0^4 - \bar{g}_{\mathrm{Na}} \bar{m}^3 h_0 - \bar{g}_{\mathrm{L}}}{C_m} & \frac{-3\bar{g}_{\mathrm{Na}} \bar{m}^2 h_0 (\bar{v} - v_{\mathrm{Na}})}{C_m} \\ 0.1(1-\bar{m}) \frac{-(e^{\frac{25-\bar{v}}{10}} - 1) + \frac{25-\bar{v}}{10} e^{\frac{25-\bar{v}}{10}}}{(e^{\frac{25-\bar{v}}{10}} - 1)^2} + \frac{2}{9} e^{-\frac{\bar{v}}{18}} \bar{m} & -0.1 \frac{25-\bar{v}}{e^{\frac{25-\bar{v}}{10}} - 1} - 4e^{-\frac{\bar{v}}{18}} \end{bmatrix}.$$

Table 3.2: Properties of the equilibrium points of (3.4).

point	coordinates (mV)	type of equilibrium	stability properties
v_e	$(113.92, 0.999)$	nodal sink	Asymptotically Stable
v_s	$(2.602, 0.0716)$	saddle point	Unstable
v_r	$(0.018, 0.053)$	nodal sink	Asymptotically Stable

The stability of the equilibrium configuration of the nonlinear system is determined by the eigenvalues λ_i of matrix $\mathbf{F}$. In particular:

- if all the eigenvalues of $\mathbf{F}$ are negative, $(\bar{v}, \bar{m})$ is asymptotically stable;
- if at least one eigenvalue of $\mathbf{F}$ has positive real part, then $(\bar{v}, \bar{m})$ is unstable.

By substituting the parameters values in Table 3.1, we find the result shown in Table 3.2. Since v_s is a saddle point, it has a stable manifold (evidenced in Fig. 3.3). It represents a separatrix in the phase plane because the trajectories starting from the left or from the right of the stable manifold have a different behavior. If the initial point of a solution is located on the left, the corresponding trajectory evolves toward the resting state v_r, while if the solution starts from a point on the right it is prevented from reaching v_r and it must end up at the excited state, v_e.

Therefore by exciting the system from the resting state, if the perturbation is large enough to cross the separatrix, it results in a large excursion in the voltage that reaches the excited state, while, if the shock strength is not sufficient to cross the manifold, the stimulus returns to v_r. This is called a *threshold phenomenon* because the stable manifold acts as a threshold, by causing the excitation of the system once the separatrix is crossed.

Whenever a solution reaches the excited state, the potential stays at v_e indefinitely and the system exhibits no return to the resting state. The main reason for this unphysical behavior is that the model does not take into account changes in h and n, which are the variables responsible for bringing the potential to the resting state. Thus it is required to reintroduce one of these variables in the model to completely describe an action potential.

FitzHugh proved that during the course of an action potential the plots of n an h versus time have similar shapes ([4], Fig.1). Then he suggested that the variable h could be eliminated by setting $h = 0.85 - n$ [5].

By following this idea and assuming that the activation of the sodium channels is faster than the evolution of the voltage (which is equivalent to

assuming that m is always in instantaneous equilibrium), Keener and Sneyd [32] proposed a fast-slow model involving the fast variable v and the slow variable n:

$$\begin{aligned} c_{\mathrm{m}}\frac{\mathrm{d}v}{\mathrm{d}t} &= -\bar{g}_{\mathrm{K}}n^4(v-v_{\mathrm{K}}) - \bar{g}_{\mathrm{Na}}m_\infty^3(v)(0.8-n)(v-v_{\mathrm{Na}}) - \bar{g}_L(v-v_L) - i_{\mathrm{appl}} \\ \frac{\mathrm{d}n}{\mathrm{d}t} &= \alpha_n(1-n) - \beta_n n \end{aligned}$$

where $m_\infty(v)$ is the equilibrium value of m ($m_\infty(v) = \alpha_m(v)/(\alpha_m(v) + \beta_m(v))$).

By replacing α_m, β_m, α_n and β_n with the relations provided by Hodgkin and Huxley [27, 4], they get

$$\begin{aligned} c_{\mathrm{m}}\frac{\mathrm{d}v}{\mathrm{d}t} &= -\bar{g}_{\mathrm{K}}n^4(v-v_{\mathrm{K}}) - \bar{g}_{\mathrm{Na}}\left(\frac{0.1\frac{25-v}{e^{\frac{25-v}{10}}-1}}{0.1\frac{25-v}{e^{\frac{25-v}{10}}-1} + 4e^{\frac{-v}{18}}}\right)^3 (0.8-n)(v-v_{\mathrm{Na}}) - i_{\mathrm{appl}} \\ &\quad - \bar{g}_L(v-v_L) \\ \frac{\mathrm{d}n}{\mathrm{d}t} &= 0.01\frac{10-v}{e^{\left(\frac{10-v}{10}\right)}-1}(1-n) - 0.125e^{\left(\frac{-v}{80}\right)}n. \end{aligned} \tag{3.8}$$

The nullclines and the vector field corresponding to this dynamical system (when $i_{\mathrm{appl}} = 0$) are shown in Fig. 3.4.

In analogy with the previous system, we observe that the coefficients α_m and α_n are different from zero for all the values of the potential. If we make use of Table 3.1, the nullclines intersect in a single point, located in $v_{\mathrm{eq}} = (-0.196, 0.315)$, so that the dynamical system has a single steady state.

The Jacobian matrix evaluated at the equilibrium point is

$$\mathbf{F} = \begin{bmatrix} -0.332 & -54.881 \\ 0.003 & -0.183 \end{bmatrix}.$$

Since $\mathrm{tr}\mathbf{F} < 0$ and $\det\mathbf{F} > 0$, the equilibrium point is stable, and more precisely it is a spiral sink. In the following analysis we show that, in the limit $c_{\mathrm{m}} \to 0$, the orbits are attracted by the stable sink.

As a matter of fact, since v is a fast variable (and small values of c_{m} highlight this statement) and n is slow, the trajectories in the phase plane are approximately horizontal except closed to the $v-$nullcline. Along this curve the orbit (dashed line in Fig. 3.4) moves slowly in the direction prescribed by the sign of $\frac{\mathrm{d}n}{\mathrm{d}t}$, but however, as we may realize from Fig. 3.4, it moves

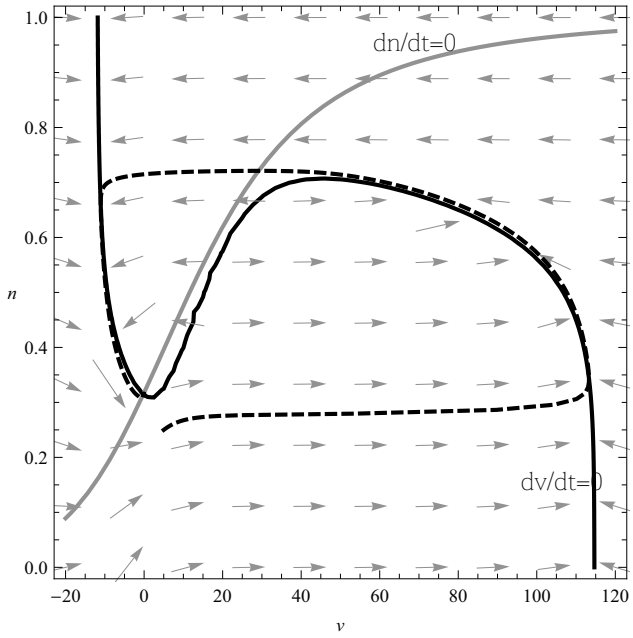

Figure 3.4: Phase portrait of system (3.8).

away from the middle branch of the $v-$nullcline toward the left and the right branches.

In particular, when the trajectory reaches the right branch, that is the decreasing part of the curve $\frac{\mathrm{d}v}{\mathrm{d}t} = 0$ which starts at the relative maximum of the cubic function, $\frac{\mathrm{d}n}{\mathrm{d}t} > 0$, so that the solution moves up until the turning point is reached. At this point, since the right branch of the slow manifold ceases to exist, the solution moves quickly to the left branch of the $v-$nullcline, identified by the decreasing portion of the nullcline that ends at its relative minimum. Here, $\frac{\mathrm{d}n}{\mathrm{d}t} < 0$, so that the trajectory proceeds approaching the steady state, and then completing the action potential. This last path corresponds to the recovery phase of the action potential.

On the other hand, if an orbit directly intersects the left branch, it remains close to it and it is guided by the vector field to the resting point.

The variables n and v are usually called the excitation and recovery variables, respectively: v controls the increase up to the excited state, while n causes the return to the equilibrium point.

The middle branch of the slow nullcline is referred to as the unstable branch. It is included between the relative minimum and maximum of the curve $\frac{\mathrm{d}v}{\mathrm{d}t} = 0$ and it acts as a threshold, exactly as the unstable manifold for the previous model. If a perturbation from v_{eq} is small enough so that v does not cross the unstable manifold, then the trajectory moves horizontally

toward the left and returns to the steady state. However, if the excursion is large enough so that v intersects the unstable manifold, then the trajectory moves quickly toward the right branch of the slow manifold, which coincides with the excited state.

The correspondence between the fast model and the fast-slow model can be recognized also in the three different states: resting, excitable and saddle (or unstable). Indeed the three intersection points between the v and m nullclines in the fast phase plane (fixed n and h) match the three branches of the v nullcline in the fast-slow model. Precisely we can say that the left branch of this nullcline corresponds to the resting state, the middle branch to the unstable state and the right one to the excited state.

An useful illustration of the previous statement is presented in Fig. 3.5 which shows the fast phase portrait with the m-nullcline (dashed line) and the variation of the v-nullcline for n increasing and h decreasing. As n grows, the unstable and the excited state, v_s and v_e, coalesce and disappear. The same behavior is observed in the fast-slow model (Fig. 3.4): as n increases, the two rightmost branches of the slow nullcline coincide in a point and then vanish.

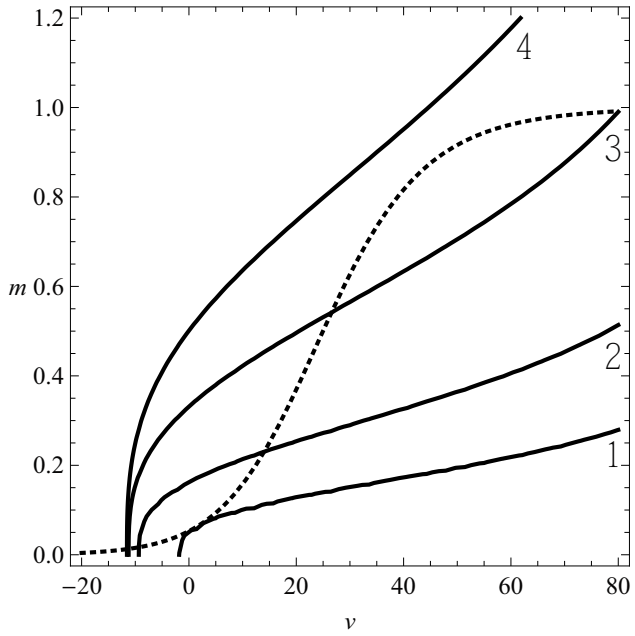

Figure 3.5: The fast phase plane as a function of the slow variables, showing the m-nullcline (dotted) and the v-nullcline (solid) for different values of the slow variables. 1) $h_0 = 0.596$, $n_0 = 0.3176$; 2) $h_0 = 0.4$, $n_0 = 0.5$; 3) $h_0 = 0.2$, $n_0 = 0.7$; and 4) $h_0 = 0.1$, $n_0 = 0.8$.

It is clear that all the assertions discussed above hold because the left and the right branches of the $v-$nullcline tend to infinity, and in particular the left branch tends to $+\infty$ for $v \to v_{\mathrm{K}}$, while the right branch goes to $-\infty$ for $v \to v_{\mathrm{Na}}$.

3.1.3 The Nagumo circuit and the FitzHugh-Nagumo system

In 1960 Nagumo proposed a simplified model of the cell membrane that summarizes the characteristics of the main ionic currents responsible for the action potential [6]. This model reproduces, in a detailed but still manageable way, the slow and the fast currents analyzed by FitzHugh in the previous systems. He built the circuit in Fig. 3.6 consisting of three components: a capacitor, that usually models the membrane capacitance, a non-linear current-voltage element representing the fast ionic currents and a resistor, an inductor and a battery in series simulating the recovery forces.

Application of the Kirchhoff current law at node A (Fig. 3.6) yields

$$i_{\mathrm{appl}} + i_{\mathrm{fast}} + i_{c_{\mathrm{m}}} + i_{\mathrm{rec}} = 0,$$

equivalent to

$$F(V_{\mathrm{m}}) + i_{\mathrm{rec}} + c_{\mathrm{m}} \frac{\mathrm{d}V_{\mathrm{m}}}{\mathrm{d}\tau} = -i_{\mathrm{appl}}.$$

Application of the Kirchhoff voltage law to the right closed loop, yields

$$V_{\mathrm{m}} - V_R - V_L - V_0 = 0,$$

that is

$$V_{\mathrm{m}} - V_0 = R i_{\mathrm{rec}} + L \frac{di_{\mathrm{rec}}}{\mathrm{d}\tau},$$

where we have used Ohm's law for the resistance (i_{rec} is the current through the resistor-inductor) and the relation linking the voltage and the current in the inductor. The τ denotes a dimensional time, while t will be used as a dimensionless time variable.

Thus we obtain the following (V_{m}, i) system

$$\begin{cases} F(V_{\mathrm{m}}) + i_{\mathrm{rec}} + c_{\mathrm{m}} \dfrac{\mathrm{d}V_{\mathrm{m}}}{\mathrm{d}\tau} = -i_{\mathrm{appl}} \\ V_{\mathrm{m}} - V_0 = R i_{\mathrm{rec}} + L \dfrac{\mathrm{d}i_{\mathrm{rec}}}{\mathrm{d}\tau}. \end{cases} \tag{3.9}$$

The next step consists in introducing dimensionless variables depending on the passive resistance of the non linear element, $R_1 = 1/F'(0)$, and the

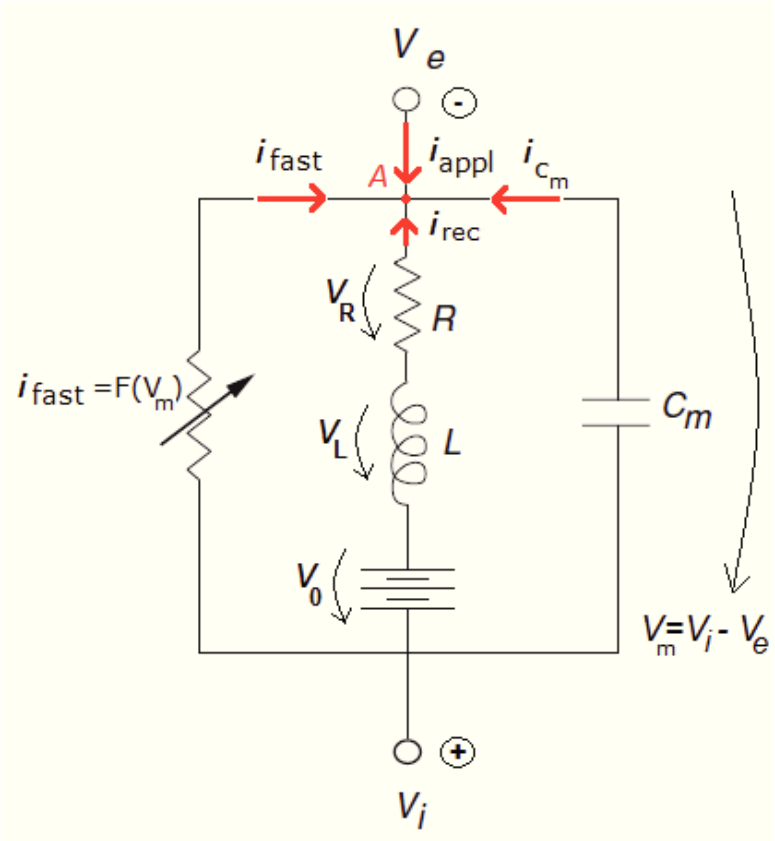

Figure 3.6: The Nagumo circuit (modified from [32]).

two stable equilibrium configurations of the differential equation $\mathrm{d}V_\mathrm{m}/\mathrm{d}\tau = -F(V_\mathrm{m})$, once we have assumed $F(V_\mathrm{m})$ of cubic shape (Fig. 3.7). The function $F(V_\mathrm{m})$ of the figure corresponds to the v-nullcline of the fast-slow phase plane, and the three zeros illustrated in Fig. 3.7 identify the three branches of the curve.

By multiplying equations (3.9) by R_1/V_1, and introducing the dimensionless variables

$$t = \tau\frac{R_1}{L} \qquad v = \frac{V_\mathrm{m}}{V_1} \qquad w = \frac{R_1}{V_1}i_\mathrm{rec} \qquad f(v) = -\frac{R_1}{V_1}F(V_\mathrm{m})$$

we get

$$\begin{cases} -f(v) + w + c_\mathrm{m}\dfrac{R_1}{V_1}\dfrac{\mathrm{d}V_\mathrm{m}}{\mathrm{d}t}\dfrac{\mathrm{d}t}{\mathrm{d}\tau} = -i_\mathrm{appl}\dfrac{R_1}{V_1} \\ R_1 v - \dfrac{R_1}{V_1}V_0 = Rw + L\dfrac{R_1}{V_1}\dfrac{\mathrm{d}i_\mathrm{rec}}{\mathrm{d}t}\dfrac{\mathrm{d}t}{\mathrm{d}\tau} \end{cases}$$

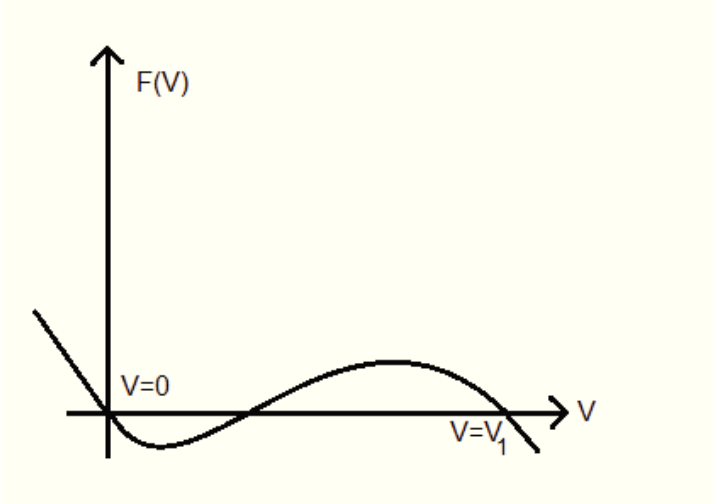

Figure 3.7: Schematic representation of the function F(V).

or

$$\begin{cases} -f(v) + w + c_{\mathrm{m}} \dfrac{R_1^2}{L} \dfrac{\mathrm{d}v}{\mathrm{d}t} = -i_{\mathrm{appl}} \dfrac{R_1}{V_1} \\ R_1 v - \dfrac{R_1}{V_1} V_0 = Rw + \dfrac{R_1^2}{V_1} \dfrac{\mathrm{d}i_{\mathrm{rec}}}{\mathrm{d}t}. \end{cases}$$

Finally, by letting $\varepsilon = R_1^2 c_{\mathrm{m}}/L$, $w_0 = i_{\mathrm{appl}} R_1/V_1$, $\gamma = R/R_1$ and $v_0 = V_0/V_1$, system (3.9) becomes:

$$\begin{cases} \varepsilon \dfrac{\mathrm{d}v}{\mathrm{d}t} = f(v) - w - w_0 \\ \dfrac{\mathrm{d}w}{\mathrm{d}t} = v - \gamma w - v_0. \end{cases} \tag{3.10}$$

Equations (3.10) are referred to as classical FitzHugh-Nagumo dynamical system. The parameters of the model need to satisfy the following requirements:

$$0 < \gamma < 1 \text{ which implies } R_1 > R, \tag{3.11}$$

$$0 < \varepsilon \ll 1 \text{ which implies } \frac{C}{L} \ll \frac{1}{R_1^2}. \tag{3.12}$$

The first request specifies a property of the membrane, so that γ is usually adjusted as a fitting parameter. The second statement takes into account the different time scales of the fast and slow currents (indeed (3.12) is a sort of a comparison between the conductance of the non linear device and that of the inductor).

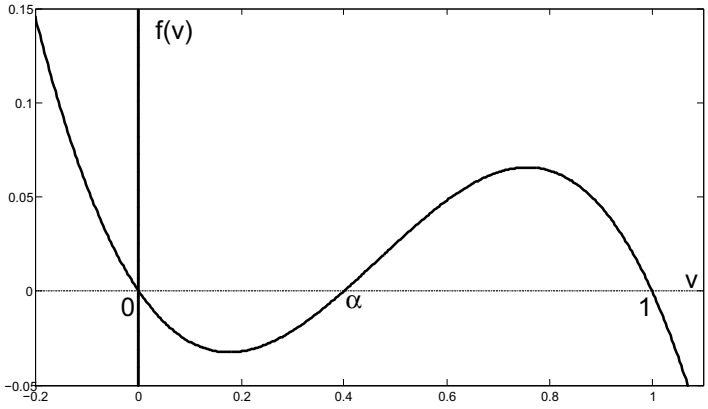

Figure 3.8: Graph of $f(v)$.

The function $f(v)$ is a cubic with three zeros. In the following we will set

$$f(v) = v(1-v)(v-\alpha),$$

with $\alpha \in (0,1)$.

In summary, the dynamical system we will study in the following is

$$\begin{cases} \varepsilon \dfrac{\mathrm{d}v}{\mathrm{d}t} = v(1-v)(v-\alpha) - w \\ \dfrac{\mathrm{d}w}{\mathrm{d}t} = v - \gamma w \end{cases} \tag{3.13}$$

where we have set $i_{\text{appl}} = 0$ and $V_0 = 0$.

The v-nullcline has a cubic form while the w-nullcline is a linear function. They are represented by the relationships

$$\begin{aligned} \frac{\mathrm{d}v}{\mathrm{d}t} = 0 &\Rightarrow w = v(1-v)(v-\alpha), \\ \frac{\mathrm{d}w}{\mathrm{d}t} = 0 &\Rightarrow w = \frac{v}{\gamma}. \end{aligned}$$

The number of intersection points between these two curves depends on the values of γ. In particular, denoting by $\gamma_{\text{cr},1} = 4/(1-\alpha)^2$, then we have:

- If $\gamma < \gamma_{\text{cr},1}$ there is a single equilibrium configuration, which corresponds to $(v, w) = (0, 0)$.

Table 3.3: Stability properties of equilibrium configurations for (3.13).

$\gamma^2\varepsilon < 1$		
	type of equilibrium	stability
$\gamma f'(v_{\rm eq}) < \gamma^2\varepsilon$	sink	stable
$\gamma f'(v_{\rm eq}) = \gamma^2\varepsilon$	center	stable
$\gamma^2\varepsilon < \gamma f'(v_{\rm eq}) < 1$	source	unstable
$\gamma f'(v_{\rm eq}) = 1$	unstable	
$\gamma f'(v_{\rm eq}) > 1$	saddle point	unstable
$\gamma^2\varepsilon = 1$		
$\gamma f'(v_{\rm eq}) < \gamma^2\varepsilon$	sink	stable
$\gamma f'(v_{\rm eq}) = \gamma^2\varepsilon$	further analysis needed	
$\gamma f'(v_{\rm eq}) > \gamma^2\varepsilon$	source	unstable
$\gamma^2\varepsilon > 1$		
$\gamma f'(v_{\rm eq}) < 1$	sink	stable
$\gamma f'(v_{\rm eq}) = 1$	stable	
$1 < \gamma f'(v_{\rm eq}) < \gamma^2\varepsilon$	saddle point	unstable
$\gamma f'(v_{\rm eq}) = \gamma^2\varepsilon$	saddle point	unstable
$\gamma f'(v_{\rm eq}) > \gamma^2\varepsilon$	saddle point	unstable

- If $\gamma = \gamma_{\rm cr,1}$ there are two equilibrium points.
- If $\gamma > \gamma_{\rm cr,1}$ three different equilibrium points arise.

By studying the Jacobian matrix of system (3.13) we can easily deduce the stability of the equilibrium configurations determined above. If we let

$$\mathbf{J} = \begin{bmatrix} \varepsilon^{-1} f'(v_{\rm eq}) & -\varepsilon^{-1} \\ 1 & -\gamma \end{bmatrix} \tag{3.14}$$

we have

$$\det \mathbf{J} = \frac{1}{\varepsilon}\left(1 - f'(v_{\rm eq})\gamma\right) \quad \text{and} \quad \operatorname{tr} \mathbf{J} = -\gamma + \frac{f'(v_{\rm eq})}{\varepsilon}. \tag{3.15}$$

Since ε and γ are assumed to be positive, it follows that whenever $f'(v_{\rm eq}) \leq 0$, the equilibrium configuration is stable. Otherwise, if $f'(v_{\rm eq}) > 0$, the sign of $\det J$ depends on whether $\gamma f'(v_{\rm eq}) \lessgtr 1$, while the sign of $\operatorname{tr} J$ changes as $f'(v_{\rm eq}) \lessgtr \gamma\varepsilon$. By matching the previous results we may derive the stability Table 3.3.

In Fig. 3.9 we depict the phase plane representation for the following values of the parameters:

$$\gamma = \frac{1}{2} \qquad \alpha = \frac{1}{10} \qquad \varepsilon = \frac{1}{100}. \tag{3.16}$$

For such values $\gamma < \gamma_{\mathrm{cr},1}$, then the unique steady state is located at the origin and, since $\gamma^2\varepsilon < 1$ and $f'(v_{\mathrm{eq}}) < \gamma\varepsilon = 5 \times 10^{-3}$, the equilibrium point is a stable sink. In this case a generic solution behaves like the trajectory of system (3.8): once it hangs the right branch of the v-nullcline, it follows the curve up to the relative maximum. Then it moves quickly on the left region, and it moves down along the left branch toward the resting state.

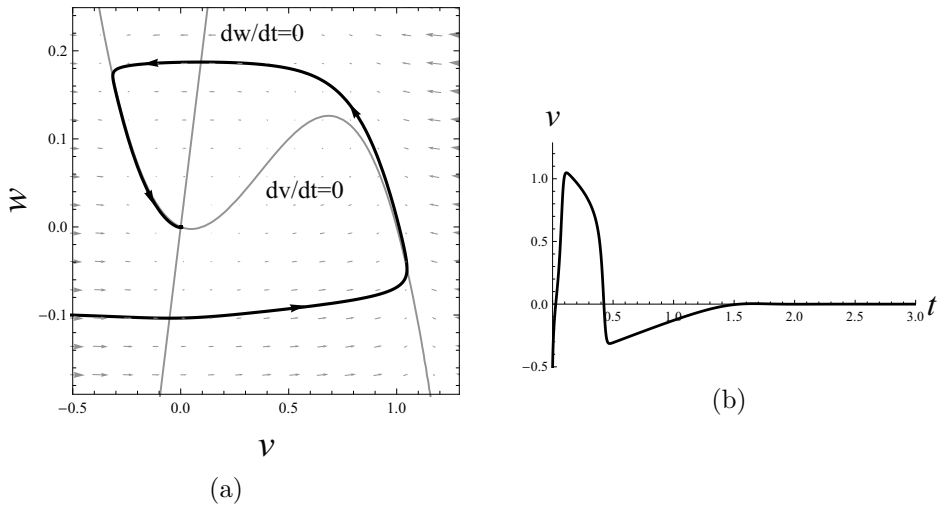

Figure 3.9: (a) FitzHugh-Nagumo phase plane with $i_{\mathrm{appl}} = 0$. (b) Plot of the potential as a function of time.

Therefore, analogously to the model (3.8), the middle branch of the v-nullcline is the unstable region in the phase plane; this means that all the points belonging to this branch are unstable and may play the role of a voltage threshold. For this reason, in the literature the authors refer to α as a voltage threshold [33, 34, 1, 35]: indeed when the point $v = \alpha$, which is also a zero of the function $f(v)$, belongs to the middle branch, it can be assumed as the threshold. That is, if the perturbation exceeds the value $v = \alpha$ the system reacts by performing a complete action potential.

With the values of the parameters in (3.16) but the current clamp $i_{\mathrm{appl}} \neq 0$ the phase portrait and the solutions change substantially. For the sake of clarity, from now on we replace the term w_0 in (3.10) with I_{appl}, in order to stress the fact that this term is linked to the density current applied to the circuit. Then the dynamical system we will analyze is

$$\begin{cases} \varepsilon \dfrac{\mathrm{d}v}{\mathrm{d}t} = v(1-v)(v-\alpha) - w + I_{\mathrm{appl}} \\ \dfrac{\mathrm{d}w}{\mathrm{d}t} = v - \gamma w. \end{cases} \tag{3.17}$$

Obviously the number of equilibria equals the number of roots of the polynomial

$$p(v) = v(1-v)(v-\alpha) - \gamma^{-1}v + I_{\text{appl}}.$$

Generally speaking, if $\gamma_{\text{cr},2}(\alpha) = 3/(1-\alpha+\alpha^2)$, we can say that:

- If $\gamma \leq \gamma_{\text{cr},2}(\alpha)$, the polynomial p is monotonically decreasing, and therefore there is a unique equilibrium configuration. We remark that $\gamma_{\text{cr},2} \in (3,4]$ when $\alpha \in (0,1)$, so that this case is the most significant in practical applications.

- If $\gamma > \gamma_{\text{cr},2}(\alpha)$, the polynomial p exhibits a relative minimum at $v = v_-$, and a relative maximum at $v = v_+$, where

$$v_\pm = \frac{1+\alpha}{3} \pm \sqrt{\frac{\gamma - \gamma_{\text{cr},2}}{3\gamma\gamma_{\text{cr},2}}}\,.$$

  When this is the case, the number of equilibrium configurations depends on the particular value of I_{appl}, as this latter parameter influences the polynomial p by simply translating it upwards or downwards.

For the values of α, γ and ε in (3.16), $\gamma < \gamma_{\text{cr},2} \doteq 3.2967$, then system (3.17) again has one equilibrium point.

Since the stability condition requires $f'(v_{\text{eq}}) < \gamma\varepsilon$, in terms of I_{appl} this happens when either $I_{\text{appl}} < I_{\text{appl},1}$ or $I_{\text{appl}} > I_{\text{appl},2}$ where $I_{\text{appl},1} \doteq 0.105$ and $I_{\text{appl},2} \doteq 1.238$ (Figs. 3.10 3.11).

At both critical values of I_{appl} a Poincaré-Andronov-Hopf bifurcation occurs [32, 36].

Indeed, when $I_{\text{appl},1} < I_{\text{appl}} < I_{\text{appl},2}$, the equilibrium point lies on the middle branch of the v-nullcline, so that it identifies an unstable configuration, and the solution behaves like in Fig. 3.12. Instead of approaching the equilibrium configuration after a finite number of cycles around the steady state, each trajectory alternates periodically between the upper and lower branches, giving rise to an infinite number of periodic solutions (limit cycle behavior).

The qualitative behavior of the phase plane of (3.17) evidences that, by varying the constitutive parameters, the solutions of the dynamical system may undergo two quite different evolutions: either they perform a finite number of cycles before remaining trapped close to the equilibrium configuration (this solution corresponds to the emission of a finite number of action potentials), or they converge towards a limit cycle (an un-physical situation which would correspond to the emission of an infinite number of action potentials). In this Thesis we deal with the first class of solutions. It is our

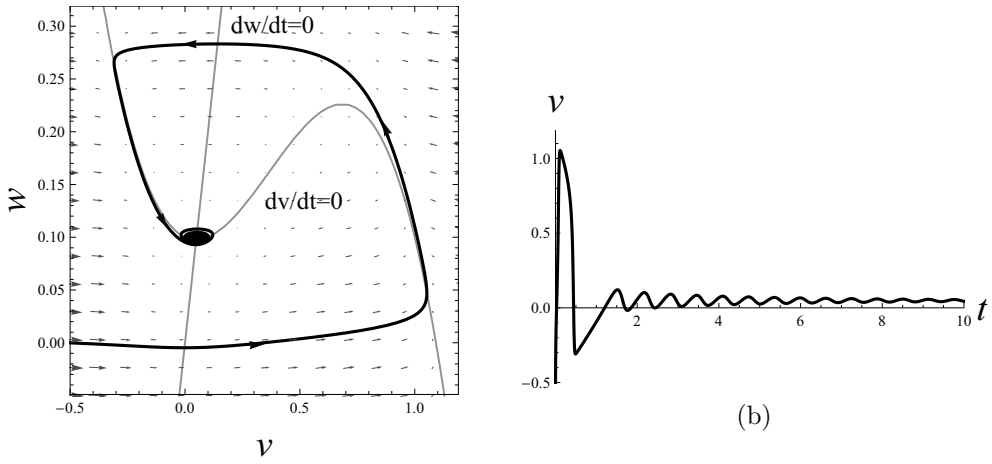

Figure 3.10: FitzHugh-Nagumo phase plane with $I_{\text{appl}} \doteq 0.105$.

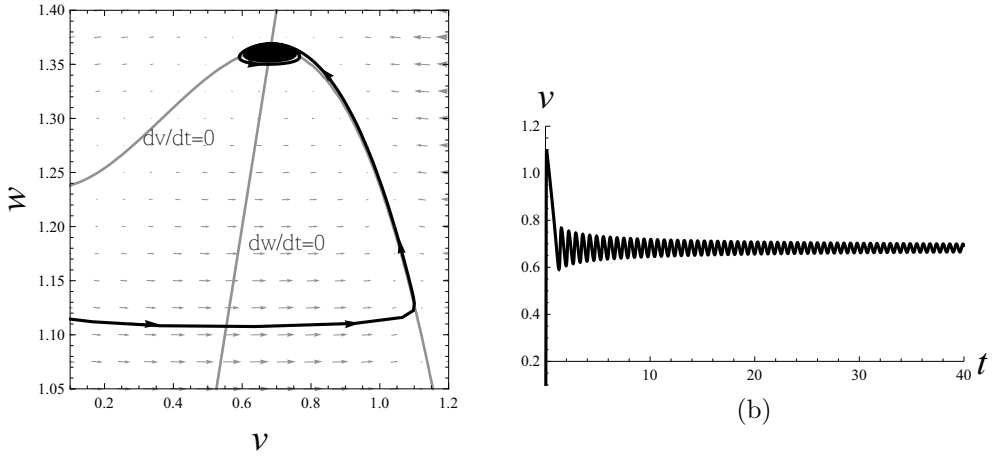

Figure 3.11: FitzHugh-Nagumo phase plane with $I_{\text{appl}} \doteq 1.238$.

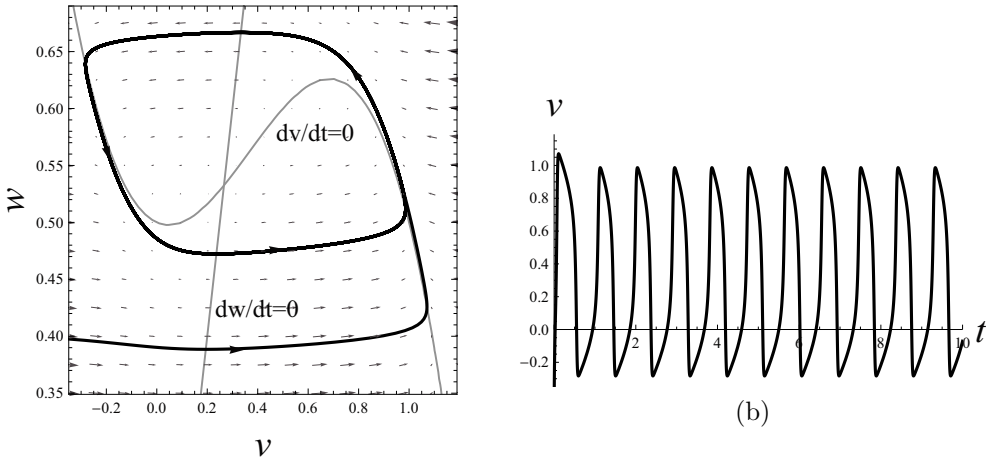

(a) (b)

Figure 3.12: FitzHugh-Nagumo phase plane with $I_{\text{appl}} = 0.5$.

aim to associate with each solution the number of cycles it performs before remaining trapped in the spiral sink, and to study how this number depends on the constitutive parameters. We will, for simplicity, limit ourselves to the case $I_{\text{appl}} = 0$, although all our treatment could easily be generalized to any value of the constitutive parameters which correspond to a single, stable equilibrium configuration.

3.2 Nonexistence of limit-cycle solutions and boundedness of the orbits

In the previous section we have shown that, when $I_{\text{appl}} = 0$ and the other constitutive parameters assume the typical values in (3.16), the orbits in the phase plane evolve toward the equilibrium oscillating around the resting value. The question we handle in this section concerns the possibility of having solutions that, for values of α, ε and γ different from (3.16), do not converge to the stable state as $t \to \infty$.

More precisely, limiting the research to the case $\gamma < \gamma_{\text{cr},1}$, so that the only equilibrium point is the origin, we analyze the possible occurrence of both periodic and unbounded solutions for (3.13) when the constitutive parameters vary in their physiological range. Indeed if there were a limit cycle solution that contains the origin, a trajectory starting out of the region enclosed by the cycle would be prevented form approaching the stable equilibrium point. Moreover, if there exist unbounded orbits (as $t \to +\infty$), they divide the

phase plane into two regions, so that solutions starting in the domain that does not contain the equilibrium point could not belong to the attraction basin of the spiral sink.

In deriving the results contained in this paragraph we mainly follow [37, 38]. These reports analyze quite different dynamical systems, but put forward the analytical methods fit to prove both the absence of limit cycles and the boundedness of the solutions. Here, we adapt their method to the dynamical system (3.13), and supplement the results with some numerical analysis.

3.2.1 Nonexistence of limit cycles: Analytical results

A simple test that proves the nonexistence of periodic solutions is the Bendixson's criterion [39], that we state in the following.

Lemma 1 (Bendixson's negative criterion)**.** *Let* $\dot{\mathbf{x}} = \mathbf{F}(\mathbf{x})$ *be a planar autonomous dynamical system, where* $\mathbf{x} = (x(t), y(t))$ *and* $\mathbf{F} = (f(x, y), g(x, y))$. *Suppose* $\mathbf{F} \in C^1(E)$ *where* E *is a simply connected region of the plane. If* $\operatorname{div} \mathbf{F} = \frac{\partial f}{\partial x} + \frac{\partial g}{\partial y}$ *is always of the same sign but not identically zero, then there are no periodic solutions within* E.

By applying this criterion to (3.13) we can say that the system has no limit cycles if

$$\frac{\partial}{\partial v}\left[\frac{1}{\varepsilon}(v(1-v)(v-\alpha)-w)\right] + \frac{\partial}{\partial w}(v-\gamma w) \neq 0,$$

and it does not change sign. This means that the discriminant of the following expression must be negative $\forall v$

$$\frac{1}{\varepsilon}(-3v^2 + 2v(1+\alpha) - \alpha) - \gamma,$$

that is

$$\frac{1}{\varepsilon^2}(1 + \alpha^2 - \alpha) - \frac{3\gamma}{\varepsilon} < 0. \tag{3.18}$$

If we consider the values of the parameters in (3.16), relation (3.18) is not satisfied, so that this criterion does not prevent the FitzHugh-Nagumo dynamical system from exhibiting periodic solution in correspondence of the values of the constitutive parameters in (3.16).

This result suggests to look for a weaker condition ensuring the nonexistence of limit cycles, since, as we have noted before, the solutions to the FitzHugh-Nagumo dynamical equations when ε, α and γ are those in (3.16) converge to the potential resting value.

Therefore, in order to search for a weaker request, we apply a variable transformations to the equations in (3.13) and make use of some theorems about Liénard systems [40, 41]. By introducing the change of variables

$$\begin{cases} x = -\varepsilon v \\ y = w + \gamma x \end{cases}$$

equations (3.13) become

$$\begin{aligned} \frac{\mathrm{d}x}{\mathrm{d}t} &= y - F(x) \\ \frac{\mathrm{d}y}{\mathrm{d}t} &= -g(x), \end{aligned} \tag{3.19}$$

where

$$\begin{aligned} F(x) &= x\left(\frac{1}{\varepsilon}\left(1+\frac{x}{\varepsilon}\right)\left(\frac{x}{\varepsilon}+\alpha\right)+\gamma\right) \\ g(x) &= x\left(\frac{\gamma}{\varepsilon}\left(1+\frac{x}{\varepsilon}\right)\left(\frac{x}{\varepsilon}+\alpha\right)+\frac{1}{\varepsilon}\right). \end{aligned}$$

An easy computation shows that the condition

$$xg(x) > 0, \quad \forall x \neq 0 \tag{3.20}$$

is equivalent to considering the origin as the unique fixed point of the system. Indeed the term multiplying x in $g(x)$ is positive for all x if $(1-\alpha)^2 - 4/\gamma < 0$, that yields $\gamma < \gamma_{\mathrm{cr},1}$.

Let $G(x) = \int_0^x \mid g(\xi) \mid d\xi$. Since condition (3.20) ensures that $g(x)$ has only one zero at $x = 0$ and that

$$\begin{aligned} g(x) > 0 \text{ if } x > 0 \\ g(x) < 0 \text{ if } x < 0 \end{aligned}$$

and assuming that α, γ and ε are positive, we get:

$$G(x) = \begin{cases} \frac{x^2}{12}\left(\frac{3\gamma}{\varepsilon^3}x^2 + 4\frac{\gamma}{\varepsilon^2}(1+\alpha)x + \frac{6}{\varepsilon}(\gamma\alpha+1)\right) & \text{if} \quad x \geq 0 \\ -\frac{x^2}{12}\left(\frac{3\gamma}{\varepsilon^3}x^2 + 4\frac{\gamma}{\varepsilon^2}(1+\alpha)x + \frac{6}{\varepsilon}(\gamma\alpha+1)\right) & \text{if} \quad x < 0 \end{cases}$$

from which we deduce that $G(x)$ is continuous on $\mathbb{R}$ and it is strictly increasing. Consequently the inverse of G exists, and we can make use of the following theorem for Lièнard systems.

Theorem 1. *[40] Suppose that the origin is the only equilibrium point and*

$$F(G^{-1}(-w)) \neq F(G^{-1}(w)) \qquad \forall w > 0 \tag{3.21}$$

Then (3.19) has no limit cycles.

We try to rephrase (3.21) in order to obtain a more straightforward expression involving α, γ and ε. Following [37], we compute the three roots of the cubic polynomial $F(x)$:

$$\begin{aligned} a &= 0 \\ b &= \frac{\varepsilon}{2}\left(-1-\alpha+\sqrt{(1-\alpha)^2-4\gamma\varepsilon}\right) \\ c &= \frac{\varepsilon}{2}\left(-1-\alpha-\sqrt{(1-\alpha)^2-4\gamma\varepsilon}\right). \end{aligned}$$

In the case

$$(1-\alpha)^2 - 4\gamma\varepsilon > 0 \tag{3.22}$$

we have $c \leq b < a$. Indeed we can easily prove that

$$b = \frac{\varepsilon}{2}\left(-1-\alpha+\sqrt{(1-\alpha)^2-4\gamma\varepsilon}\right) < \frac{\varepsilon}{2}\left(-1-\alpha+\sqrt{(1-\alpha)^2}\right) = -\varepsilon\alpha < 0.$$

We come to the following theorem.

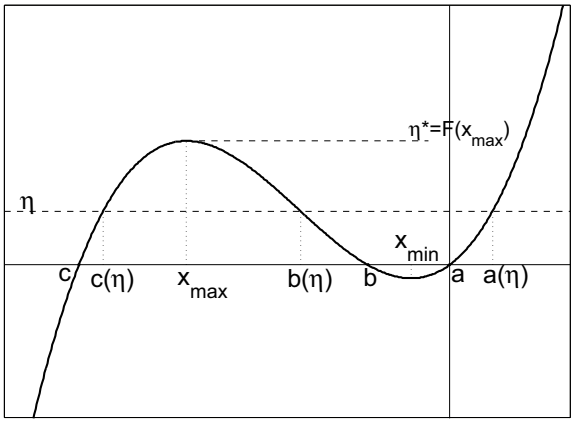

Figure 3.13: Plot of the cubic polynomial $F(x)$, illustrating the arrangement of its roots, and the position of its relative maximum and minimum.

Theorem 2. *[37] Let $a(\eta) \geq b(\eta) \geq c(\eta)$ denote the roots of the equation $F(x) = \eta$, where $\eta \in [0, \eta^*]$, $\eta^* = F(x_{max})$, and x_{max} denotes the point of local maximum of F (see fig. 3.13). Then condition (3.21) is equivalent to*

$$(G(a(\eta)) + G(b(\eta)) \neq 0) \wedge (G(a(\eta)) + G(c(\eta)) \neq 0) \quad \forall \eta \in (0, \eta^*]. \tag{3.23}$$

If, moreover, x_{min} denotes the point of local minimum of F, holds $c(\eta) \leq x_{max} \leq b(\eta) \leq x_{min} < a(\eta)$ holds.

Proof. Let $G(c(\eta)) = G_c \qquad G(b(\eta)) = G_b \qquad G(a(\eta)) = G_a$. Since G is strictly increasing and $c(\eta) < b(\eta) < a(\eta)$, we have

$$G(c(\eta)) < G(b(\eta)) < G(a(\eta)).$$

We also have

$$\eta = F(a(\eta)) = F(b(\eta)) = F(c(\eta))$$

that is

$$\eta = F(G^{-1}(G_a)) = F(G^{-1}(G_b)) = F(G^{-1}(G_c)). \tag{3.24}$$

Now, suppose that $G(a(\eta)) = -G(b(\eta))$ and $G(a(\eta)) = -G(c(\eta))$, that is $G_a = -G_b$ and $G_a = -G_c$. Then (3.24) becomes

$$\eta = F(G^{-1}(G_a)) = F(G^{-1}(-G_a))$$

which yields the contradiction of (3.21). This proves that (3.21) is equivalent to (3.23). □

Let us now evaluate $G(a(\eta))$

$$G(a(\eta)) = \frac{a^2(\eta)}{12}\left(\frac{3\gamma}{\varepsilon^3}a^2(\eta) + 4\frac{\gamma}{\varepsilon^2}(1+\alpha)a(\eta) + \frac{6}{\varepsilon}(\gamma\alpha+1)\right). \tag{3.25}$$

By considering the following equivalence

$$F(a(\eta)) - \eta = 0 = \frac{a^3(\eta)}{\varepsilon^3} + \frac{a^2(\eta)}{\varepsilon^2}(1+\alpha) + a(\eta)(\gamma + \frac{\alpha}{\varepsilon}) - \eta \tag{3.26}$$

we can subtract from (3.25) the quantity

$$\frac{1}{12}(3\gamma a(\eta) + \varepsilon\gamma(1+\alpha))(\frac{a^3(\eta)}{\varepsilon^3} + \frac{a^2(\eta)}{\varepsilon^2}(1+\alpha) + a(\eta)(\gamma + \frac{\alpha}{\varepsilon}) - \eta) \tag{3.27}$$

and we get

$$\begin{aligned} G(a(\eta)) =& \frac{1}{12}\left[a^2(\eta)\left(\frac{6}{\varepsilon} - 3\gamma^2 - \frac{\gamma}{\varepsilon}(-\alpha+1+\alpha^2)\right)\right. \\ &\left. + a(\eta)\left(3\gamma\eta - \varepsilon\gamma(1+\alpha)(\gamma+\frac{\alpha}{\varepsilon})\right) + \varepsilon\gamma(1+\alpha)\eta\right]. \end{aligned}$$

Similar computations can be made for $b(\eta)$ and $c(\eta)$, provided that we add the expression (3.27) computed for $b(\eta)$ and $c(\eta)$

$$\begin{aligned} G(b(\eta)) =& -\frac{1}{12}\left[b^2(\eta)\left(\frac{6}{\varepsilon} - 3\gamma^2 - \frac{\gamma}{\varepsilon}(-\alpha+1+\alpha^2)\right)\right. \\ &\left. + b(\eta)\left(3\gamma\eta - \varepsilon\gamma(1+\alpha)(\gamma+\frac{\alpha}{\varepsilon})\right) + \varepsilon\gamma(1+\alpha)\eta\right], \end{aligned}$$

$$G(c(\eta)) = -\frac{1}{12}\left[c^2(\eta)\left(\frac{6}{\varepsilon} - 3\gamma^2 - \frac{\gamma}{\varepsilon}(-\alpha + 1 + \alpha^2)\right)\right.$$
$$\left. + c(\eta)\left(3\gamma\eta - \varepsilon\gamma(1+\alpha)(\gamma + \frac{\alpha}{\varepsilon})\right) + \varepsilon\gamma(1+\alpha)\eta\right].$$

Then, with the above relations, (3.23) becomes

$$\left(\frac{6}{\varepsilon} - 3\gamma^2 - \frac{\gamma}{\varepsilon}(-\alpha + 1 + \alpha^2)\right)(a(\eta) + b(\eta)) \neq$$
$$-3\gamma\eta + \varepsilon\gamma(1+\alpha)(\gamma + \frac{\alpha}{\varepsilon}) \qquad \forall\eta \in (0, \eta^*]$$

$$\left(\frac{6}{\varepsilon} - 3\gamma^2 - \frac{\gamma}{\varepsilon}(-\alpha + 1 + \alpha^2)\right)(a(\eta) + c(\eta)) \neq$$
$$-3\gamma\eta + \varepsilon\gamma(1+\alpha)(\gamma + \frac{\alpha}{\varepsilon}) \qquad \forall\eta \in (0, \eta^*]$$

where $\eta^* > 0$.

Let now $\eta \to 0$. The right hand side in the previous relations becomes $\varepsilon\gamma(1+\alpha)(\gamma + \frac{\alpha}{\varepsilon}) > 0$, then

$$a(\eta) \to a = 0 \qquad b(\eta) \to b < 0 \qquad c(\eta) \to c < 0.$$

So the left hand side is negative if

$$\frac{6}{\varepsilon} - 3\gamma^2 - \frac{\gamma}{\varepsilon}(-\alpha + 1 + \alpha^2) > 0. \tag{3.28}$$

Then, if (3.28) holds, for $\eta \to 0$ we have

$$\left(\frac{6}{\varepsilon} - 3\gamma^2 - \frac{\gamma}{\varepsilon}(-\alpha + 1 + \alpha^2)\right)(a(\eta) + b(\eta)) < -3\gamma\eta + \varepsilon\gamma(1+\alpha)(\gamma + \frac{\alpha}{\varepsilon}) \tag{3.29}$$

$$\left(\frac{6}{\varepsilon} - 3\gamma^2 - \frac{\gamma}{\varepsilon}(-\alpha + 1 + \alpha^2)\right)(a(\eta) + c(\eta)) < -3\gamma\eta + \varepsilon\gamma(1+\alpha)(\gamma + \frac{\alpha}{\varepsilon}). \tag{3.30}$$

Since (3.23) must hold for all $\eta \in (0, \eta^*]$, inequalities in (3.29) and (3.30) can not change sign; moreover $c(\eta) < b(\eta)$ $\forall\eta \in (0, \eta^*]$, then we come to the following proposition.

Proposition 1. [37] If (3.28) holds, condition (3.23) is equivalent to

$$\left(\frac{6}{\varepsilon} - 3\gamma^2 - \frac{\gamma}{\varepsilon}(-\alpha + 1 + \alpha^2)\right)(a(\eta) + b(\eta)) <$$
$$-3\gamma\eta + \varepsilon\gamma(1+\alpha)(\gamma + \frac{\alpha}{\varepsilon}) \qquad \forall\eta \in (0, \eta^*]. \tag{3.31}$$

We can take a step forward by introducing a new parameter ξ and studying the solutions of the equation

$$F(x) - F(\xi) = 0, \qquad \text{for } \xi \in [c, x_{\max}).$$

By substituting in the previous equation the expression for F we obtain

$$(x - \xi)(x^2 + x(\xi + \varepsilon + \alpha\varepsilon) + (\xi + \varepsilon)(\xi + \alpha\varepsilon) + \gamma\varepsilon^2) = 0.$$

The roots of this equation are ξ, $a(\xi)$ and $b(\xi)$, where $a(\xi)$ and $b(\xi)$ solve

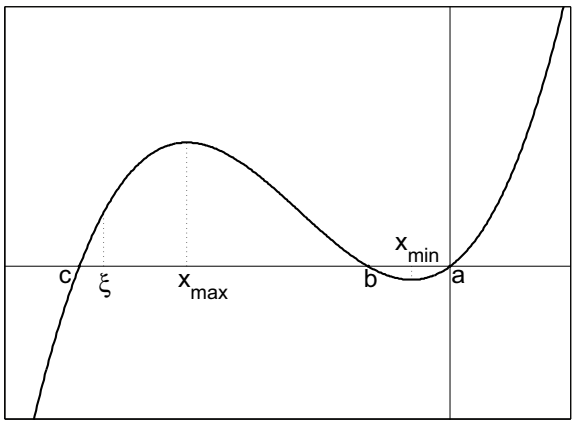

Figure 3.14: Rendering of the parameter ξ.

the following system

$$\begin{cases} a(\xi) + b(\xi) = -(\xi + \varepsilon + \alpha\varepsilon) \\ a(\xi)b(\xi) = (\xi + \varepsilon)(\xi + \alpha\varepsilon) + \gamma\varepsilon^2. \end{cases}$$

By substituting $\eta = F(\xi)$ in (3.31) and the first of the previous relations, we get

$$\begin{aligned} H(\xi) := &- \xi^3 \left(\frac{3\gamma}{\varepsilon^3}\right) - \frac{3\gamma}{\varepsilon^2}(1 + \alpha)\xi^2 - \xi \left(\frac{\gamma}{\varepsilon}(\alpha + 1)^2 + 6\left(\gamma^2 - \frac{1}{\varepsilon}\right)\right) + \\ &(6 - 2\gamma^2\varepsilon - \gamma(1 - \alpha)^2)(1 + \alpha) > 0 \qquad \forall \xi \in [c, x_{\max}). \end{aligned} \tag{3.32}$$

We are now in a position to introduce the main result.

Theorem 3. *[37] The dynamical system (3.13) does not have limit cycles if (3.18) holds, or if the following statements are simultaneously verified*

$$\gamma - 4/(1-\alpha)^2 < 0; \tag{3.33}$$

$$\frac{3\gamma}{\varepsilon} - \frac{1}{\varepsilon^2}(1+\alpha^2-\alpha) < 0; \tag{3.34}$$

$$4\gamma\varepsilon - (1-\alpha)^2 < 0; \tag{3.35}$$

$$-\frac{6}{\varepsilon} + 3\gamma^2 + \frac{\gamma}{\varepsilon}(-\alpha+1+\alpha^2) < 0; \tag{3.36}$$

$$-H(c) < 0; \tag{3.37}$$

$$-H'(c) < 0. \tag{3.38}$$

Proof. The first inequality guarantees that (3.13) has one equilibrium point, (3.34) indicates that parameters violate (3.18), (3.35) ensures that $F(x)$ has three real zeros, (3.36) allows to employ Proposition 1 while (3.37) and (3.38) guarantee that (3.32) holds.

Indeed, since we consider $\gamma^2\varepsilon < 1$ (see section 3.1.3), the discriminant of $H'(\xi)$ is greater than zero, so H has a local maximum and a local minimum at

$$\begin{cases} \xi_{\min} & = -\frac{\varepsilon(1+\alpha)}{3} - \frac{\varepsilon}{3\gamma}\sqrt{-6(\gamma^3\varepsilon-\gamma)} \\ \xi_{\max} & = -\frac{\varepsilon(1+\alpha)}{3} + \frac{\varepsilon}{3\gamma}\sqrt{-6(\gamma^3\varepsilon-\gamma)}. \end{cases}$$

We observe also that (3.36) implies that

$$\xi_{\min} < x_{\max} = -\frac{(1+\alpha)\varepsilon}{3} + \frac{\varepsilon}{3}\sqrt{1+\alpha^2-\alpha-3\gamma\varepsilon}.$$

In conclusion (3.37) and (3.38) ensure that (3.32) is satisfied. □

In the plane (γ, ε) we can identify the region where the parameters satisfying inequalities (3.33)-(3.38) must be inspected. In Fig. 3.15 we represent this region for different values of α. Note that $H(c)$ is defined if $4\gamma\varepsilon-(1-\alpha)^2 < 0$, that is for the points lying below the solid line in Fig. 3.15. In this region (and in particular in the grey region) $-H(c) < 0\ \forall\gamma, \varepsilon$.

It is worth making some observations on Fig. 3.15 in order to better understand the behavior of the admissible parameters region.

1. The hyperbola $3\gamma\varepsilon - 1 - \alpha^2 + \alpha = 0$ is above the hyperbola $4\gamma\varepsilon - (1-\alpha)^2 = 0\ \forall\alpha$. This is because

$$\frac{\alpha^2+1-\alpha}{3\gamma} > \frac{(1-\alpha)^2}{4\gamma} \Rightarrow \alpha^2 + 2\alpha + 1 > 0$$

that is true $\forall\alpha$.

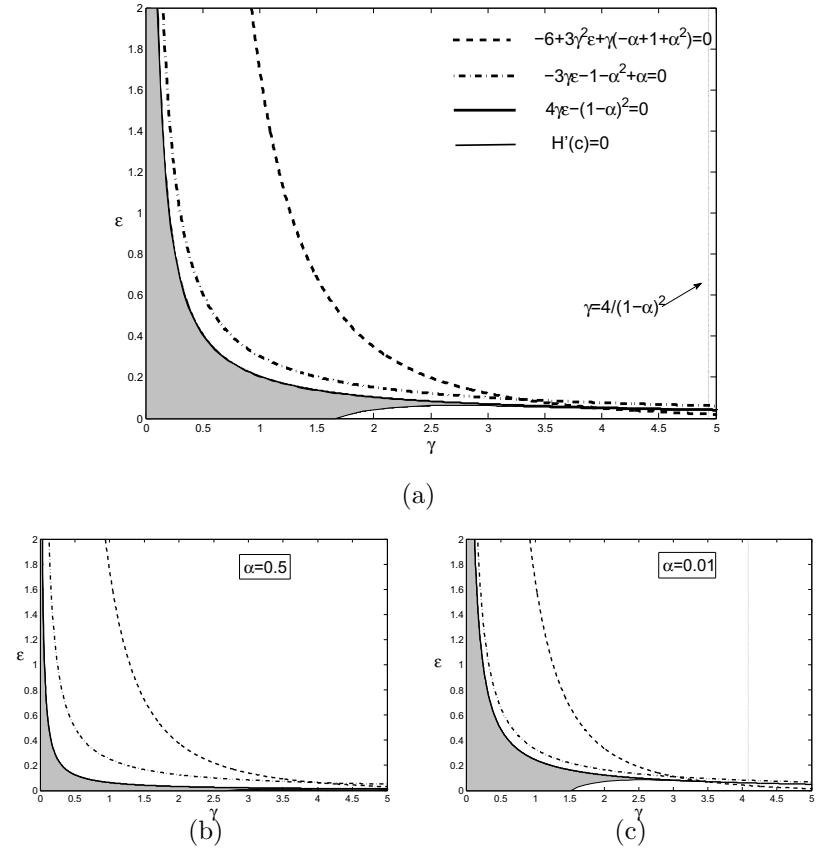

Figure 3.15: Representation of the region where the parameters satisfying inequalities (3.33)-(3.38) must be found in the (γ, ε) plane with (a) $\alpha = 0.1$, (b) $\alpha = 0.5$ and (c) $\alpha = 0.01$.

2. Let us write the equation $H'(c) = 0$,

$$-\left(-1-\alpha-\sqrt{(1-\alpha)^2-4\gamma\varepsilon}\right)^2\left(\frac{9\gamma}{4}\right)-3\gamma(1+\alpha)\left(-1-\alpha-\right.$$
$$\left.\sqrt{(1-\alpha)^2-4\gamma\varepsilon}\right)-\gamma(\alpha+1)^2-6\varepsilon\gamma^2+6=0.$$

Let $\gamma_{\mathrm{cr},3}(\alpha)=\frac{6}{(\alpha-2)^2}$. When $\varepsilon\to 0$, $\gamma\to\gamma_{\mathrm{cr},3}(\alpha)$, that is for $\varepsilon\to 0$, the equation $H'(x_3)=0$ has solutions $\forall\alpha\neq 2$. In particular we can say that $\forall\gamma<\gamma_{\mathrm{cr},3}(\alpha)$, $\exists\varepsilon_{cr}(\alpha)$ such that for $0<\varepsilon<\varepsilon_{cr}(\alpha)$ the FitzHugh-Nagumo dynamical system does not have limit cycle solutions.

3. Consider now the curves (a) $6+3\gamma^2\varepsilon+\gamma\varepsilon(-\alpha+1+\alpha^2)=0$, (b) $4\gamma\varepsilon-(1-\alpha)^2=0$ and (c) $H'(c)=0$. In Fig. 3.16 we represent with a solid line the γ-coordinate of the intersection point between (b) and (c) by varying the parameter α, with a dashed line the γ-coordinate of the intersection point between (a) and (b). The intersection points between (a) and (c) are two: the first coincides with the one between (a) and (b) while the second is represented by a dotted line. It has a critical value for $\alpha=2-\sqrt{3}$ for which (a) and (c) do not intersect each other.

   It can be easily proved that the dashed line is above the solid one for all α. Then we can conclude that the grey region in Fig. 3.15 is delimited $\forall\alpha$ by the intersection point between (b) and (c). In the following we will call the γ-coordinate of this point $\gamma_{\mathrm{cr},4}$.

4. The critical values $\gamma_{\mathrm{cr},3}(\alpha)$ and $\gamma_{\mathrm{cr},4}(\alpha)$ are decreasing functions of α. Indeed, Figs. 3.15(b) and 3.15(c) show that, as α decreases, $\gamma_{\mathrm{cr},3}(\alpha)$ decreases and also the intersection point between the curves (b) and (c) reduces its value.

5. Let us analyze the behavior of the curve $-6+3\gamma^2\varepsilon+\gamma(-\alpha+1+\alpha^2)=0$ for large or small γ. For $\gamma\to\infty$, $\varepsilon=\frac{\alpha-1-\alpha^2}{3}\frac{1}{\gamma}+\frac{2}{\gamma^2}$, so the first order approximation of ε is $\frac{\alpha-1-\alpha^2}{3\gamma}$. On the other hand, for $\gamma\to 0$, $\varepsilon\sim\frac{2}{\gamma^2}$.

6. Let us now perform the same analysis for $H'(c)=0$. For $\gamma\to 0$ we have

$$-\frac{9}{4}\gamma(1+\alpha+\sqrt{(1-\alpha)^2-4\gamma\varepsilon})^2+3\gamma(1+\alpha)(1+\alpha+\sqrt{(1-\alpha)^2-4\gamma\varepsilon})$$
$$-6\varepsilon\gamma^2+6\sim 0. \tag{3.39}$$

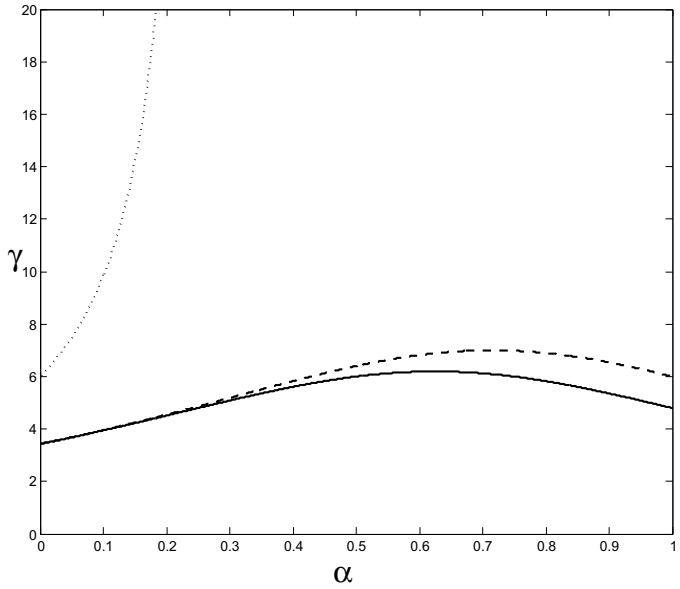

Figure 3.16: γ-coordinate of the intersection points between (a) $6 + 3\gamma^2\varepsilon + \gamma\varepsilon(-\alpha + 1 + \alpha^2) = 0$, (b) $4\gamma\varepsilon - (1-\alpha)^2 = 0$ and (c) $H'(c) = 0$. Solid line, dashed line and dotted line represent respectively the intersection point between (b) and (c), (a) and (b) and (a) and (c).

If $1 < \varepsilon < \frac{1}{\gamma}$, that is $\varepsilon\gamma \to 0$, (3.39) becomes $6 \sim 0$ which is false. If $\frac{1}{\gamma} < \varepsilon < \frac{1}{\gamma^2}$, that is $\varepsilon\gamma \to \infty$ and $\varepsilon\gamma^2 \to 0$ (3.39) becomes

$$-\frac{9}{4}\gamma(1+\alpha+\sqrt{-4\gamma\varepsilon})^2 + 3\gamma(1+\alpha)(1+\alpha+\sqrt{-4\gamma\varepsilon}) + 6 \sim 0. \quad (3.40)$$

Since $H'(c)$ is equal to 0 for a finite γ, see Fig. 3.15, for $\gamma \to 0$ in $H'(c)$ $\varepsilon < 0$, so that $-4\gamma\varepsilon > 0$. Then (3.40) becomes

$$-9\gamma(-\gamma\varepsilon) + 3\gamma(1+\alpha)\sqrt{-4\gamma\varepsilon} + 6 \sim 0.$$

By neglecting $\sqrt{\gamma\varepsilon}$ with respect to $\gamma\varepsilon$ we get

$$9\gamma^2\varepsilon + 6 \sim 0 \Rightarrow 6 \sim 0,$$

which is false again.

The final case we have to analyze is $\varepsilon > \frac{1}{\gamma^2}$, that yields $\varepsilon\gamma \to \infty$ and $\varepsilon\gamma^2 > 1$. Consequently (3.39) is

$$-9\gamma(-\gamma\varepsilon) + 3\gamma(1+\alpha)\sqrt{-4\gamma\varepsilon} - 6\varepsilon\gamma^2 + 6 \sim 0.$$

Again by ignoring $\sqrt{\gamma\varepsilon}$ with respect to $\gamma\varepsilon$ it remains $3\gamma^2\varepsilon + 6 \sim 0 \Rightarrow \varepsilon \sim \frac{2}{\gamma^2}$ that is consistent with the initial hypothesis, $\varepsilon\gamma^2 > 1$.

Conclusively, for $\gamma \to 0$, $\varepsilon \sim \frac{2}{\gamma^2}$.

For $\gamma \to \infty$, $H'(c) = 0$ is not defined. Indeed the curves $4\gamma\varepsilon - (1-\alpha)^2 = 0$ and $H'(c) = 0$ intersect each other for a finite $\gamma = \gamma_{\mathrm{cr},4}$ (see Fig. 3.16). If $\gamma > \gamma_{\mathrm{cr},4}$, $H'(c)$ is not defined.

To sum up, for $\gamma \to 0$, the curves $3\gamma\varepsilon - 1 - \alpha^2 + \alpha = 0$ and $4\gamma\varepsilon - (1-\alpha)^2 = 0$ behave like $1/\gamma$, while $-6 + 3\gamma^2\varepsilon + \gamma(-\alpha + 1 + \alpha^2) = 0$ and $H'(c) = 0$ behave like $2/\gamma^2$. For $\gamma \to \infty$ the first three curves behave like $1/\gamma$ whereas $H'(c) = 0$ is not defined.

If we now verify inequalities (3.33)-(3.38) when the parameters are those in (3.16), we obtain:

$$(3.33) \Rightarrow -3.5404 < 0 \qquad (3.34) \Rightarrow -8950 < 0 \qquad (3.35) \Rightarrow 0.7900 < 0$$
$$(3.36) \Rightarrow -553.7500 < 0 \qquad (3.37) \Rightarrow -H(c) = -0.6425 < 0$$
$$(3.38) \Rightarrow -H'(c) = -421.1724 < 0,$$

being $c = -0.0099$. In particular we infer that for the physiological values of the constitutive parameters in (3.16) the system does not have limit cycles.

3.2.2 Nonexistence of limit cycles: Numerical results

If the parameters $\varepsilon, \alpha, \gamma$ assume values outside the grey region in Fig. 3.15, the existence of limit cycle solutions for the FitzHugh-Nagumo model is not excluded by the results in the preceding section. Therefore in this section we report the evidence obtained by means of a number of numerical investigations from which we may deduce that, also for the parameter values we did not test in the previous paragraph, the dynamical system (3.13) does not possess limit cycles. The method we use is the following.

We parameterize the nullcline $w = v/\gamma$, for $w < 0$, by a curvilinear coordinate s (see Fig. 3.17). Then we study a trajectory starting from any $0 < s_0 < \infty$. Let $s_1 = f(s_0)$ be the point where this trajectory crosses the nullcline $w = v/\gamma$ for the first time during its evolution. Then the trajectory is a limit cycle if $s_1 = s_0$.

Fig. 3.18 shows the numerical calculation of $f(s)$ $\forall s \in (0, 2]$ for different values of α ε and γ. The plots on the right side represent the zoom of $f(s)$ close to $s = 0$. The numerical results clearly evidence that $f(s) < s$ for all s, so that there are not limit cycles. The indication consistently confirmed by the plots in Fig. 3.18 has been indeed tested for several different values of

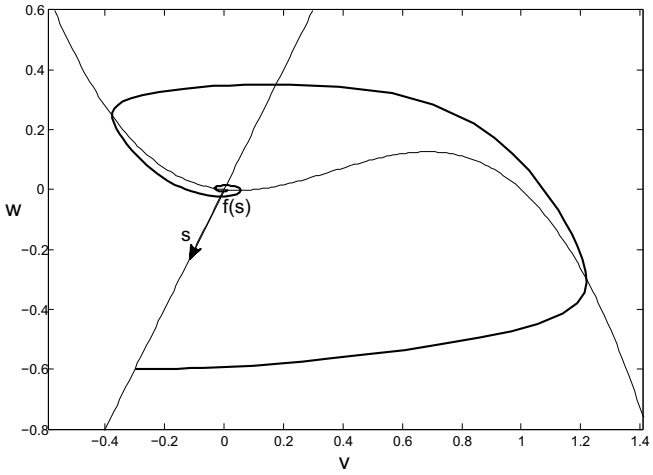

Figure 3.17: Characterization of the numerical method used to show the nonexistence of periodic solutions to (3.13).

the constitutive parameters. More precisely, the variation of α and γ within their physiological range does not affect consistently the behavior of $f(s)$. Slightly more remarkable, and therefore explicitly reported in the plots in Fig. 3.18, is the increase of f with ε, though $f(s)$ remains always sensibly smaller than s, even for physiologically-large values of $\varepsilon(\varepsilon \approx 1)$.

3.2.3 Boundedness of the solutions

As we have already noted at the beginning of this section, if there exists a solution which is unbounded for $t \to +\infty$, the phase plane separates into two regions, one of which contains the origin. Then, since trajectories cannot cross each other, solutions starting out from the region that encloses the equilibrium point, never reach the resting state. In this section we look for conditions that prevent system (3.13) from having unbounded solutions.

For all the computations we refer to [37] and [38]. In these papers it is shown that, if the origin is the unique fixed point of (3.13), it is an attractor for the whole $\mathbb{R}^2$ plane except for a bounded set. This means that the solutions must be bounded. A sketch of the proof is presented in the following.

By a suitable change of variables, equations (3.13) assume a more affordable shape, since it becomes quite easy to construct a Lyapunov function for

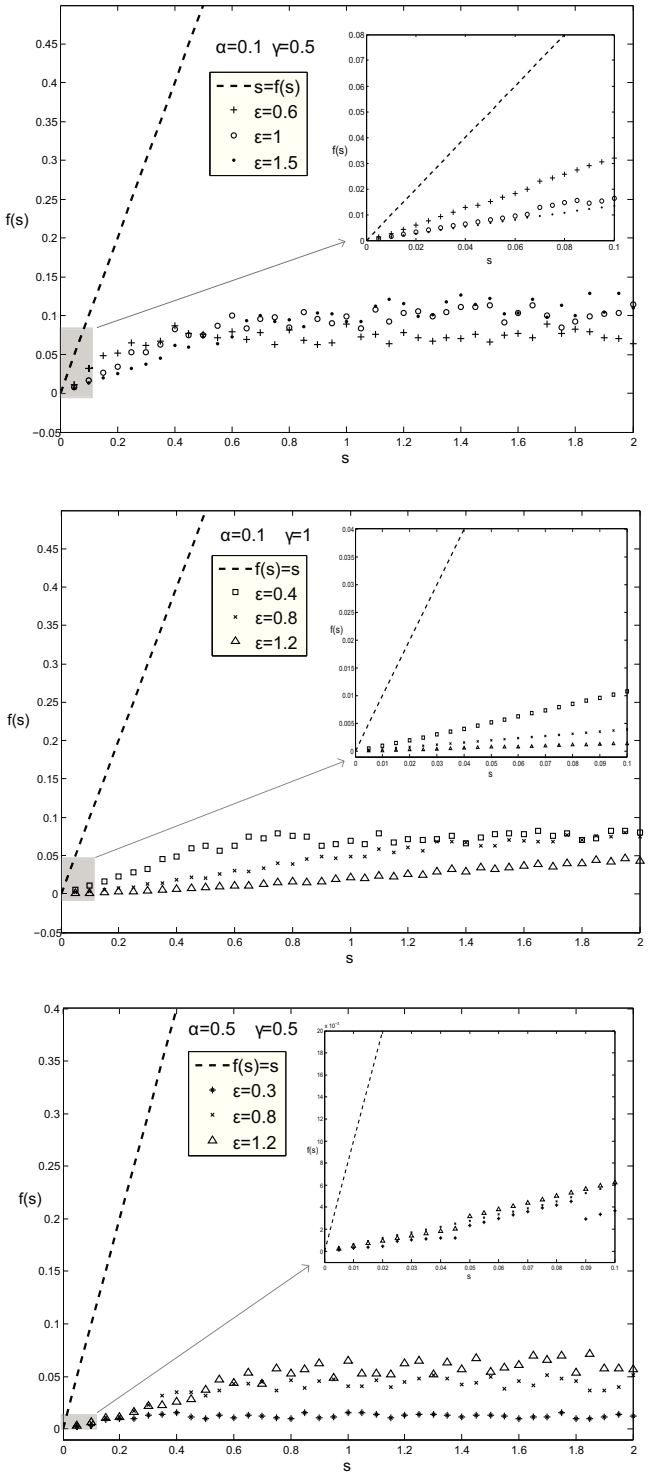

Figure 3.18: Numerical estimate of $|f(s)|$ for $s \in (0, 2]$ for different values of ε, α and γ.

the transformed system. To this aim let

$$\begin{cases} u = v - v_e \\ s = w - w_e \end{cases}, \qquad \begin{cases} y = u - \gamma s \\ x = s \end{cases}$$

where $(v_e, w_e) = (0, 0)$ is the equilibrium point of (3.13). System (3.13) becomes

$$\begin{aligned} \frac{\mathrm{d}x}{\mathrm{d}t} &= y \\ \frac{\mathrm{d}y}{\mathrm{d}t} &= \frac{1}{\varepsilon}(-y f_1(x, y) - g_1(x)) \end{aligned} \tag{3.41}$$

where

$$\begin{aligned} f_1(x, y) &= y^2 + y(3\gamma x - b_2) + 3\gamma^2 x^2 - b_1 - 2b_2\gamma x + \gamma \\ g_1(x) &= -b_1\gamma x - b_2\gamma^2 x^2 + \gamma^3 x^3 + x \end{aligned}$$

and $b_1 = f'(v_e)$, $b_2 = \frac{f''(v_e)}{2}$, being $f(v) = v(1-v)(v-\alpha)$. If $(v_e, w_e) = (0, 0)$, $b_1 = -\alpha$ and $b_2 = (1 + \alpha)$. Define for system (3.41) the function

$$V(x, y) = \frac{y^2}{2} + \frac{G(x)}{\varepsilon},$$

where $G(x) = \int_0^x g_1(\xi)d\xi = \frac{x^2}{12}\left(6(\alpha\gamma + 1) - 4(1 + \alpha)\gamma^2 x + 3\gamma^3 x^2\right)$. We have

$$\dot{V}(x, y) = y\dot{y} + \frac{g_1(x)}{\varepsilon}\dot{x} = -\frac{y^2}{\varepsilon} f_1(x, y).$$

If we show that V is a Lyapunov function for (3.41), we can deduce that its solutions are bounded. The only equilibrium point for (3.41) is the origin. Then, set $(x_e, y_e) = (0, 0)$, $V(x, y)$ is a Lyapunov function for (x_e, y_e) if

- $V(x_e, y_e) = 0$ and $V(x, y) > 0$ if $(x, y) \neq (x_e, y_e)$;

- $\dot{V}(x, y) \leq 0$ in $\mathbb{R}^2 \setminus (x_e, y_e)$.

In order to prove that the first statement is satisfied, let us rewrite V as

$$V(x, y) = \frac{y^2}{2} + \frac{x^2}{12\varepsilon} h(x)$$

where $h(x) = 6(\alpha\gamma+1) - 4(1+\alpha)\gamma^2 x + 3\gamma^3 x^2$ is a parabola. The discriminant of $h(x)$ is

$$\triangle = 16(1 + \alpha)^2\gamma^4 - 72(\alpha\gamma + 1)\gamma^3.$$

Then, if $\triangle < 0$, $h(x) > 0\ \forall x$ and consequently $V(x,y) > 0\ \forall (x,y) \neq (0,0)$. Note that $\triangle < 0$ is equivalent to $\gamma < 9/(2+2\alpha^2-5\alpha) = \gamma_{\mathrm{cr},5}$. Since $\gamma_{\mathrm{cr},1} < \gamma_{\mathrm{cr},5}$ for all $\alpha > 0$, when the dynamical system (3.13) has one equilibrium point, only the case $\triangle < 0$ occurs.

As a general rule, if $\triangle \geq 0$, then $h(x)$ has two zeros, x_1 and x_2, and a local minimum point x^*. If we define

$$\bar{y} = \inf\{y > 0 \mid \frac{y^2}{2} + \frac{(x^*)^2}{12\varepsilon} h(x^*) > 0\}$$

then $\bar{y} < \infty$. Therefore the set where $V(x,y) < 0$ is a subset of $\mathcal{A} = \{(x,y) \in \mathbb{R}^2 \mid x_1 < x < x_2, \mid y \mid < \bar{y}\}$ which is bounded. Then $V(x,y) > 0$ outside of this bounded set.

It remains to prove the second requirement. We can say that

$$\dot{V} < 0 \quad \Leftrightarrow f_1(x,y) > 0 \text{ and } y \neq 0.$$

It can be easily shown that $f_1(x,y)$ is an elliptic paraboloid. Indeed, the quadratic form associated to $f_1(x,y)$ is represented by the matrix

$$\mathbf{B} = \begin{bmatrix} 3\gamma^2 & 3/2\gamma & 0 \\ 3/2\gamma & 1 & 0 \\ 0 & 0 & 0 \end{bmatrix}.$$

The eigenvalues of $\mathbf{B}$ are: $\lambda_1 = 0$, $\lambda_2 = 3/2\gamma^2 + 1/2 + \sqrt{9\gamma^4 + 1 + 3\gamma^2}/2$ and $\lambda_3 = 3/2\gamma^2 + 1/2 - \sqrt{9\gamma^4 + 1 + 3\gamma^2}/2$. Then, since the eigenvalues different from 0 are both positive, $f_1(x,y)$ is an elliptic paraboloid. If we label the minimum point of the quadratic form by $(x_{\min}, y_{\min})$, it is clear that if $f_1(x_{\min}, y_{\min}) > 0$, then the paraboloid is always positive. Since

$$x_{\min} = \frac{1+\alpha}{3\gamma}, \qquad y_{\min} = 0,$$

the value of f_1 at the minimum point is $f_1(x_{\min}, y_{\min}) = -\frac{(1+\alpha)^2}{3} + \alpha + \gamma = S$. Therefore, $f_1(x,y) > 0\ \forall (x,y)$ if and only if $S > 0$, that is $\gamma > (\alpha^2 - \alpha + 1)/3 = 1/\gamma_{\mathrm{cr},2}$ (see section 3.1.3).

We can easily show that $1/\gamma_{\mathrm{cr},2} < \gamma_{\mathrm{cr},1}$ if $-1 < \alpha < 2.554$, while $1/\gamma_{\mathrm{cr},2} > \gamma_{\mathrm{cr},1}$ otherwise. Since the physiological values of α are in the interval $[-1, 2.554]$, typically $1/\gamma_{\mathrm{cr},2} < \gamma_{\mathrm{cr},1}$, then, for $1/\gamma_{\mathrm{cr},2} < \gamma < \gamma_{\mathrm{cr},1}$, $S > 0$ while, for $\gamma < 1/\gamma_{\mathrm{cr},2}$, $S < 0$. If $S < 0$, $f_1(x,y)$ has a negative minimum. But since f_1 is a paraboloid, $\exists (\hat{x}, \hat{y})$ such that $f_1(x,y) > 0$ in $\mathcal{B} = \{(x,y) \in \mathbb{R}^2 | \mid x \mid < \hat{x}, \mid y \mid < \hat{y}\}$. Then the set where $\dot{V} > 0$ is bounded by $\mathcal{B}$. Obviously $\dot{V} = 0$ if $y = 0$ or $f_1(x,y) = 0$. In conclusion, we have proved that, when the origin is

the only equilibrium point of (3.13), V is a Lyapunov function for the fixed point of (3.41) on whole of the plane except for a bounded set. This set is detected by $\mathcal{C} = \{(x, y) \in \mathbb{R}^2 | \mid x \mid > \hat{x}, \mid y \mid > \hat{y}\}$. Then the solutions $(x(t), y(t))$ to (3.41) must be bounded. Finally, since

$$\begin{cases} v = y + \gamma x + v_e \\ w = x + w_e \end{cases}$$

we deduce that if $(x(t), y(t)) < \infty$ for $t > 0$, than also the solutions $(v(t), w(t))$ to (3.13) are bounded as $t > 0$. This proves that the origin is an asymptotically stable attractor for all the orbits.

3.3 Generalized FitzHugh-Nagumo models

In recent years has increasingly asserted the idea that the cardiac mechanical activity is influenced by the electrophysiological mechanisms that drive the potential wave spreading through cardiac tissue. At the same time, the propagation of the electrical flow is affected by the mechanical properties of the tissue since changes in fiber length influence the electrical activity via the so called *mechano-electrical feedback* [42, 43, 44]. Therefore, a more realistic description of the cardiac action potential should also model the laws regulating the information exchanged between the mechanical and electrical environment in the heart.

In this section we make a first attempt to improve the FitzHugh-Nagumo model by accounting for the influence of the depolarization wave propagation on the mechanical characteristics of the cardiomyocytes. This influence is clearly evidenced by the consideration that changes in the electrical properties, occurring at a micro-scale, cause the macroscopic contraction of the cardiac fibers. Then we aim to explicitly describe in the model how the electric flow modifies the physiological parameters, that contain information on the intrinsic characteristic of the tissue.

The most simple way for acting in accordance with this approach is to introduce a dependence on v of the model parameters, so that a modification in the membrane potential can affect the constitutive variables. In the following we will choose ε as a function of v, thus considering that the ratio between the time constants of the fast current and the slow current depends on the membrane potential. The system we obtain is

$$\begin{cases} \varepsilon(v)\dfrac{\mathrm{d}v}{\mathrm{d}t} = v(1-v)(v-\alpha) - w \\ \dfrac{\mathrm{d}w}{\mathrm{d}t} = v - \gamma w. \end{cases} \tag{3.42}$$

The choice of the expression for $\varepsilon(v)$ can be suggested either by a physiological reasoning or by analytical arguments. We will present, in the next, two different procedures described in the article by Ambrosi et al. [45], where the analytical derivation is developed, and in the paper by Aliev and Panfilov [25] where the law for $\varepsilon(v)$ is fitted to experimental measures. Then we will compare the outcomes obtained from these two methods with empirical studies recovered in the literature, in order to understand if our results are compatible with the real physiological behavior.

In [45] a more complete model is studied. Indeed Ambrosi et al. located system (3.13) in a spatial framework that accounts for the spatial coupling of the cardiac cells and consequently for the transmission of the electric signal through cellular linking.

Their model involves the diffusion of the action potential through myocyte interconnections (i.e gap junctions), so that the propagation velocity of the electric impulse is influenced not only by the transmembrane currents but also by axial flows that spread the potential through the heart tissue. The equations characterizing this new model are derived from the cable equation fitted to the neuronal behavior [32]. Such equation represents the mathematical description of a spatial structure that involves many circuits of Fig. 3.6 coupled together by an axial current flow, simulating a fiber, or a tissue, of adjacent cells electrically coupled.

Then, the three-dimensional extension of the FitzHugh-Nagumo equations is a system of a diffusion-reaction equation for the potential v and a reaction-transport equation for the gate variable w

$$\begin{cases} \varepsilon_0 \dfrac{\partial v}{\partial t} + \mathrm{div}(\dot{\mathbf{x}} v) - \mathrm{div}(\mathbf{D}\mathrm{grad} v) = v(1-v)(v-\alpha) - w \\ \dfrac{\partial w}{\partial t} + \mathrm{div}(\dot{\mathbf{x}} w) = v - \gamma w \end{cases} \tag{3.43}$$

where $\mathrm{div}(\dot{\mathbf{x}} v)$ represents a convection term describing the transport due to the displacement of the material itself, $\mathrm{div}(\mathbf{D}\mathrm{grad} v)$ accounts for the spatial distribution of the myocytes and $\mathbf{D}$ is the diffusion tensor. The symbols grad and div are respectively the gradient and the divergence with respect to the spatial coordinates, that characterize the present configuration of the body. We have replaced ε by ε_0 in order to distinguish between the constant parameter ε in (3.13) and the function $\varepsilon(v) = \epsilon_0 \hat{\varepsilon}(v)$. Forms equivalent to the dynamical system (3.43) can be found in [46, 43, 35, 25].

In this section we follow the calculations made in [45]. Then, at the final step, we let the diffusion coefficient tend to zero, thus considering again a description that neglects the spatial bonds between the cardiomyocytes, according to the 0D setting typical of the classical FitzHugh-Nagumo model.

We assume $\mathbf{D}$ as an isotropic diffusivity tensor, namely $\mathbf{D} = d\mathbf{I}$ and we consider that the tissue undergoes large deformations.

By rewriting the dynamical system (3.43) in a material frame of reference, which is assumed to coincide with the undeformed configuration, we obtain

$$\begin{cases} \varepsilon_0 \dfrac{\partial}{\partial t}(Jv) = \mathrm{Div}(d\mathrm{Div}(Jv\mathbf{F}^{-T})\mathbf{F}^{-T}) + Jv(1-v)(v-\alpha) - Jw \\ \dfrac{\partial}{\partial t}(Jw) = Jv - J\gamma w \end{cases} \tag{3.44}$$

where Div and Grad denote the divergence and the gradient operators with respect to the material coordinates X_i, $i = 1, 2, 3$ and $J = \det \mathbf{F}$, $\mathbf{F}$ being the deformation gradient ($F_{i,j} = \partial x_i / \partial X_j$).

To obtain (3.44) we made use of the relations linking the volume and area elements in spatial coordinates to the same elements in the reference configuration:

$$\mathrm{d}v = J\mathrm{d}V, \quad n\mathrm{d}a = J\mathbf{F}^{-T}N\mathrm{d}A.$$

By considering now that the following statement hold

$$\mathrm{Div}(\varphi\mathbf{S}) = \varphi\mathrm{Div}\mathbf{S} + \mathbf{S}\mathrm{Grad}\varphi \qquad \forall \varphi, \mathbf{S}$$

where φ and $\mathbf{S}$ are a scalar and a tensor field respectively, and by making use of the Piola identity

$$\mathrm{Div}(J\mathbf{F}^{-T}) = 0 \quad \text{for } F_{i,j} = \partial x_i / \partial X_j \quad \text{and } J = \det \mathbf{F}$$

(3.44) becomes

$$\begin{cases} \varepsilon_0 \dfrac{\partial}{\partial t}(Jv) = \mathrm{Div}(Jd\mathbf{C}^{-1}\mathrm{Grad}v) + Jv(1-v)(v-\alpha) - Jw \\ \dfrac{\partial}{\partial t}(Jw) = Jv - J\gamma w \end{cases} \tag{3.45}$$

where $\mathbf{C} = \mathbf{F}^T\mathbf{F}$ is the right Cauchy-Green strain tensor.

As in [45], we make an elementary hypothesis assuming that, in the undeformed configuration, at any material point $\mathbf{X}$ the cardiac fibers are ordered according to one direction $\mathbf{n}(\mathbf{X})$. In other words, we assume the following form of $\mathbf{F}$

$$\mathbf{F} = \mathbf{I} + \gamma(v)\mathbf{n} \otimes \mathbf{n}$$

where $\gamma(v)$ prescribes the contraction of the cardiomyocytes along the direction $\mathbf{n}$.

If we now consider a one-dimensional domain, representing a cardiac fiber, and we assume the simplest expression for $\gamma(v)$, namely the contraction of

the fibers linearly depending on the potential field, the tensor field $\mathbf{F}$ becomes the scalar field

$$F = 1 - \beta v. \tag{3.46}$$

where β is the proportionality factor. Then system (3.45) changes into

$$\begin{cases} \varepsilon_0 \dfrac{\partial}{\partial t}((1-\beta v)v) = d\dfrac{\partial}{\partial X}(\dfrac{1}{1-\beta v}\dfrac{\partial v}{\partial X}) + (1-\beta v)v(1-v)(v-\alpha) - (1-\beta v)w \\ \dfrac{\partial (1-\beta v)w}{\partial t} = (1-\beta v)(v-\gamma w). \end{cases} \tag{3.47}$$

Relation (3.46) is certainly a too simplified and therefore unrealistic constitutive prescription for the activation of the contraction. Indeed the mechanisms underlying the muscle stretch involve concentration of calcium ions and are described by more complicated functional relations than the simple direct proportionality between the contraction and the potential [47, 16, 42]. Nevertheless, considering so a simple relation allows us to make a first step toward a more realistic model than the traditional FitzHugh-Nagumo without leading to needless complications of the problem.

According to (3.46), in the depolarization phase, i.e. for a positive potential difference, $-\beta v < 0$ so that the fiber undergoes a contraction. The physiological value of β is 0.3, since a typical muscle contraction requires a 30% strain.

Performing time derivatives in (3.47), the limit $d \to 0$ yields the following spatially-independent model

$$\begin{cases} \varepsilon_0 \dfrac{1-2\beta v}{1-\beta v}\dfrac{\mathrm{d}v}{\mathrm{d}t} = v(1-v)(v-\alpha) - w \\ \dfrac{\mathrm{d}w}{\mathrm{d}t} - \dfrac{\beta}{1-\beta v}\dfrac{\mathrm{d}v}{\mathrm{d}t}w = v - \gamma w, \end{cases}$$

and with some further calculations

$$\begin{cases} \varepsilon_0 \dfrac{1-2\beta v}{1-\beta v}\dfrac{\mathrm{d}v}{\mathrm{d}t} = v(1-v)(v-\alpha) - w \\ \dfrac{\mathrm{d}w}{\mathrm{d}t} = \dfrac{\beta}{\varepsilon_0(1-2\beta v)}w(v(1-v)(v-\alpha) - w) + v - \gamma w. \end{cases} \tag{3.48}$$

The v-nullclines are $v = \frac{1}{\beta}$ and $w = v(1-v)(v-\alpha)$ while the w-nullclines result from the equivalence

$$\frac{\beta}{\varepsilon_0(1-2\beta v)}w(v(1-v)(v-\alpha) - w) + v - \gamma w = 0$$

which is a second order equation in w admitting, in general, two solutions $w_1 = f_1(v)$ and $w_2 = f_2(v)$.

The existence of w_1 and w_2 is bound to the positiveness of the following sixth order polynomial

$$\begin{aligned} P(v) =& \beta^2 v^6 - 2\beta^2(\alpha+1)v^5 + (\beta^2(\alpha+1)^2 + 2\beta(\alpha\beta - 2\beta\varepsilon\gamma))v^4 + \\ &+ (2\beta\varepsilon\gamma - 2\beta(\alpha\beta - 2\beta\varepsilon\gamma)(\alpha+1))v^3 + ((\alpha\beta - 2\beta\varepsilon\gamma)^2 - 8\beta^2\varepsilon - \\ &- 2\beta\varepsilon\gamma(\alpha+1))v^2 + (4\beta\varepsilon + 2\varepsilon\gamma(\alpha\beta - 2\beta\varepsilon\gamma))v + \varepsilon^2\gamma^2. \end{aligned}$$

Figures 3.19 and 3.20 show the graph of $P(v)$ for different values of the parameters α, ε_0 and β (changing of γ does not affect substantially the plot of the polynomial). From these diagrams we may deduce that, for the physiological range of values of the parameters, there exists always an interval where $P(v) < 0$.

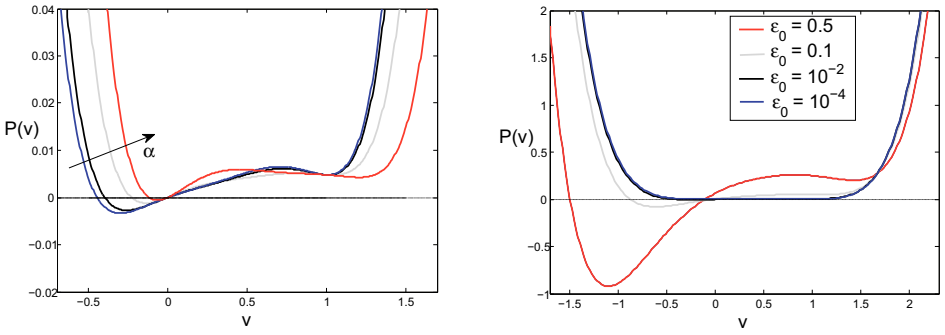

(a) (b)

Figure 3.19: (a) Plot of the polynomial $P(v)$ for $\gamma = 0.5$, $\beta = 0.3$, $\varepsilon_0 = 0.01$ and for $\alpha = 0.1, 0.3, 0.5, 1$. (b) Plot of the polynomial $P(v)$ for $\gamma = 0.5$, $\beta = 0.3$, $\alpha = 0.1$ and for different values of ε_0.

For this reason in the phase portrait of the dynamical system (3.48), shown in Figs. 3.21 and 3.22, there is a range of values of v, which is about $(-0.2, 0)$, where the two w-nullclines are not defined.

Figure 3.22 is a schematic representation of the vector field behavior of the dynamical system. We should note that the line $v_{\text{cr}} = \frac{1}{2\beta}$ represents a critical region for the equations.

Indeed, when the potential assumes this critical value, the first equation of (3.48) yields $\mathrm{d}v/\mathrm{d}t = \infty$. Moreover, in the case $w > v(1-v)(v-\alpha)$, if $v \to v_{\text{cr}}^-$, $\mathrm{d}v/\mathrm{d}t < 0$ then the potential is decreasing (see Fig. 3.22), while, if $v \to v_{\text{cr}}^+$, $\mathrm{d}v/\mathrm{d}t > 0$ and the potential is growing. Therefore a trajectory never really reaches the point v_{cr}.

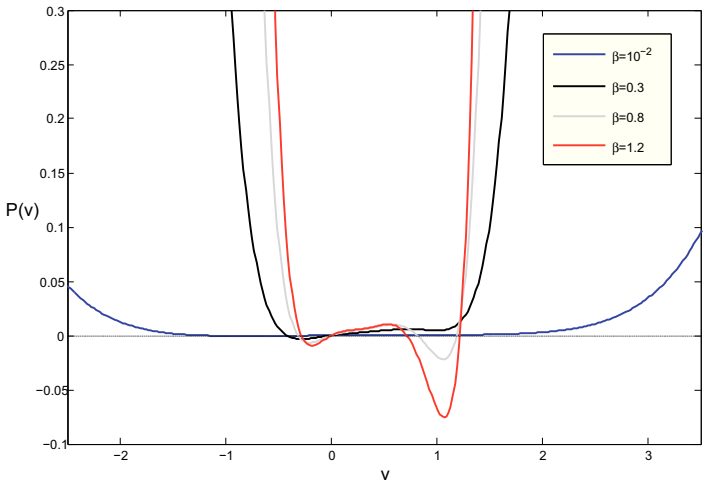

Figure 3.20: Plot of the polynomial $P(v)$ for $\gamma = 0.5$, $\alpha = 0.1$, $\varepsilon_0 = 0.01$ and for different values of β.

On the contrary, in the case $w < v(1-v)(v-\alpha)$, for $v \to v_{\rm cr}^-$, $\mathrm{d}v/\mathrm{d}t > 0$ while for $v \to v_{\rm cr}^+$, $\mathrm{d}v/\mathrm{d}t < 0$; consequently the solution oscillates around the critical line.

The above observations yield the conclusion that the phase plane portrait of dynamical system (3.48) is certainly more involved than that of (3.13), since some singular features of the trajectories emerge. However the abnormal behavior of the solutions can be connected to the linear dependence (3.46) assumed for the functional relation $F(v)$. Indeed, equation (3.46) is to be interpreted as a linear Taylor expansion close to the equilibrium value $v = 0$, and the first-order truncation of the series gives rise to the occurrence of representation errors.

The equilibrium points of system (3.48) are:

$$P_{\rm eq,1} = (0,0) \quad P_{\rm eq,2-3} = \left(0, \frac{1+\alpha \pm \sqrt{1-\gamma_{\rm cr,1}/\gamma}}{2}\right)$$

$$P_{\rm eq,4-5} = \left(\frac{1}{\beta}, \frac{-\xi \pm \sqrt{\xi^2 - 4\varepsilon\beta^4}}{2\beta^3}\right)$$

where $\xi = 1 - \beta(1-\alpha) + \alpha\beta^2 - \gamma\varepsilon\beta^2$.

$P_{\rm eq,1}$ and $P_{\rm eq,2-3}$ result from the intersections between the curve $w = v(1-v)(v-\alpha)$ and the w-nullclines. Indeed, for the points on the cubic nullcline and for small values of w, the second equation in (3.48) becomes

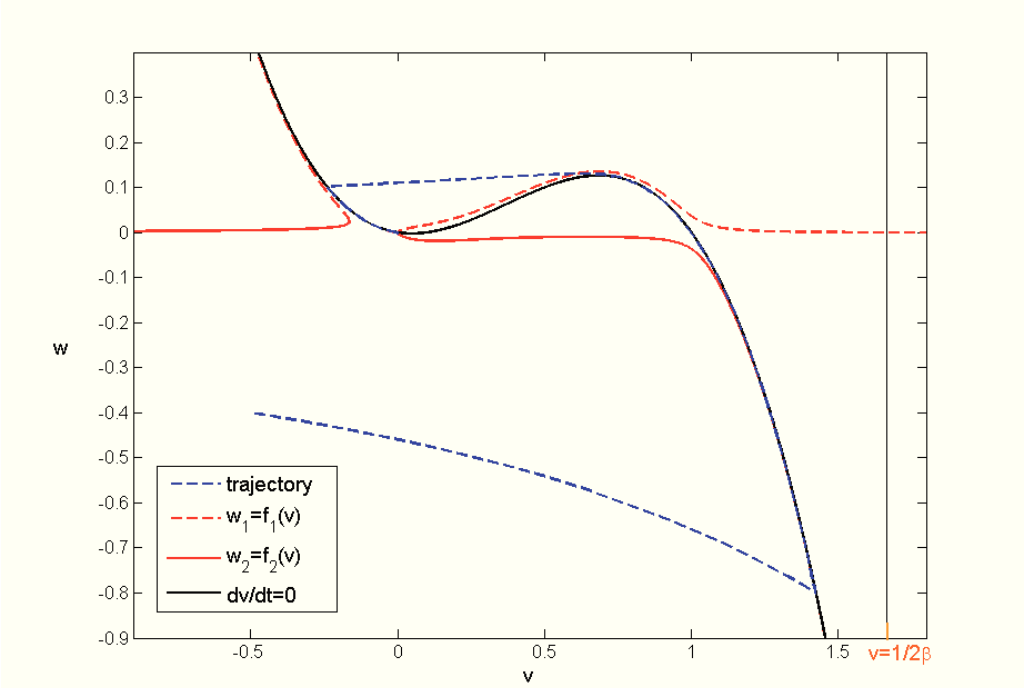

Figure 3.21: Phase plane of (3.48) with $\alpha = 0.1$, $\epsilon_0 = 10^{-3}$, $\gamma = 0.5$ and $\beta = 0.3$.

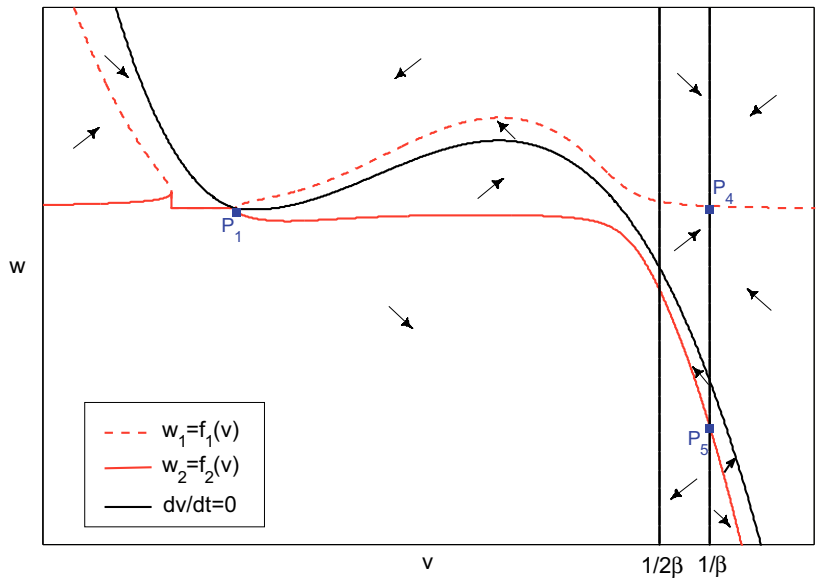

Figure 3.22: Schematic description of the vector field of (3.48).

$\mathrm{d}w/\mathrm{d}t = v - \gamma w$, that equals the second equation in (3.13).

Furthermore, if $\gamma < \gamma_{\mathrm{cr},1}$, the origin only survives as a steady state, and, since the Jacobian matrix of (3.48), evaluated in $P_{\mathrm{eq},1}$, is equivalent to $(3.14)|_{(0,0)}$, $P_{\mathrm{eq},1}$ is a nodal sink.

$P_{\mathrm{eq},4-5}$ are the intersections between $v = 1/\beta$ and the w-nullclines (see Fig. 3.22). The vector field around the equilibrium configurations in $P_{\mathrm{eq},4-5}$ suggests that $P_{\mathrm{eq},4}$ may correspond to a stable configuration, while $P_{\mathrm{eq},5}$ to an unstable equilibrium.

However this two equilibria become meaningless once realized that, before reaching the value $v = 1/\beta$, the solution intersects the critical region $v = v_{\mathrm{cr}}$, and, as we already commented, is prevented from moving toward the value $v = 1/\beta$.

In conclusion we can state that, if $\gamma < \gamma_{\mathrm{cr},1}$, a solution of (3.48) (blue dashed line in Fig. 3.21) qualitatively performs the same behavior showed for the model (3.13). After an external shock that moves the orbit out from the equilibrium state in the origin, the trajectory hangs the right branch of the v nullcline until it is possible, then it moves on the left region and approaches the steady state following the stable branch of the fast nullcline.

For this reason, in the next chapters, we will analyze equations (3.48) neglecting the behavior of the trajectories for $v \geq 1/2\beta$. Indeed our aim is to study the amplitude of the oscillations of the potential before the resting state is achieved, then we should admit the system has only one stable equilibrium point, $P_{\mathrm{eq},1}$, and the potential assumes values less than v_{cr}. That is, for our purposes we consider that models (3.13) and (3.48) perform similar behaviors in the phase plane.

3.3.1 The Aliev-Panfilov model

In 1996 Aliev and Panfilov [25] proposed a refinement of the FitzHugh-Nagumo scheme, with the purpose of reproducing more precisely the shape of the cardiac action potential. More precisely, they succeed in mimicking the plateau phase of the cardiac action potential - a feature which is absent in the FitzHugh-Nagumo model. To this aim they calibrated the constitutive parameters of the model by fitting the simulated restitution curve to that experimentally developed and by considering again the dependence of some physiological parameters from the variables of the system.

They propose the following equations

$$\begin{aligned} \frac{\mathrm{d}v}{\mathrm{d}t} &= -kv(v-1)(v-\alpha) - vw \\ \frac{\mathrm{d}w}{\mathrm{d}t} &= \varepsilon(v,w)(-w - kv(v-\alpha-1)) \end{aligned} \tag{3.49}$$

where

$$\varepsilon(v,w) = \varepsilon_0 + \frac{\mu_1 w}{v+\mu_2},$$

k controls the magnitude of the transmembrane current, and μ_1 and μ_2 are computed in order to approximate as well as possible the shape of the action potential.

In particular, following a result by Elharrar and Surawicz [48], they approximated the shape of the restitution curve by the formula

$$\text{APD} = \frac{\text{CL}}{\text{a CL} + \text{b}}$$

where APD is the duration of the action potential, defined as the time interval in which the voltage remains above the activation threshold (v_{thr}) [49], and CL denotes the cycle length, that is the sum of APD and diastolic interval. a and b are coefficients adjusted to reproduce as well as possible the experimental action potential.

With this formula, Aliev and Panfilov computed different restitution curves for different values of μ_1 and μ_2, and they detected the best approximation with the values $\mu_1 = 0.2$ and $\mu_2 = 0.3$.

The nullclines of system (3.49), shown in Fig. 3.23, are respectively:

$$\begin{array}{lll} v = 0 \qquad w = k(-v^2 + v(1+\alpha) - a) & \Rightarrow & \mathrm{d}v/\mathrm{d}t = 0 \\ w = k(-v^2 + v(\alpha+1)) \qquad w = -\varepsilon_0/\mu_1(\mu_2 + v) & \Rightarrow & \mathrm{d}w/\mathrm{d}t = 0. \end{array}$$

Then the equilibrium points are:

$$\begin{array}{c} P_{\text{eq},1} = (0,0) \quad P_{\text{eq},2} = (0, -\varepsilon_0 \dfrac{\mu_2}{\mu_1}) \\ P_{\text{eq},3-4} = \dfrac{k\zeta \mp \sqrt{k^2\zeta^2 - 4k(k\alpha + \varepsilon_0\mu_2/\mu_1)}}{2k} \end{array} \tag{3.50}$$

where $\zeta = 1 + \alpha + \varepsilon_0/\mu_1$.

With the values of the parameters specified in [25], i.e. $k = 8$, $\alpha = 0.15$, $\varepsilon_0 = 0.002$, the equilibrium configurations in (3.50) are respectively a nodal sink, a saddle point, a nodal source and a saddle point.

Note that, again, there exists a critical value for the potential corresponding to a singularity of the system (dotted line in Fig. 3.23) such that, for finite values of w, if $v = -\mu_2$, $\mathrm{d}w/\mathrm{d}t \to \infty$. Nevertheless we will see next that action potentials starting with a positive value of v do never approach this value, as they are not allowed to change sign.

Looking at the vector field depicted in Fig. 3.23, we can deduce the behavior of the solutions starting from different initial points. Consider the

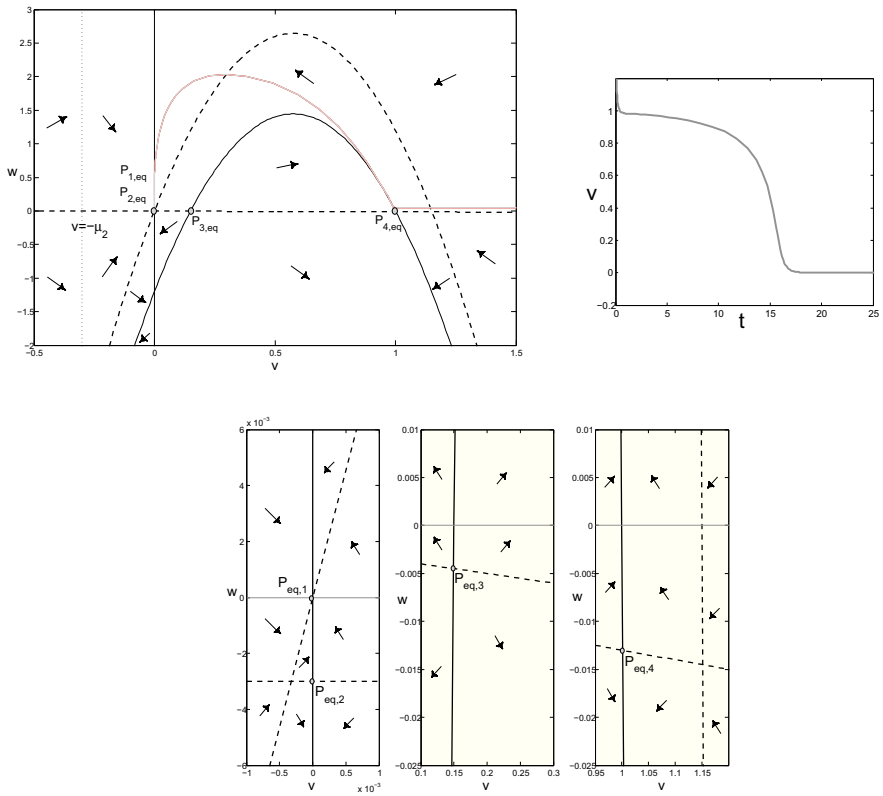

Figure 3.23: Top left: Nullclines and vector field of the dynamical system (3.49). The dashed lines are the w-nullclines, while the continuous lines are the v-nullclines. Top right: Example of a v-trajectory exhibiting the characteristic plateau phase. Bottom: Enlargement of the phase plane in correspondence of the equilibrium points.

region enclosed by the dashed parabola, with $w < -\varepsilon_0 \frac{v+\mu_2}{\mu_1}$ and $v > -\mu_2$. The orbits starting in this region evolve with $\mathrm{d}w/\mathrm{d}t < 0$ and moves towards infinity for $w \to -\infty$. Then again trajectories starting with $w < -\varepsilon_0 \frac{v+\mu_2}{\mu_1}$ and $v > -\mu_2$ and in the region out of the dashed parabola, tend to $-\infty$ for $w \to -\infty$, provided $w < -\varepsilon_0 \frac{v+\mu_2}{\mu_1}$ for all $t > 0$, even if initially they grow with $\mathrm{d}w/\mathrm{d}t > 0$.

On the other hand, for $w > -\varepsilon_0 \frac{v+\mu_2}{\mu_1}$ and $v > -\mu_2$, solutions are all attracted by the spiral sink at the origin. In particular, if the initial point is such that $-\varepsilon_0 \frac{v+\mu_2}{\mu_1} < w_0 < k(-v^2 + v(1+a) - a)$, then the corresponding trajectory reaches the decreasing branch of the nullcline $w = k(-v^2 + v(1+a) - a)$ (continuous parabola), hangs on it following the vector field until the turning point is attained, then it reaches the other fast nullcline $v = 0$ and eventually approaches the sink in $P_{\mathrm{eq},1}$ as $t \to \infty$.

If (v_0, w_0) is such that $w_0 > k(-v^2 + v(1+a) - a)$ and $v_0 > 0$, since $\mathrm{d}v/\mathrm{d}t < 0$ the solution may join the parabola $w = k(-v^2 + v(1+a) - a)$ and then behave as described before, or, if it does not cross the fast nullcline, it may directly achieve the value $v = 0$ and consequently reach the equilibrium state.

When $-\mu_2 < v_0 < 0$ and $w_0 > k(-v^2 + v(1+a) - a)$, orbits evolve with $\mathrm{d}v/\mathrm{d}t > 0$ towards the $w-$axis and ends at the origin for $t \to \infty$.

Finally, if a solution starts on the left of the line $v = -\mu_2$, it diverges to $\pm\infty$ depending on whether $w \gtrless -\varepsilon_0 \frac{v+\mu_2}{\mu_1}$.

By noting that the vertical axis $v = 0$ is itself a trajectory, we easily infer that the potential v is not allowed to change its sign during an action potential, since the $w-$axis can not be intersected by other trajectories. A clear consequence of this observation is that a solution starting with a positive v_0 does never reach the singular value $v = -\mu_2$.

In conclusion, since our goal is to examine oscillations of the potential around the rest state, we must allow the potential to be negative, then we should exclude system (3.49) from our analysis.

3.3.2 Choices for $\varepsilon(v)$

The dynamical systems examined in the previous section are paradigmatic examples that prove the aptitude of some generalized FitzHugh-Nagumo type models for reproducing in a more realistic way the physiological mechanisms underlying the cardiac action potential. These models make use of the dependence on v of the constitutive parameter ε to account, in a very simple way, for the electro-mechanical coupling. In the Aliev-Panfilov model the relation defining this dependence has been driven by a physical request, while

in the other case an analytical procedure has led to a functional relation for $\varepsilon(v)$. However in both models the parameter ε is inversely proportional to v, then it decreases as the potential grows (Fig. 3.24).

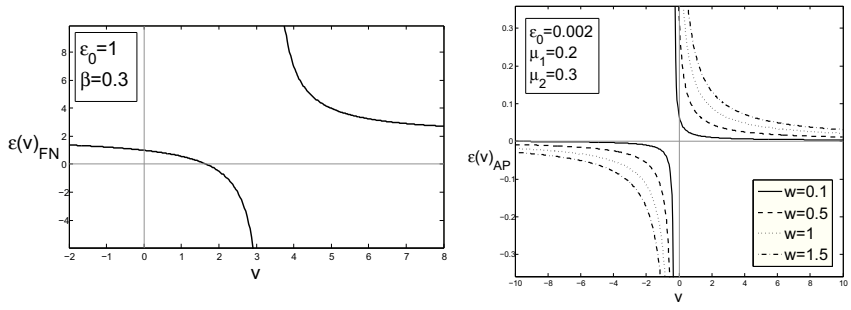

(a) (b)

Figure 3.24: Plot of $\varepsilon(v)$ in (3.48) and in (3.49). Negative values of $\varepsilon(v)$ are accounted for the sake of clarity.

As we have already noted, ε represents a time parameter for the model and expresses the ratio between the fast and slow dynamics of the two variables. ε makes explicit that the evolution of the action potential happens on two timescales: the fast dynamics of the membrane potential and the slow adaption current.

The rapid phases of the action potential have to be correlated to the voltage-gated Na^+ channels that open rapidly during membrane depolarization, while voltage-gated K^+ channels generate the recovery flow responsible for the action potential repolarization [14]. Two types of K^+ currents are involved in the cardiac action potential: the transient outward K^+ currents that cause the early rapid repolarization (phase 1 in section 1.5) and the delayed rectifying K^+ currents determining the return to the diastolic potential (phase 3 in section 1.5).

On the basis of these observations, in order to understand if the relations for $\varepsilon(v)$ in (3.48) and (3.49) are physiologically reasonable, we have compared them with the time constants evolution of the fast and slow membrane currents.

The results of such a research are discussed in the following.

Figure 3.25 shows the time constants of the fast Na^+ currents (τ_m) and of the delayed rectifier and transient outward K^+ currents (τ_{ua} and τ_{oa}) presented in [50]. Ramirez, Courtemanche and Nattel used the Luo-Rudy formulation for the ions currents and the representation of the model parameters is compared with experimental data proving that the theoretical outcomes

approximatively fit the empirical measures.

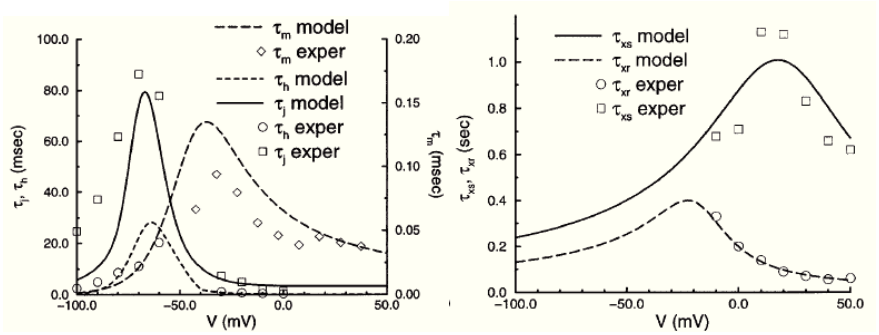

(a) (b)

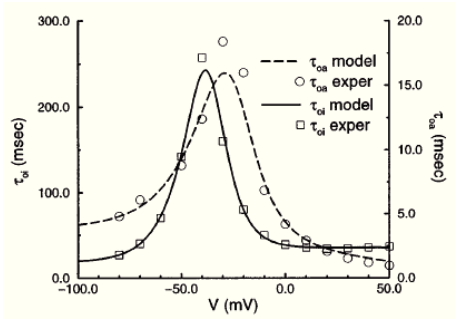

(c)

Figure 3.25: (a) Gating variable time constants of the fast Na^+ currents as a function of the potential. τ_m is the activation timescale, τ_h corresponds to the fast inactivation and τ_j to the slow inactivation. (b) Gating variable time constants of the delayed rectifier K^+ currents as a function of the potential. τ_{xs} is the slow current time constant while τ_{xr} models the rapid current. (c) Gating variable time constants of the transient outward K^+ currents as a function of the potential. τ_{oa} and τ_{oi} are the activation and inactivation timescales respectively (from [50]).

We observe that, at least for positive values of the potential, both the experimental traces (depicted in Fig. 3.25 with symbols $\diamond$, $\circ$ and $\square$) and the model curves reflect the decreasing evolution of $\varepsilon(v)$ with the increase of v. The mismatch between the graph in Fig. 3.25 and 3.24 for negative values of the potential may be ascribed to the dimensionless setting of the FitzHugh-Nagumo model, that causes the resting potential to be 0 unlike the physiological value is about -85 mV.

Similar plots are shown in Fig. 3.26 from [51], where the decreasing behavior of the time constants is more evident in the plots 3.26(a) and 3.26(c). Indeed the experimental data shown here follow quite faithfully the hyperbolic behavior of $\varepsilon(v)$ in Fig. 3.24.

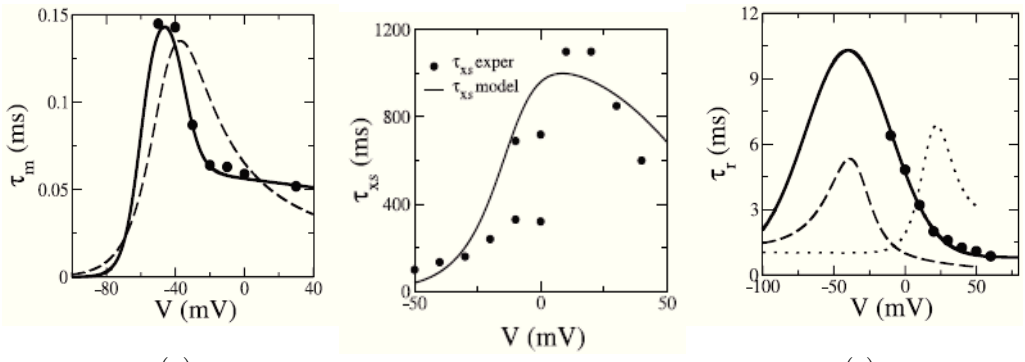

(a) (b) (c)

Figure 3.26: (a) Activation time constant of Na^+ currents. The solid line is the simulation by Tusscher et al. while the dashed line derives from the Luo-Rudy model. Symbols • denote the experimental data. (b) Activation time constant of the slow delayed rectifier current. (c) Activation time constants of the transient outward current. The solid line describes the model parameters of Tusscher et al., the dashed curve reports the simulations in [50] and the dotted line derives from the model by Priebe and Beuckelman (from [51]).

In the final analysis, we mention a simple assumption made in [52] which may summarize all the comparisons made up to now. Keldermann, Nash and Panfilov refer to a reaction-diffusion mechanics system based on the Aliev-Panfilov model where the ratio between the time scale of the activation and the recovery process is defined as

$$\varepsilon(v) = \begin{cases} 1 & \text{for } v < 0.05 \\ 0.1 & \text{for } v \geq 0.05. \end{cases} \tag{3.51}$$

Such a discontinuous function clarifies the net reduction of the time scale parameter after a fixed value of the potential near the resting state. Then the feature evidenced by (3.51) could be interpreted as follows: small values of the transmembrane potential do not affect the dynamics of the two variables but there exists a small interval for v where the ratio between the time scales of the evolution of v and w undergo a large decrease, then settling itself to a new small value. In other words, there exists a range for the potential v where the time scales of the two evolution variables are remarkably different, thus

highlighting the slow and the fast processes that determine the occurrence of the action potential.

Chapter 4

Mathematical modeling of DAD

4.1 Introduction

This chapter is devoted to the main topic of this Thesis, that is the possibility of modeling DAD occurrence in the framework of extended FitzHugh-Nagumo models. It is our goal to merge the simple structure of the FitzHugh-Nagumo type model, described in the previous chapters, with the characterization of the DAD phenomenon for the cardiac action potential presented in chapter 2.

We associate the occurrence of DAD with the existence of particular solutions of the dynamical systems, that we will call *spike solutions*. These particular orbits essentially perform a certain number of finite-amplitude oscillations (spikes) around the equilibrium configuration and then approach the resting state. Our analysis will focus on the first spike after the main upstroke, because it reasonably simulates a delayed after depolarization. Indeed, on the one side, if it triggers DAD, the subsequent evolution is to be modified to account for the effects of the new heartbeat. On the other hand, if the primary spike is not strong enough to induce DAD, neither will be the following spikes, which have lower intensity than the first in order to allow the trajectory to approach the stable equilibrium configuration.

Moreover an interesting challenge will be the tuning of DAD amplitude that best simulates a suprathreshold depolarization and may trigger a secondary action potential.

The starting point of this study is the paper by Tonnelier [53], where the spike solutions for a piecewise-linear FitzHugh-Nagumo model were introduced. Since in the piecewise-linear approximation the motion equations

may be integrated analytically, Tonnelier performed some analytical computations to find conditions on the parameters of the model for the appearance of a spike in the solution.

We derived from this article the definition of spike solution, then we focused on the non linear system (3.13) reproducing similar investigations. Namely we look for requirements on the constitutive parameters that allow the characterization of the occurrence of DAD in the model. Obviously our analysis is substantially a numerical study, since we examine a nonlinear dynamical model.

Afterwards, in order to improve the representation of the cardiac potential, we amplified the research by studying spike solutions in generalized models, and more precisely for the dynamical system (3.48).

4.2 A piecewise-linear approximation to the FitzHugh-Nagumo model

In [53] the following piecewise linear system is analyzed:

$$\begin{aligned} \frac{\mathrm{d}v}{\mathrm{d}t} &= -\lambda v + \mu h(v-a) - w + I_{\mathrm{appl}} \\ \frac{\mathrm{d}w}{\mathrm{d}t} &= bv \end{aligned} \tag{4.1}$$

where h is the Heaviside step function, and the constitutive parameters satisfy the following requirements: $\lambda > 0$, $\mu > 0$, $a > 0$, $b > 0$ and $\mu > \lambda a$.

It should be observed that in (4.1) $\varepsilon = 1$ and $\gamma = 0$. However the role of ε is carried out by b, because if $b \ll 1$ the time scale of the equations differs and v assumes a fast dynamic while w becomes the slow variable. The vanishing of the parameter γ is a simplification that allows the analysis of the excitable regime only, neglecting all other possible equilibrium states.

Figure 4.1 shows the phase plane portait of (4.1): the w-nullcline coincides with the $v-$axis and the v-nullcline has a cubic-like shape, due to the restriction $\mu > \lambda a$.

The only equilibrium point is the origin and it is locally stable if $g'(0)$ is negative, where $g(v) = -\lambda v + \mu h(v-a)$. In fact, since the Jacobian matrix of (4.1) evaluated at the origin is

$$J = \begin{bmatrix} g'(0) & -1 \\ b & 0 \end{bmatrix},$$

the fixed point is stable if and only if $g'(0) < 0$. Then, since the distributional derivative of $g(v)$ is $-\lambda$ for $v \lessgtr a$ and $\mu\delta(a)$ for $v = a$, if $\lambda > 0$, the origin is a stable sink.

In this case, after an initial input for which the potential crosses the line $[-\lambda a, -\lambda a + \mu]$, the solution (plotted in Fig. 4.1 (a) with a black continuous line) returns to the equilibrium state, completing the action potential, as shown in Fig. 4.1 (b).

Owing to the direction of the vector field, the segment $[-\lambda a, -\lambda a + \mu]$ can be intersected only in the extreme points.

A *spike solution* for system (4.1) is defined as an orbit which, while evolving towards the origin, performs a finite number of spikes N_{sp}. A spike is defined as the number of times that a solution crosses a fixed, positive threshold with positive left time-derivative $\dot{v}^-$. In [53] this threshold is set to be $v_{\text{thr}} = a$ which is the minimum point of the cubic-like nullcline. Therefore whenever $(v(t), w(t))$ crosses the line $v = a$ with $-\infty < w(t) \leq 0$, an additional spike is counted. Moreover, the count of N_{sp} includes also the initial condition if $v(t_0) = v_0 > v_{\text{thr}}$, in order to take into account the perturbation necessary to drive the system to v_0 from the neighborhood of the stable equilibrium configuration.

Tonnelier analytically proved the following results.

Proposition 2. [53] For $\lambda^2 > 4b$, there exists a spike solution when $a < v_0 < \frac{\mu}{\lambda}$. This solution only presents a single spike.

This is the case shown in Fig. 4.1: the only spike is due to the initial pulse $(v_0, 0)$ ($w_0 = 0$ is considered in order to simplify the study).

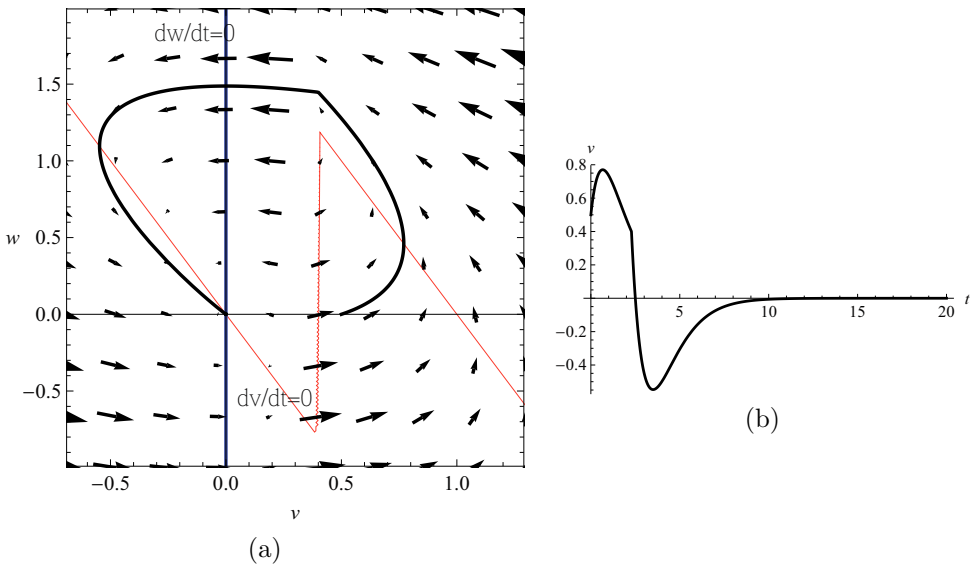

Figure 4.1: (a) Phase portrait of system (4.1) with $\lambda = 2$, $\mu = 2$, $a = 0.4$ and $b = 0.5$. (b) Plot of the potential versus time.

Proposition 3. [53] For $\lambda^2 < 4b$, the spike solution of system (4.1) is able to present more than one action potentials.

A two-spike solution is depicted in Fig. 4.2. The plot on the left evidences the occurrence of a spontaneous action potential caused by the exceeding of the threshold $v = a$.

4.3 Spike solutions in the classical FitzHugh-Nagumo model

In this section we apply the definition of spike solution to the FitzHugh-Nagumo dynamical system (3.13), and we will study how N_{sp} depends on the constitutive parameters. As we have said above, given the non-linearity of the problem, our results mainly arise from the numerical integration of the FitzHugh-Nagumo motion equations corresponding to particular initial conditions. All the results presented in this section have been published in [54].

In order to shorten the presentation we here assume $v_{\text{thr}} > 0$, $I_{\text{appl}} = 0$ and $\gamma < \gamma_{\text{cr},1}$, so that there exists a unique equilibrium configuration $(v_{\text{eq}}, w_{\text{eq}}) = (0, 0)$, corresponding to a spiral sink.

Definition 1. ([54]) Let $(v(t), w(t))$ be a solution of the dynamical system

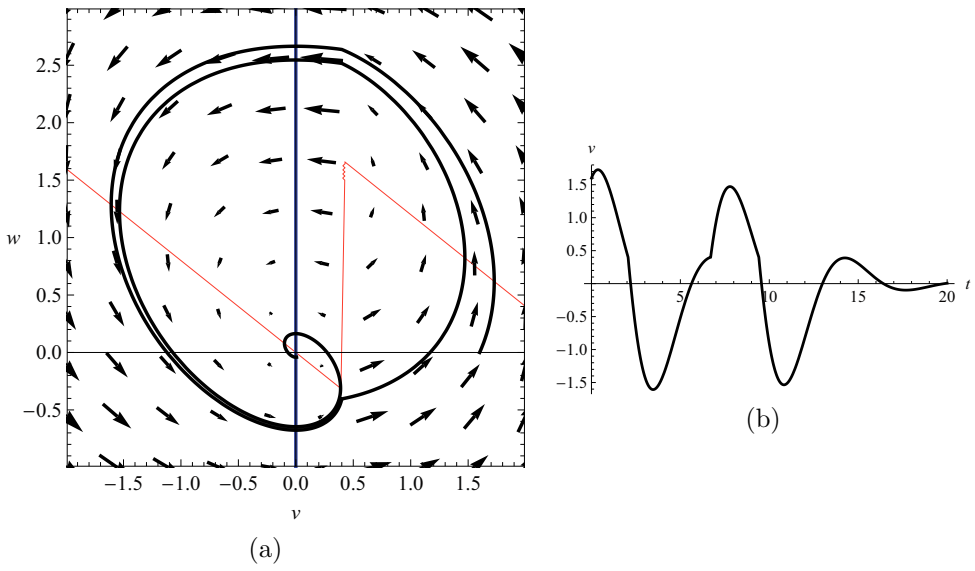

Figure 4.2: (a) Phase portrait of system (4.1) with $\lambda = 0.8$, $\mu = 2$, $a = 0.4$, $b = 1$ and $(v_0, w_0) = (1.6, 0)$. (b) Plot of the potential versus time.

(3.13) which satisfies the initial condition $(v(0), w(0)) = (v_0, w_0)$, and converges towards a stable equilibrium configuration, that is, such that

$$\lim_{t\to\infty} (v(t), w(t)) = (v_{\rm eq}, w_{\rm eq}).$$

We define number of spikes of such solution the integer number of solutions of the equation $v(t) = v_{\rm thr}$ with $t > 0$ and $\dot{v} > 0$, with the prescription that $N_{\rm sp}$ is to be augmented by 1 whenever $v_0 > v_{\rm thr}$.

Since the functions on the right-hand side of the motion equations are continuous functions, $\dot{v}^+ = \dot{v}^-$ so that in the previous definition we have not specified the nature of the derivative.

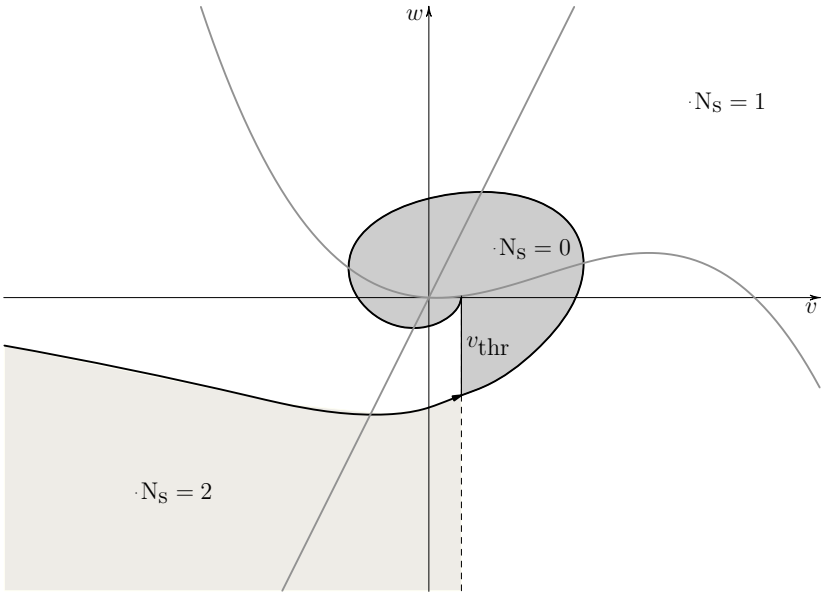

Figure 4.3: Representation of the separatrix $(\tilde{v}(t), \tilde{w}(t))$ starting from $(v_{\rm thr}, f(v_{\rm thr}))$ and computed backwards in time.

The strategy we follow to study the occurrence of spike solutions for (3.13) is based on the selection in the phase plane of a particular orbit which acts as a separatrix for the characterization of $N_{\rm sp}$. It is the trajectory $(\tilde{v}(t), \tilde{w}(t))$ such that $(v_0, w_0) = (v_{\rm thr}, f(v_{\rm thr}))$ (Fig. 4.3).

Such a solution performs only one spike for $t > 0$, which corresponds to the initial condition $v(0) = v_0 = v_{\rm thr}$, because for any $t > 0$ the equation $\tilde{v}(t) = v_{\rm thr}$ has no solution. This statement can be easily proved by contradiction. In fact let us observe that, since the initial point of the separatrix belongs to the v-nullcline and being $v_{\rm thr} > 0$ (which implies $\tilde{w}(0) < \tilde{v}(0)/\gamma$),

the following relations hold

$$\dot{\tilde{v}}(0) = 0 \qquad \dot{\tilde{w}}(0) > 0. \tag{4.2}$$

Then for a positive and sufficiently small t, the second of (4.2) yields $\tilde{w}(t) > \tilde{w}(0)$, which, in turn, implies $\dot{v}(t) < 0$. In other words, the trajectory initially moves in the half-plane $\tilde{v}(t) < v_{\text{thr}}$ (Fig. 4.4).

If we assume that $(\tilde{v}(t), \tilde{w}(t))$ should cross the threshold once more for $t > 0$, it must intersect the curve $(v, f(v))$ for some $v < 0$ (point P_1 in Fig. 4.4) and then it could cross $v = v_{\text{thr}}$ at some $w < f(v_{\text{thr}})$ (point P_2 in Fig. 4.4). Indeed we must notice that, due to the vector field direction

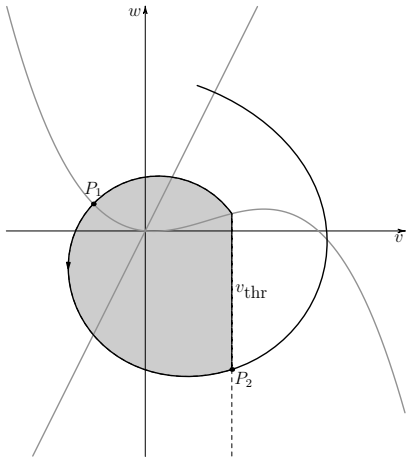

Figure 4.4: Hypothetic behavior of the trajectory $(\tilde{v}(t), \tilde{w}(t))$ exploited to prove by contradiction the one-spike property of the separatrix when $t > 0$.

sketched in Fig. 3.9, if at time $\hat{t}$ a generic solution $(v(t), w(t))$ crosses the line $v = v_{\text{thr}}$ with $\dot{v}(\hat{t}) > 0$, then $w(\hat{t}) < f(v_{\text{thr}})$.

After the crossing point P_2, the trajectory, by definition 1, should evolve toward the equilibrium configuration as $t \to \infty$. It means that it must enter the grey region evidenced in Fig. 4.4 which contains the equilibrium point, so that the solution is forced to cross itself.

This is an impossible circumstance that derives from the uniqueness of the solution for a dynamical system.

In conclusion, we have proved that the separatrix $(\tilde{v}(t), \tilde{w}(t))$ is a one-spike solution of (3.13) for $t > 0$.

From the same property of the impossible self-crossing of the trajectories, we can derive the peculiar feature of the separatrix, namely the partition of the phase plane determined every time that it intersects the threshold line $v = v_{\text{thr}}$ with $w < f(v_{\text{thr}})$ for $t < 0$.

Such partition is evidenced in Fig. 4.3 with the domains painted in different grey tones. Each domain is characterized by a specific value of $N_{\rm sp}$, meaning that a solution starting from a point in one domain, carries out a number of spikes equal to $N_{\rm sp}$ associated with that domain.

4.3.1 Spike solutions with a variable threshold

Initially, and in order to follow the threshold choice in [53], we have studied the case $v_{\rm thr} = v_{\rm min}$, where $v_{\rm min}$ is the value of the potential at which the cubic function $f(v)$ attains a relative minimum,

$$v_{\rm min} = \frac{1 + \alpha - \sqrt{1 + \alpha^2 - \alpha}}{3}. \tag{4.3}$$

The chosen value depends on the parameter α, which, as we have already observed, contains information on the threshold for the depolarization needed to generate the potential upstroke. Then, from a conceptual point of view, this seems the best choice for $v_{\rm thr}$, as it is related to the intrinsic potential threshold of the model.

However we will prove by numerical simulations that $v_{\rm min}$ is not a good value for the definition of spike solutions, because it generates non physiologically reasonable results. As a consequence, we will choose below a specific value for $v_{\rm thr}$, independent of any physiological parameter.

The numerical analysis developed in this section focuses on the study of the negative-time behavior of the separatrix $(\tilde{v}(t), \tilde{w}(t))$, such that $(\tilde{v}_0, \tilde{w}_0) = (v_{\rm min}, f(v_{\rm min}))$, by varying the constitutive parameters in their physiological range. For each simulation, our aim is to keep track of the number of intersections of the trajectory, integrated backward in time, with the threshold half-line $(v_{\rm min}, w)$, with $w < f(v_{\rm min})$.

We remind that, for $t > 0$ and for any values of the parameters, the separatrix has only one spike (occurring at the initial time).

In a very first simulation, we have computed, for a fixed value of γ, the values of ε and α for which there exist trajectories with $N_{\rm sp} \geq 2$. The results are illustrated in Fig. 4.5 and are to be interpreted as follows.

Let $\alpha_{\rm cr}(\bar{\varepsilon}, \bar{\gamma})$ (for $\bar{\gamma} = 0.5, 0.6, 0.8$) be the abscissa of the point belonging to the curve associated with $\bar{\gamma}$, having $\bar{\varepsilon}$ as y-coordinate. Then, there exist trajectories in the phase plane, with $N_{\rm sp} \geq 2$, for $\gamma = \bar{\gamma}$ and $\varepsilon = \bar{\varepsilon}$, if and only if $\alpha < \alpha_{\rm cr}(\bar{\varepsilon}, \bar{\gamma})$. The plot evidences that, if α is large enough, only no-spikes or single-spike trajectories exist.

Indeed, if we let $\alpha_{\rm max}(\bar{\gamma})$ be the maximum value of $\alpha_{\rm cr}(\varepsilon, \bar{\gamma})$ for the curve corresponding to $\bar{\gamma}$, then, for any $\alpha \geq \alpha_{\rm max}(\bar{\gamma})$, the separatrix is a one-spike solution $\forall t$, then only solutions with $N_{\rm sp} \leq 1$ can be found.

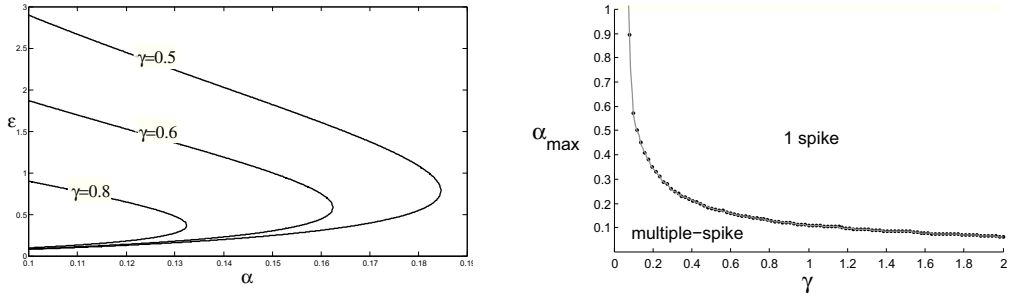

Figure 4.5: (a) Critical values of α and ε for the existence of multiple-spikes solutions when $\gamma = 0.5, 0.6, 0.8$. (b) Behavior of the function $\alpha_{\max}(\gamma)$ defined in the text.

Figure 4.5b illustrates how $\alpha_{\max}$ depends on γ (for γ in the physiological range of values): as γ increases, the maximum value of α, that ensures the existence of trajectories with $N_{\rm sp} \geq 2$, largely decreases. This result has not a clear physical confirmation, since γ is a fitting parameter.

Figure 4.6 reports the results of a similar study, in which however α is kept fixed and γ is allowed to vary.

Therefore let $(\gamma_{\rm cr}(\bar{\varepsilon}, \bar{\alpha}), \bar{\varepsilon})$ be a point belonging to the curve associated with $\alpha = \bar{\alpha}$ ($\bar{\alpha} = 0.1, 0.3, 0.5$). Then, there exist trajectories with $N_{\rm sp} \geq 2$, for $\alpha = \bar{\alpha}$ and $\varepsilon = \bar{\varepsilon}$, if and only if $\gamma < \gamma_{\rm cr}(\bar{\varepsilon}, \bar{\alpha})$. In this case, also, the plot evidences the existence of $\gamma_{\max}(\bar{\alpha})$ representing the maximum value of $\gamma_{\rm cr}(\varepsilon, \bar{\alpha})$ for the curve corresponding to $\bar{\alpha}$. For any $\gamma \geq \gamma_{\max}(\bar{\alpha})$, only solutions with $N_{\rm sp} \leq 1$ can be found.

A noteworthy difference emerges when comparing Figs. 4.5 and 4.6. Indeed, from Fig. 4.6 we deduce that, for any α, multiple-spikes solutions happen to exist even if ε is very large, provided γ is small enough. On the contrary, in Fig. 4.5, choosing $\alpha < \alpha_{\max}(\bar{\gamma})$, multiple-spikes solutions exist only for $\varepsilon_1(\alpha) < \varepsilon < \varepsilon_2(\alpha)$.

The previous analysis (and in particular Fig. 4.5) shows that decreasing the parameter α raises the probability of having solutions with two or more spikes. In addition, we can prove that, as critical values of α become smaller and smaller, solutions with higher-order spikes are involved, meaning that, if $\alpha \to 0$, orbits oscillate many times around the resting state.

This effect is illustrated in Fig. 4.7. Fixed $\alpha = 10^{-2}$ (a value ten times smaller than the typical physiological choice $\alpha = 10^{-1}$), we have studied the ondet of regions with multiple spikes by varying γ and ε. In this case, even for quite small values of ε (note the multiplying factor 10^{-3} in the y-axis)

and physiological values of γ, trajectories can perform up to five (and more) spikes.

From a physiological point of view, the onset of orbits with many spikes suggests that the depolarization exceeds the activation threshold many times consecutively. This is an un-physical phenomenon since, after a delayed after depolarization had overtaken the threshold, a triggered action potential occurs, then the following suprathreshold DADs can not happen.

In Fig. 4.8 we can see the separatrix $(\tilde{v}(t), \tilde{w}(t))$ when it performs many spikes. Moreover Fig. 4.9(a) shows, for each spike and for different values of

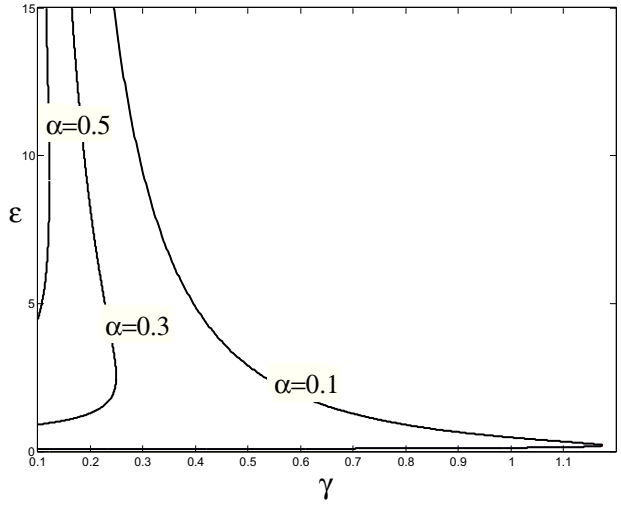

Figure 4.6: Critical values of γ and ε for the existence of multiple-spikes solutions when $\alpha = 0.1, 0.3, 0.5$.

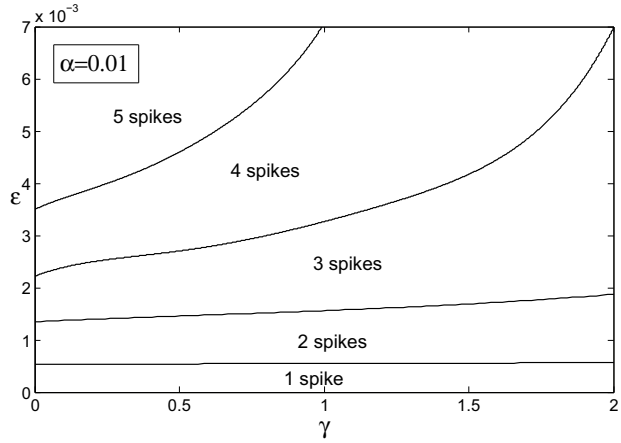

Figure 4.7: Occurrence of multiple-spike solutions when $\alpha = 10^{-2}$.

ε, the value of v of the intersection point between the separatrices (associated with each ε) and the v-nullcline which occurs after the spike (black points in Fig. 4.8). This value corresponds to the maximum value attained by the variable v. In Fig. 4.9(b) we have represented the value of w at which the trajectories cross the threshold v_{thr} (red points in Fig. 4.8). In both pictures different graphs correspond to trajectories exhibiting different numbers of spikes.

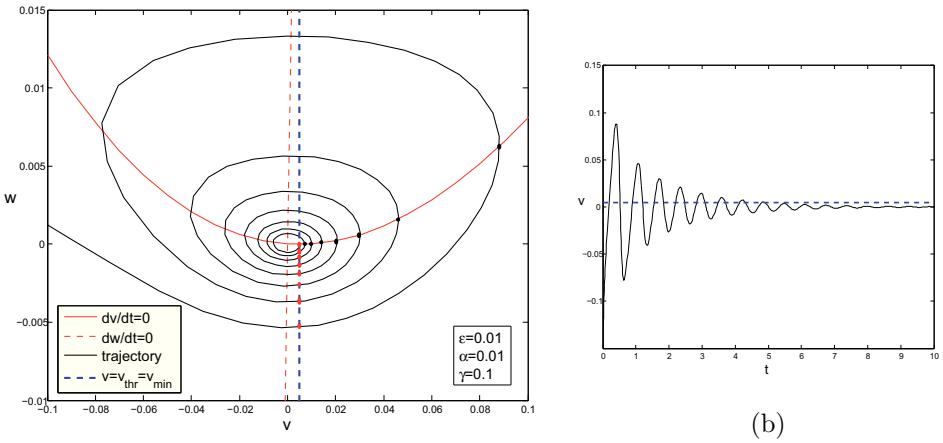

(a) (b)

Figure 4.8: Representation of the separatrix $((\tilde{v})(t), (\tilde{w})(t))$ when it performs many spikes for $t < 0$.

It clearly emerges from this analysis that the greatest values reached by both variables is much smaller than 1. This fact is a signal that pictures like the one in Fig. 4.8 clearly evidence. Figure 4.8 simply represents a zoomed view of the phase plane near the origin and the spikes performed by the solution are the small oscillations of the orbit near the equilibrium point, caused by the attraction of the spiral sink [55]. As a matter of fact, as we noticed in chapter 3, the equilibrium configuration is a spiral sink, which implies that the converging orbits perform an infinite number of turns about the equilibrium configuration. These turns may correspond to the spikes.

In support of this argument it should be noted that in most of the literature, the action potential simulated by non-dimensional models show the main upstroke amplitude of order of 1 [43, 25, 44, 56, 57]. In [57], for instance, Wedge studied the effects of changing in the parameters on the action potential and they concluded that the non-dimensional potential v ranges essentially from -1 to 1 during the upstroke, whatever the values of ϵ, α and γ. Analogous investigations for w confirm that the recovering variable also

ranges over the same interval as v, for any values of the physiological parameters.

Then, the behaviors shown in Fig. 4.8 and 4.9 do not involve the main depolarization wave of the cardiac action potential, so that they can not conveniently reproduce the onset of the secondary spike after the main action potential.

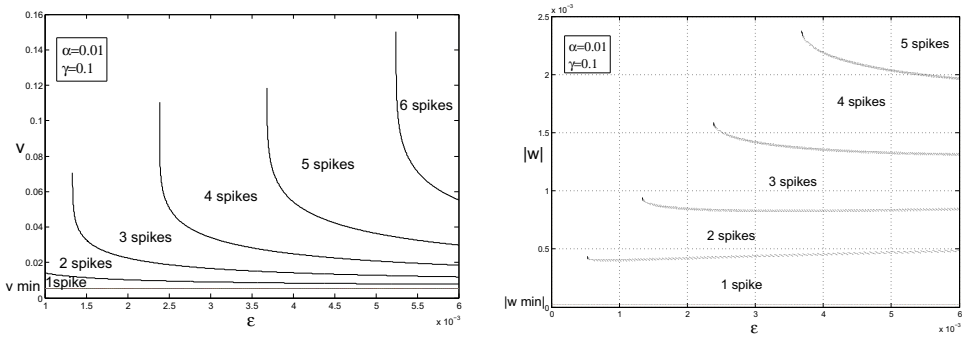

(a) (b)

Figure 4.9: (a) Values of the abscissa v of the intersection point between the orbit $((\tilde{v})(t), (\tilde{w})(t))$ and the v-nullcline which occurs after the spike. (b) Absolute value of the intersection point between $((\tilde{v})(t), (\tilde{w})(t))$ and the threshold v_{thr} for $-\infty < w \leq 0$.

This detailed investigation, that proves the odd behavior of the solutions under some circumstances, yields the conclusion that our choice of v_{thr} must be discussed in detail.

4.3.2 Spike solutions with a fixed threshold

Together with the results of the previous paragraph, to justify the need of a better choice for v_{thr}, we should observe that in the small-α limit, the threshold $v_{\text{thr}} = v_{\min}$ tends to 0, because from (4.3) we deduce that $v_{\min} = \frac{1}{2}\alpha + O(\alpha^2)$ when $\alpha \to 0$ (Fig. 4.10). Hence, as the threshold approaches the equilibrium point, multi-spikes solutions are more likely to occur since, as we have just noticed, near the resting state the solutions wrap themselves an infinity of times due do the spiral attraction of the origin. It is therefore evident that we need a more reliable description, which may be independent of the constitutive variables of the model.

According to this purpose, in the following we will consider that the threshold v_{thr} is set by an external factor. This represents also a more realistic choice, since the threshold needed to propagate an excitation depends on mechanical properties related to the contraction of the cardiac muscle, which are

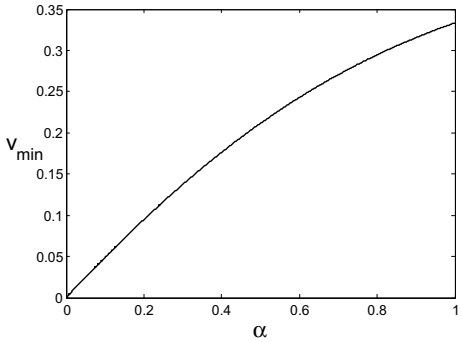

Figure 4.10: Representation of the function $v_{\min}(\alpha)$.

not represented among the constitutive parameters of the FitzHugh-Nagumo model. Indeed, the threshold needed is almost fixed in most of the literature.

Since the aim of this work is to simulate the DAD phenomenon, and in particular to detect suprathreshold DADs, which may trigger arrhythmic episodes, we are interesting in comparing the values of v_{thr}, defined in our analysis, with the depolarization threshold that causes the occurrence of a secondary action potential.

In the literature we found that the potential value necessary to trigger an action potential ranges over the interval $(-65, -60)$ mV. We mention [17] where v_{thr} is set to 65 mV, [18] where $v_{\text{thr}} = -62.9$ mV, [58] that estimates the interval $(-70, -60)$ mV and [52] where v_{thr} is approximately $-60mV$. Luo and Rudy [16] interestingly computed the threshold depolarization required to trigger a spontaneous action potential in terms of $[Ca^{2+}]$ in the sarcoplasmic reticulum.

With the above values for v_{thr}, we can infer that, since the whole amplitude of the upstroke is about 120 mV (from -80 mV to 40 mV), the potential value the DAD must exceed to generate an aftercontraction is about 1/8 of the magnitude of an action potential. Then, in a qualitative way, if we adapt this estimate to the normalized variables of the FitzHugh-Nagumo model, recalling that the adimensionalized potential v in (3.13) varies from 0 to about 1 during the upstroke [56], we can say that, if the secondary spike reaches the value of about 0.125 of the action potential magnitude, it may induce cardiac arrhythmia. In the next we will refer to this value as $v_{\text{thr,phy}}$.

We should underline, however, that the comparison between v_{thr} and $v_{\text{thr,phy}}$ represents only a qualitative test and is not sufficient to deduce the occurrence of a triggered action potential. Indeed system (3.13) does not model the propagation of the secondary spike and in particular it does not contain a tool that starts an action potential if the potential exceeds a fixed threshold. Nevertheless, we can certainly state that if the difference $|v_{\text{thr}} - v_{\text{thr,phy}}|$ is small enough, our model is reasonably realistic.

In the following analysis the values of the parameters α, γ and ε that ensure the onset of spike-solutions for system (3.13) are discussed.

Firstly, assuming that γ attains some fixed values and varying α and ε, we proved that there exists a critical value for α that restricts the possibility of having two-spikes solutions. These specific values are illustrated in Fig. 4.11 for different choices of v_{thr} and for different values of γ. Hence, when v_{thr} is fixed to some particular value, the corresponding $\alpha_{\text{cr}}(v_{\text{thr}}, \bar{\gamma})$, determined by the continuous line associated with $\bar{\gamma}$, is such that there exist multi-spike solutions for any value of $\alpha < \alpha_{\text{cr}}(v_{\text{thr}}, \bar{\gamma})$, while there are no multi-spike solutions (whatever the value of ε) if $\alpha \geq \alpha_{\text{cr}}(v_{\text{thr}}, \bar{\gamma})$.

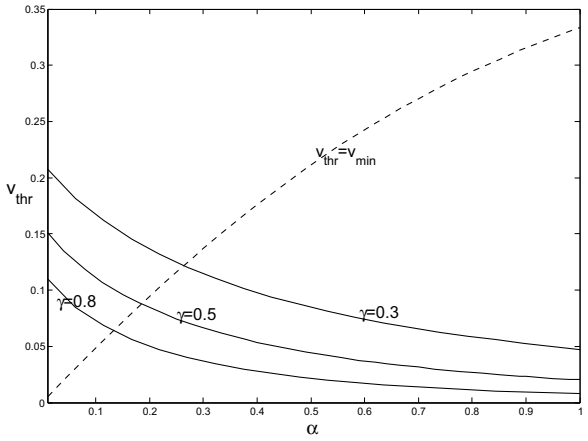

Figure 4.11: Critical values of α for the existence of multi-spikes solutions for different values of the potential threshold and for some values of γ.

Note that the value $v_{\text{thr}} = v_{\text{thr,phy}}$ can be attained, although not so easily.

The dashed line in Fig. 4.11 represents the threshold $v_{\text{thr}} = v_{\text{min}}$ for different values of α. It is worth comparing Fig. 4.11 with Fig. 4.5(a). In fact the intersection points between the continuous curves and the line $v = v_{\text{min}}$ in Fig. 4.11 correspond to the values $\alpha_{\text{max}}(\gamma)$ in Fig. 4.5.

This means that, for $\gamma = \bar{\gamma}$ and for $v_{\text{thr}} = v_{\text{min}}$, the critical value of α that determines the disappearance of multi-spike solutions is exactly the value $\alpha_{\text{max}}(\bar{\gamma})$ detected in Fig. 4.5.

Figure 4.12 shows a two-spike separatrix for $\gamma = 0.3$, $\alpha = 0.1$, $\varepsilon = 0.76$ and $v_0 = v_{\text{thr}} = 0.16$. The left plot represents the trajectory for $t < 0$, while the right graph describes the action potential performed by this solution. Conversely to what seen in Fig. 4.8, we can observe here that the variables v and w ranges over the appropriate interval detected in the literature.

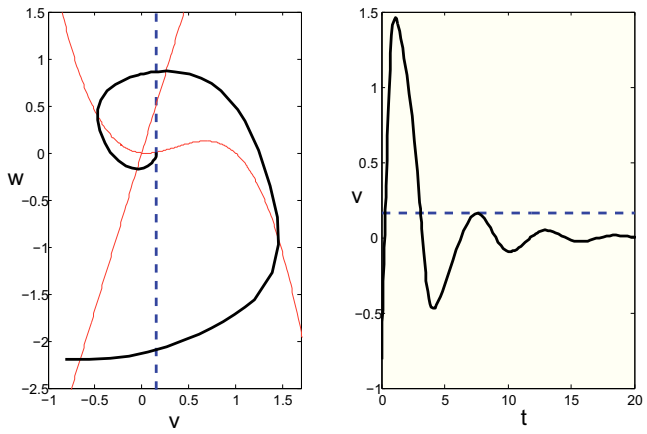

Figure 4.12: A two-spike separatrix in the phase plane and the corresponding action potential ($\gamma = 0.3$, $\alpha = 0.1$, $\varepsilon = 0.76$ and $v_0 = v_{\text{thr}} = 0.16$).

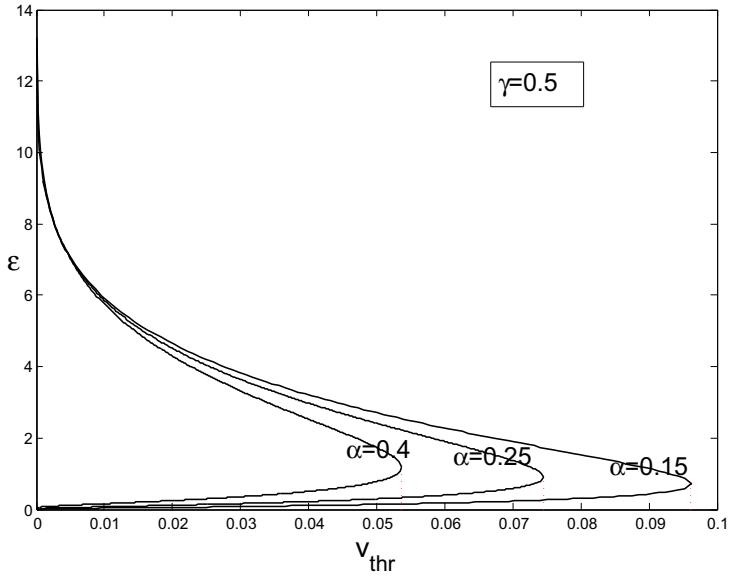

Figure 4.13: Range of values for ε for the existence of multi-spike solutions for different values of the potential threshold and for some values of α.

Furthermore, to complete the study, we found the values of ε that guarantee the occurrence of two-spike solutions, α and γ being fixed.

The results are shown in Fig. 4.13 when $\gamma = 0.5$. Setting $v_{\text{thr}} = \bar{v}_{\text{thr}}$, system (3.13) owns orbits with multiple spikes if and only if $\varepsilon_{\min}(\bar{v}_{\text{thr}}, \bar{\alpha}) < \varepsilon < \varepsilon_{\max}(\bar{v}_{\text{thr}}, \bar{\alpha})$, with $\bar{\alpha} = 0.15, 0.25, 0.4$. When v_{thr} is small enough the minimum admissible value of $\varepsilon(\bar{v}_{\text{thr}}, \bar{\alpha})$ is close to zero even if it maintains a finite value since an infinitesimal ε makes the trajectories approaching the origin almost horizontally. On the other hand, as $v_{\text{thr}} \to 0$ the maximum value of ε moves asymptotically to $+\infty$, meaning that a small extra-spike in the action potential is not affected by values of ε great enough.

It is clear from Fig. 4.13 that the choice of the potential threshold that determines the emergence of multi-spike solutions is bounded by a critical value $v_{\text{thr,cr}}$ (for a fixed α). Indeed, by setting $\alpha = \bar{\alpha}$, the existence of solutions with more than one spike is ensured by a potential threshold belonging to the interval $(0, v_{\text{thr,cr}}(\bar{\alpha}))$, identified by the red dashed line in Fig. 4.13.

In conclusion, as we could expect, the choice of v_{thr} is not completely free, but it is limited by some upper bound, which depends on the values of α and γ.

4.4 Spike-induced traveling pulses

The previous sections showed that an important property of the dynamical system (3.13) is to reproduce perturbations in the action potential that have reference to the delayed after-depolarization occurring in the cardiac action potential. The amplitude of these perturbations is a crucial feature, since, in dependence of its value, the DADs can be classified as suprathreshold or subthreshold. In the presence of a suprathreshold depolarization a spontaneous impulse can be activated, and the cardiomyocytes, which have not jet reached a relaxed state, may be re-excited.

In this section we are interested in studying the possible propagation of the DAD-triggered impulse. Indeed we would to analyze the conditions that cause the spike-induced action potential to generate a traveling wave that spreads into the whole cardiac tissue and may influence the heart contractions. This research requires the characterization of a spatial domain representing the cardiac texture through which the potential wave propagates. In particular we have to account for the dependence of the variables (v, w) from a spatial coordinate, so that the motions equations they must satisfy become spatially-dependent.

For the sake of simplicity, we will consider in the following the one-

dimensional extension of the FitzHugh-Nagumo equations,

$$\begin{aligned} \varepsilon \frac{\partial v}{\partial t} &= \frac{\partial^2 v}{\partial x^2} + v(1-v)(v-\alpha) - w \\ \frac{\mathrm{d}w}{\mathrm{d}t} &= v - \gamma w \end{aligned} \tag{4.4}$$

where we accounted for only the diffusion term (that involves the second derivative of v) and the diffusion coefficient is set to 1. Moreover the dynamics of the gating variable w is assumed to be independent from the spatial framework.

The study of traveling pulse solutions for the dynamical system (4.4) requires the close examination of two issues. First of all, if the model is refined with the description of the diffusion process for which the potential wave is transmitted form a cell to its neighbors, the occurrence of secondary oscillations in the signal evolution will obey quite different constraints than those studied for the spatial- independent model (3.13). Indeed the mechanisms of interaction between the myocytes generate a dispersion of the potential, and the force of the initial electric impulse will be reduced since, during its propagation, some energy is lost. For this reason we should expect that the existence of two-spike solutions will be verified for values of the constitutive parameters slightly different from those found in the previous analysis, and, more in general, the extra-spikes in the action potential will occur under more restrictive circumstance.

However, although the previous observation is to be considered, we will develop here the study with the parameter's range valid for (3.13), since the general structure of the results does not substantially change.

Secondly, for the existence of a traveling wave solution in the FitzHugh-Nagumo model some further conditions on the parameters must hold [34, 59, 60, 61, 62]. Therefore, it is obvious that, for our aims, the parameter requirements that allow for the onset of a traveling wave must be supplemented with the prescriptions on the constitutive parameters for having two-spike trajectories in the model. More precisely, we have to make sure that there exist values of the parameters for which the appearance of both a propagation pulse and a two-spike solution occur. This last question can be partially answered here. Indeed some interesting results from [34] can be easily adapted to our contest, as they prove some inequalities the parameters should satisfy for the propagation of traveling pulses.

Obviously, by presenting here the analysis suggested in [34] we can not be expected to exhaust the topic. It is our aim to simply support, with an easy argument, our perception that the dynamical system (3.13) can simulates

in a complete way the consequences of the DAD occurrence on the heart activity.

4.4.1 Traveling pulses in the FitzHugh-Nagumo model

To look for traveling pulse solutions, we introduce the coordinate $\xi = x + ct$, where c is the wave speed, and we rewrite the dynamical system (4.4) in the new frame of reference. Note that if $c > 0$ the wave moves form right to left, while if $c < 0$ it propagates in the other direction.

By replacing the dynamic variables $v(x,t)$ and $w(x,t)$ with $v = \varphi(x+ct)$ and $w = \psi(x+ct)$ in (4.4), we obtain a system of ordinary differential equations

$$\begin{aligned} \varepsilon c\varphi' &= \varphi'' + f(\varphi) - \psi \\ c\psi' &= \varphi - \gamma\psi \end{aligned} \tag{4.5}$$

where the apex denotes the derivative with respect to ξ and $f(\varphi) = \varphi(1-\varphi)(\varphi-\alpha)$.

According with the definition of traveling wave solution [32, 34, 59], we assume that

$$\lim_{|\xi|\to\infty} \varphi(\xi) = \lim_{|\xi|\to\infty} \varphi'(\xi) = \lim_{|\xi|\to\infty} \psi(\xi) = 0 \tag{4.6}$$

meaning that the pulse connects the same rest point because it starts and is completed at the steady state of the motion equations (which in the framework of our analysis is the origin). The condition on the derivative of ϕ underlines that the transition must happen in a smooth way.

Then, according to [34], if we assume that the functions φ and ψ are regular enough, we can multiply the first equation of (4.5) by φ and the second equation by ψ and we can integrate the resulting system with respect to the variable ξ from $-\infty$ to ∞. That is we can write

$$\begin{aligned} \varepsilon c \int_{-\infty}^{\infty} \varphi\varphi' \mathrm{d}\xi &= \int_{-\infty}^{\infty} \varphi\varphi'' \mathrm{d}\xi + \int_{-\infty}^{\infty} \varphi f(\varphi) \mathrm{d}\xi - \int_{-\infty}^{\infty} \varphi\psi \mathrm{d}\xi \\ c \int_{-\infty}^{\infty} \psi\psi' \mathrm{d}\xi &= \int_{-\infty}^{\infty} \psi\varphi \mathrm{d}\xi - \gamma \int_{-\infty}^{\infty} \psi^2 \mathrm{d}\xi. \end{aligned}$$

By noting that $\varphi\varphi' = 1/2(\varphi^2)'$ and $\psi\psi' = 1/2(\psi^2)'$, and by taking account for the hypothesis in (4.6) we integrate by parts and obtain

$$\int_{-\infty}^{\infty} \varphi f(\varphi) \mathrm{d}\xi = \int_{-\infty}^{\infty} (\varphi')^2 \mathrm{d}\xi + \int_{-\infty}^{\infty} \varphi\psi \mathrm{d}\xi \tag{4.7a}$$

$$\gamma \int_{-\infty}^{\infty} \psi^2 \mathrm{d}\xi = \int_{-\infty}^{\infty} \psi\varphi \mathrm{d}\xi. \tag{4.7b}$$

Analogously, if we multiply the first of (4.5) by φ' and the second by ψ' and we again integrate, we get

$$\begin{aligned}\varepsilon c\int_{-\infty}^{\infty}(\varphi')^2\mathrm{d}\xi &= \int_{-\infty}^{\infty}\varphi'\varphi''\mathrm{d}\xi+\int_{-\infty}^{\infty}\varphi' f(\varphi)\mathrm{d}\xi-\int_{-\infty}^{\infty}\varphi'\psi\mathrm{d}\xi\\ c\int_{-\infty}^{\infty}(\psi')^2\mathrm{d}\xi &= \int_{-\infty}^{\infty}\psi'\varphi\mathrm{d}\xi-\gamma\int_{-\infty}^{\infty}\psi'\psi\mathrm{d}\xi.\end{aligned}$$

Then, by observing that $\varphi'\varphi''=1/2(\varphi'^2)'$ and integrating by parts

$$\begin{aligned}\varepsilon c\int_{-\infty}^{\infty}(\varphi')^2\mathrm{d}\xi &= -\int_{-\infty}^{\infty}\varphi\frac{\mathrm{d}f(\varphi)}{\mathrm{d}\xi}\mathrm{d}\xi-\int_{-\infty}^{\infty}\varphi'\psi\mathrm{d}\xi\\ c\int_{-\infty}^{\infty}(\psi')^2\mathrm{d}\xi &= \int_{-\infty}^{\infty}\psi'\varphi\mathrm{d}\xi.\end{aligned}$$

The term $\int_{-\infty}^{\infty}\varphi\frac{\mathrm{d}f(\varphi)}{\mathrm{d}\xi}\mathrm{d}\xi$ can be developed as follows

$$\begin{aligned}&\int_{-\infty}^{\infty}\varphi\frac{\mathrm{d}f(\varphi)}{\mathrm{d}\xi}\mathrm{d}\xi=\int_{-\infty}^{\infty}(-3\varphi^3+2\varphi^2(1+\alpha)-\alpha\varphi)\varphi'\mathrm{d}\xi=\\ &\qquad(-3\varphi^3+2\varphi^2(1+\alpha)-\alpha\varphi)\varphi\mid_{-\infty}^{\infty}-\int_{-\infty}^{\infty}\varphi(-9\varphi^2+4\varphi(1+\alpha)-\alpha)=0,\end{aligned}$$

so that we have

$$\begin{aligned}\varepsilon c\int_{-\infty}^{\infty}(\varphi')^2\mathrm{d}\xi &= -\int_{-\infty}^{\infty}\varphi'\psi\mathrm{d}\xi\\ c\int_{-\infty}^{\infty}(\psi')^2\mathrm{d}\xi &= \int_{-\infty}^{\infty}\psi'\varphi\mathrm{d}\xi.\end{aligned}\tag{4.8}$$

Since $\int_{-\infty}^{\infty}\varphi'\psi\mathrm{d}\xi=-\int_{-\infty}^{\infty}\varphi\psi'\mathrm{d}\xi$ from (4.8) we derive

$$\varepsilon\int_{-\infty}^{\infty}(\varphi')^2\mathrm{d}\xi=\int_{-\infty}^{\infty}(\psi')^2\mathrm{d}\xi.\tag{4.9}$$

We now multiply the second of (4.5) by φ and we integrate

$$c\int_{-\infty}^{\infty}\varphi\psi'\mathrm{d}\xi=\int_{-\infty}^{\infty}\varphi^2\mathrm{d}\xi-\gamma\int_{-\infty}^{\infty}\varphi\psi\mathrm{d}\xi.\tag{4.10}$$

Relations (4.7b) and (4.10) yield

$$\int_{-\infty}^{\infty}\varphi^2\mathrm{d}\xi=c\int_{-\infty}^{\infty}\varphi\psi'\mathrm{d}\xi+\gamma^2\int_{-\infty}^{\infty}\psi^2\mathrm{d}\xi\tag{4.11}$$

and by making use of (4.9) and (4.7b), (4.7a) can be rewritten as

$$\int_{-\infty}^{\infty} \varphi f(\varphi) \mathrm{d}\xi = \frac{1}{\varepsilon} \int_{-\infty}^{\infty} (\psi')^2 \mathrm{d}\xi + \gamma \int_{-\infty}^{\infty} \psi^2 \mathrm{d}\xi. \tag{4.12}$$

Moreover from (4.11) we get

$$\int_{-\infty}^{\infty} \varphi f(\varphi) \mathrm{d}\xi = \frac{1}{\varepsilon} \int_{-\infty}^{\infty} (\psi')^2 \mathrm{d}\xi - \frac{c}{\gamma} \int_{-\infty}^{\infty} \varphi \psi' \mathrm{d}\xi + \frac{1}{\gamma} \int_{-\infty}^{\infty} \varphi^2 \mathrm{d}\xi. \tag{4.13}$$

By taking account also for the second of (4.8), (4.13) becomes

$$\int_{-\infty}^{\infty} \varphi f(\varphi) \mathrm{d}\xi = \varepsilon^{-1} \int_{-\infty}^{\infty} (\psi')^2 \mathrm{d}\xi - \frac{c^2}{\gamma} \int_{-\infty}^{\infty} (\psi')^2 \mathrm{d}\xi + \frac{1}{\gamma} \int_{-\infty}^{\infty} \varphi^2 \mathrm{d}\xi$$

that is

$$\int_{-\infty}^{\infty} \left[\frac{\varphi^2}{\gamma} - \varphi f(\varphi) \right] \mathrm{d}\xi = \left(\frac{c^2}{\gamma} - \frac{1}{\varepsilon} \right) \int_{-\infty}^{\infty} (\psi')^2 \mathrm{d}\xi. \tag{4.14}$$

Let us now modify condition (4.12) according to (4.8). We obtain

$$\int_{-\infty}^{\infty} \varphi f(\varphi) \mathrm{d}\xi = \frac{1}{c\varepsilon} \int_{-\infty}^{\infty} \varphi \psi' \mathrm{d}\xi + \gamma \int_{-\infty}^{\infty} \psi^2 \mathrm{d}\xi$$

and by (4.11)

$$\int_{-\infty}^{\infty} \varphi f(\varphi) \mathrm{d}\xi = \frac{1}{c^2\varepsilon} \int_{-\infty}^{\infty} (\varphi^2 - \gamma^2 \psi^2) \mathrm{d}\xi + \gamma \int_{-\infty}^{\infty} \psi^2 \mathrm{d}\xi.$$

All these calculations yield the final expression

$$\int_{-\infty}^{\infty} \left[\frac{1}{c^2\varepsilon} \varphi^2 - \varphi f(\varphi) \right] \mathrm{d}\xi = \gamma \left(\frac{\gamma}{c^2\varepsilon} - 1 \right) \int_{-\infty}^{\infty} \psi^2 \mathrm{d}\xi. \tag{4.15}$$

Let us now rewrite the integrand of the left-hand side of (4.14) as

$$\varphi^2 \left[\frac{1}{\gamma} + (\varphi - 1)(\varphi - \alpha) \right] = \varphi^2 \left[\left(\varphi - \frac{1+\alpha}{2} \right)^2 + \frac{1}{\gamma} - \frac{(1-\alpha)^2}{4} \right] \tag{4.16}$$

If $\gamma < \gamma_{\mathrm{cr},1}$ the previous expression is positive $\forall \varphi, \alpha, \gamma$. Consequently in (4.14) it must hold

$$c^2 > \frac{\gamma}{\varepsilon}.$$

Accounting for this last statement, (4.15) yields

$$\frac{1}{c^2\varepsilon} \varphi^2 - \varphi f(\varphi) < 0 \tag{4.17}$$

which is a second order inequality in φ and has solutions if and only if $(1+\alpha)^2 - 4(\alpha + (\varepsilon c^2)^{-1}) > 0$, that is $c^2 > 4/(\varepsilon(1-\alpha)^2) > \gamma/\varepsilon$.

In conclusion, in the case $\gamma < \gamma_{\mathrm{cr},1}$ we have found a lower bound for the wave speed c, and precisely

$$c > \frac{2}{\sqrt{\varepsilon}(1-\alpha)}. \tag{4.18}$$

We now would to search for an upper bound for c. To this aim, let be $\Phi(\xi) = (\varphi(\xi), \psi(\xi))^T$. System (4.5) becomes

$$\Phi' = \begin{bmatrix} \frac{1}{\varepsilon c}\frac{\mathrm{d}^2}{\mathrm{d}\xi^2} & -\frac{1}{\varepsilon c} \\ \frac{1}{c} & -\frac{-\gamma}{c} \end{bmatrix} \Phi + \begin{bmatrix} \frac{f(\varphi)}{\varepsilon c} \\ 0 \end{bmatrix}.$$

If we multiply by Φ^T we obtain

$$\varphi\varphi' + \psi\psi' = \frac{\varphi\varphi''}{\varepsilon c} + \frac{\psi}{c}\varphi - \frac{\varphi\psi}{\varepsilon c} - \psi^2\frac{\gamma}{c} + \frac{\varphi f(\varphi)}{\varepsilon c},$$

and integrating this expression between $-\infty$ and ξ yields

$$\begin{aligned} &\frac{1}{2}\varphi^2 + \frac{1}{2}\psi^2 = \frac{1}{\varepsilon c}\varphi\varphi_\eta\,|_{-\infty}^{\xi} - \frac{1}{\varepsilon c}\int_{-\infty}^{\xi}(\varphi_\eta)^2\mathrm{d}\eta + \frac{1}{c}\int_{-\infty}^{\xi}\varphi\psi\mathrm{d}\eta - \\ &\frac{1}{\varepsilon c}\int_{-\infty}^{\xi}\varphi\psi\mathrm{d}\eta - \frac{\gamma}{c}\int_{-\infty}^{\xi}\psi^2\mathrm{d}\eta + \frac{1}{\varepsilon c}\int_{-\infty}^{\xi}\varphi f(\varphi)\mathrm{d}\eta. \end{aligned} \tag{4.19}$$

Owing to the second relation of (4.5) we can write

$$\frac{1}{c}\int_{-\infty}^{\xi}\varphi\psi\mathrm{d}\eta - \frac{\gamma}{c}\int_{-\infty}^{\xi}\psi^2\mathrm{d}\eta = \frac{1}{c}\int_{-\infty}^{\xi}\psi(c\psi_\eta)\mathrm{d}\eta = \frac{1}{2}\psi^2,$$

so that (4.19) becomes

$$\frac{1}{2}\varphi^2 = \frac{1}{\varepsilon c}\varphi\varphi_\eta - \frac{1}{\varepsilon c}\int_{-\infty}^{\xi}(\varphi_\eta)^2\mathrm{d}\eta - \frac{1}{\varepsilon c}\int_{-\infty}^{\xi}\psi(c\psi_\eta + \gamma\psi)\mathrm{d}\eta + \frac{1}{\varepsilon c}\int_{-\infty}^{\xi}\varphi f(\varphi)\mathrm{d}\eta,$$

where we have replaced φ with $c\psi_\eta + \gamma\psi$. By performing some calculations we get the equation

$$\frac{1}{2}\varphi^2 = \frac{1}{2\varepsilon c}(\varphi^2)_\eta - \frac{1}{\varepsilon c}\int_{-\infty}^{\xi}(\varphi_\eta)^2\mathrm{d}\eta - \frac{1}{2\varepsilon}\psi^2 - \frac{\gamma}{\varepsilon c}\int_{-\infty}^{\xi}\psi^2\mathrm{d}\eta + \frac{1}{\varepsilon c}\int_{-\infty}^{\xi}\varphi f(\varphi)\mathrm{d}\eta$$

from which we easily derive the following inequality

$$\frac{1}{2}\varphi^2 \le \frac{1}{2\varepsilon c}(\varphi^2)_\eta + \frac{1}{\varepsilon c}\int_{-\infty}^{\xi}\varphi f(\varphi)\mathrm{d}\eta. \tag{4.20}$$

We now claim

$$\varphi f(\varphi) - \frac{(1-\alpha)^2}{4}\varphi^2 \leq 0.$$

Indeed, by recalling the calculation made in (4.16) we can write

$$\varphi f(\varphi) - \frac{(1-\alpha)^2}{4}\varphi^2 = \varphi^2\left[-\left(\varphi - \frac{1+\alpha}{2}\right)^2 + \frac{(1-\alpha)^2}{4} - \frac{(1-\alpha)^2}{4}\right] =$$
$$\varphi^2\left[-\left(\varphi - \frac{1+\alpha}{2}\right)^2\right] \leq 0.$$

Therefore (4.20) can be written

$$\varphi^2 \leq \frac{1}{\varepsilon c}(\varphi^2)_\eta + \frac{(1-\alpha)^2}{2\varepsilon c}\int_{-\infty}^{\xi}\varphi^2 \mathrm{d}\eta.$$

Let be $G(\xi) = \int_{-\infty}^{\xi}\varphi^2 \mathrm{d}\eta$. The previous inequality yields

$$G'' - \varepsilon c G' + \frac{(1-\alpha)^2}{2}G \geq 0.$$

If we now set

$$G(\xi) = H(\xi)e^{\frac{c\varepsilon}{2}\xi} \tag{4.21}$$

we find that $H(\xi)$ satisfies the following differential inequality

$$H'' \geq \left(\frac{\varepsilon^2 c^2}{4} - \frac{(1-\alpha)^2}{2}\right)H.$$

Owing to the definition of $G(\xi)$,

$$H(\xi) = e^{-\frac{c\varepsilon}{2}\xi}\int_{-\infty}^{\xi}\varphi^2 \mathrm{d}\eta \geq 0. \tag{4.22}$$

Then, if the inequality $c^2\varepsilon^2 \geq 2(1-\alpha)^2$ also holds, we get

$$H'' \geq 0 \qquad \forall \xi \in (-\infty, \infty),$$

meaning that H is convex. In the following we prove that $H'' \geq 0$ if and only if $H \equiv 0$, so that if $c^2\varepsilon^2 \geq 2(1-\alpha)^2$ the only existing traveling wave solution for (4.5) has a constant value.

Let us start the analysis by considering the behavior of H for $\xi \to +\infty$. It is clear that, if $\varphi \in L^2(-\infty, \infty)$, then $\lim_{\xi\to+\infty} H(\xi) = 0$. While, if φ

is not a L^2 function in the interval $(-\infty, \infty)$, the following two cases may occur:

$$\lim_{\xi \to +\infty} H(\xi) = \infty,$$
$$\lim_{\xi \to +\infty} H(\xi) = 0.$$

The first condition implies $G(\xi) \to +\infty$, due to (4.21), and, from (4.22), $\varphi \to +\infty$ that contradicts the requirements in (4.6) and then yields the non existence of traveling pulse.

Assume now that the second condition holds, and let us study $H(\xi)$ for $\xi \to -\infty$. The traveling wave definition yields

$$\lim_{\xi \to -\infty} \varphi(\xi) = 0, \tag{4.23}$$

then the cubic polynomial $f(\varphi)$ can be approximated as

$$f(\varphi) = -\varphi^3 + \varphi^2(\alpha + 1) - \alpha\varphi \sim -\alpha\varphi$$

and, consequently, we can linearize system (4.5) obtaining

$$\begin{aligned} \varepsilon c\varphi' &= \varphi'' - \alpha\varphi - \psi \\ c\psi' &= \varphi - \gamma\psi. \end{aligned} \tag{4.24}$$

By rewriting (4.24) in terms of the only variable φ, we obtain the following ordinary differential equation

$$\varphi''' + \varphi''\left(\frac{\gamma}{c} - \varepsilon c\right) - \varphi'(\alpha + \gamma\varepsilon) - \varphi\left(\frac{1}{c} + \frac{\gamma\alpha}{c}\right) = 0. \tag{4.25}$$

Because of condition (4.23), φ can be represented as an exponential for $\xi \to -\infty$, that is

$$\varphi \sim Ae^{m_1\xi} \qquad \text{for } \xi \to -\infty$$

where $m_1 > 0$ is the largest root of the equation obtained by replacing in (4.25) the exponential form of φ, i. e.

$$m^3 - m^2\left(\varepsilon c - \frac{\gamma}{c}\right) - m(\alpha + \gamma\varepsilon) - \left(\frac{1}{c} + \frac{\gamma\alpha}{c}\right) = 0.$$

Since $c^2 > \gamma/\varepsilon$, all the coefficients in the previous equation are negative, except for that of the third order term. Then, the polynomial has only one positive root. More particularly, we can say that $m_1 > c$, because the value of the polynomial for $m = c$ is negative.

An important consequence of this result is that φ approaches the null value as $\xi \to -\infty$ with a rate at least equal to the decay of $e^{c\xi}$. Then (4.22) implies that $H(\xi) \to 0$ as $\xi \to -\infty$.

These findings complete the analysis, since the following statement has been shown

$$\text{if} \qquad c^2\varepsilon^2 \geq 2(1-\alpha)^2 \qquad \lim_{|\xi|\to\infty} H(\xi) = 0.$$

Due to the convexity of H, from the previous assertion we deduce $H \equiv 0$ and, from (4.22), $\varphi \equiv 0$. Therefore for the existence of a non-constant traveling pulse of (4.5) the inequality $c^2\varepsilon^2 < 2(1-\alpha)^2$ must hold, and this is equivalent to say that the wave speed must respect the upper limit

$$c < \sqrt{2}\frac{(1-\alpha)}{\varepsilon}. \tag{4.26}$$

By comparing (4.18) and (4.26), we discover that the constitutive parameters must satisfy the following relation

$$\varepsilon < \frac{(1-\alpha)^4}{2} \tag{4.27}$$

so that a potential wave propagates along a cardiac fiber. Therefore, setting $\varepsilon_{\mathrm{cr,w}}(\alpha) = \frac{(1-\alpha)^4}{2}$, we can say that the dynamical system (4.5) possesses traveling pulse solutions for a fixed $\alpha = \bar{\alpha}$, only if $\varepsilon < \varepsilon_{\mathrm{cr,w}}(\bar{\alpha})$.

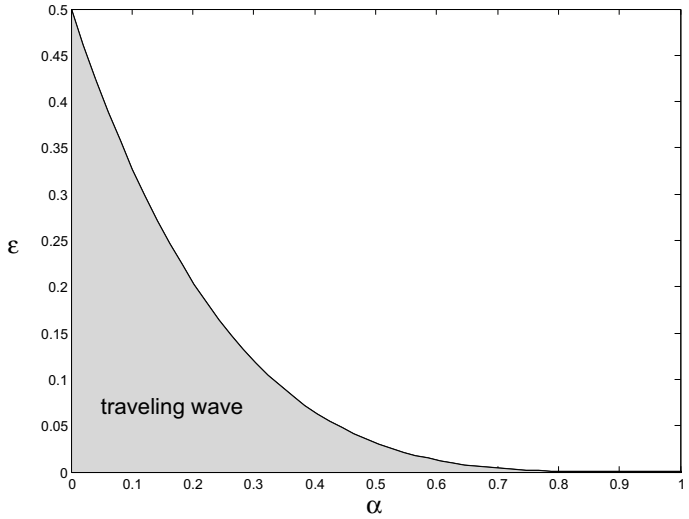

Figure 4.14: Representation of condition (4.27). The grey domain contains the values of ε that allow the definition of traveling wave solutions for (4.5).

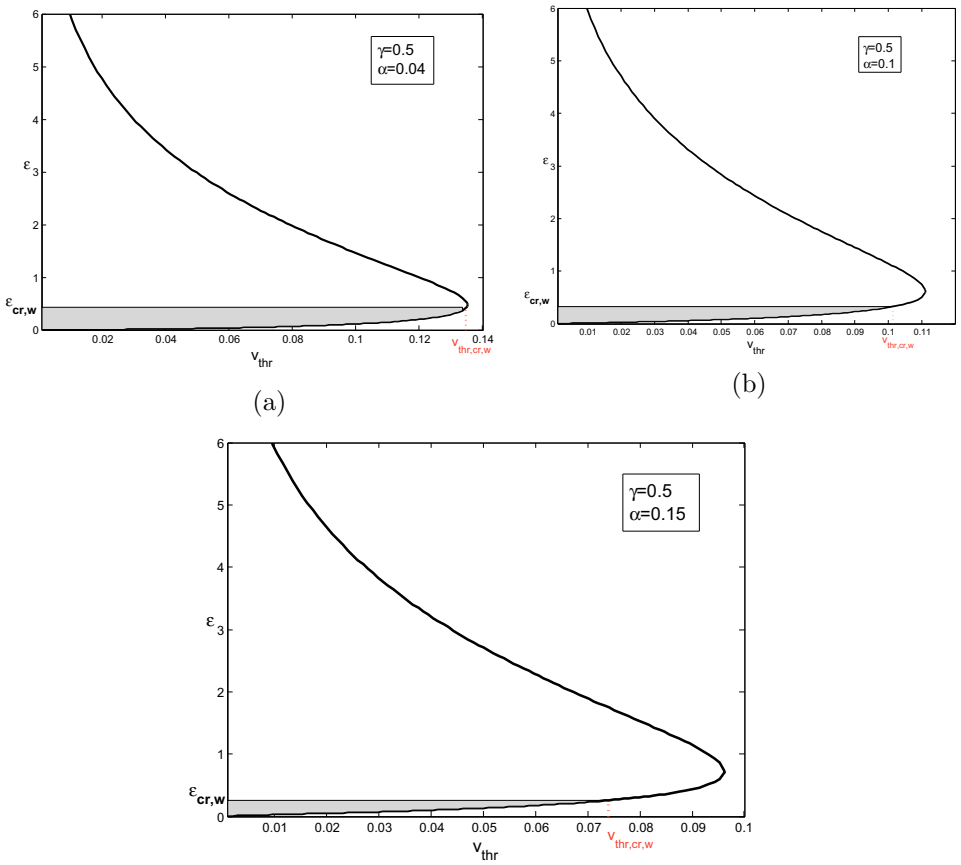

Figure 4.15: Critical value of the threshold corresponding to $\varepsilon_{\mathrm{cr,w}}$ for $\alpha = 0.04, 0.1, 0.15$.

4.4.2 Parameters characterization for DAD onset

Inequality (4.27) is displayed in Fig. 4.14. The evidenced region encloses all the admissible values of ε, corresponding to each $\alpha \in (0, 1]$, that allow us to define of a traveling wave solution for (4.4).

Recalling what we noted in the introduction to this section, the first step we should make if we aim at investigating the possible propagation of a secondary spike throughout the tissue, is comparing the values $\varepsilon_{\mathrm{cr,w}}(\alpha)$ with critical values of ε that guarantee the occurrence of two-spike solutions in (4.5). This admissible range of ε is shown in Fig. 4.13, for some values of α and v_{thr}.

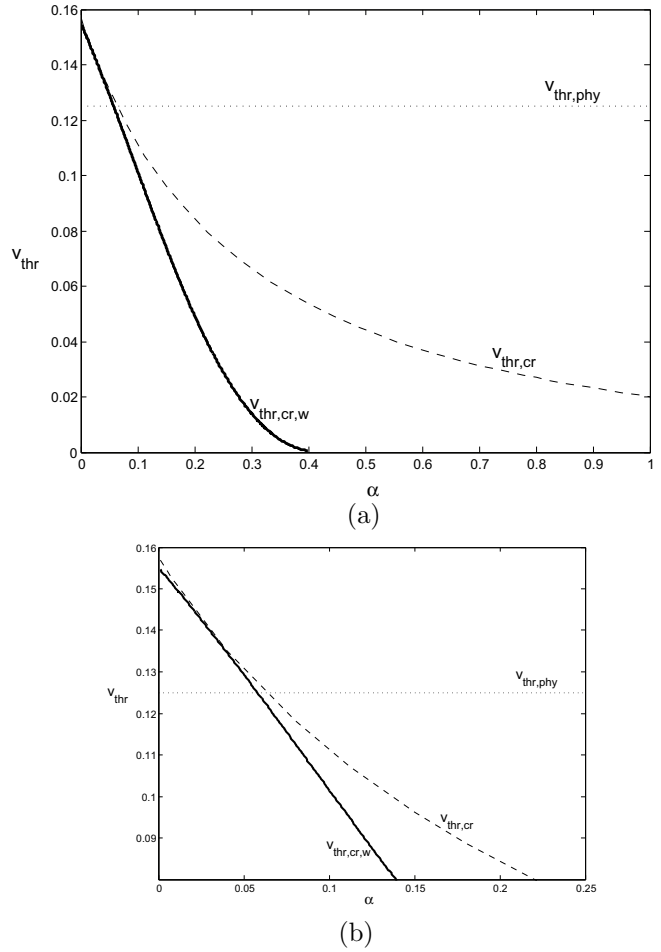

Figure 4.16: (a) Behavior of $v_{\mathrm{thr,cr,w}}$ for $\alpha \in (0, 4]$ compared with the critical threshold required to have two-spike solutions. (b) Zoomed view of the area where the curves are very close.

Let us consider, for instance, $\bar{\alpha} = 0.15$, so that $\varepsilon_{\mathrm{cr,w}}(0.15) \sim 0.2610$. It can be easily verified that, for choices of v_{thr} large enough, $\varepsilon_{\mathrm{cr,w}}(0.15) < \varepsilon_{\min}(v_{\mathrm{thr}}, 0.15)$, therefore the secondary spike that eventually follows the main electrical upstroke if $\varepsilon_{\min}(v_{\mathrm{thr}}, 0.15) < \varepsilon < \varepsilon_{\max}(v_{\mathrm{thr}}, 0.15)$, does not evolve because it immediately dies out.

In other words, there exists a critical value of the threshold, $v_{\mathrm{thr,cr,w}}$ such that, if $v_{\mathrm{thr}} > v_{\mathrm{thr,cr,w}}$ a secondary spike, if arises, does not propagate in the cardiac fibers. Such a value can be detected in Fig. 4.15 from the intersection point between the line $\varepsilon = \varepsilon_{\mathrm{cr,w}}(\alpha)$ and the curve corresponding to the chosen α. This special value of the threshold and the line $\varepsilon = \varepsilon_{\mathrm{cr,w}}$ mark off an area in Fig. 4.15 where the extra-spikes may generate a depolarization wave. Then, if the time scale parameter exceeds the critical value two circumstances arise: either an after-depolarization appears but the triggered action potential is not transmitted to the adjacent cells, or the potential does not oscillate after the main impulse.

As $\alpha \to 0$, $v_{\mathrm{thr,cr,w}}$ increases and the grey region if Fig. 4.15 is extended. This behavior is evidenced in Fig. 4.16, where we described $v_{\mathrm{thr,cr,w}}$ as a function of α and we compared the resulting curve with the behavior of $v_{\mathrm{thr,cr}}(\alpha)$ for $\gamma = 0.5$ (already shown in Fig. 4.11), where $v_{\mathrm{thr,cr}}$ is the value of the threshold depicted with a red dashed line in Fig. 4.13 . It is clear that the value of $v_{\mathrm{thr,cr,w}}$ rapidly decreases in the interval $(0, 0.4]$ and for $\alpha > 0.4$ it assumes so small values that they can be approximated with the null value. This means that for $\alpha > 0.4$ all the secondary oscillations that may arise do not affect the electrical process and in particular there is no risk of arrhythmias occurring.

At the same time, as α decreases, the difference between the two critical thresholds, the one representing the upper limit for the occurrence of traveling pulses and the other bounding from above the onset of two-spike trajectories, is reduced. Fig. 4.16 clearly shows that $v_{\mathrm{thr,cr,w}} < v_{\mathrm{thr,cr}}\ \forall\alpha$, and in particular that the two curves do not have common points, even if, in a small interval, they are very close each other. Then we evince that for all $\alpha \in (0, 1]$ and for γ fixed to its physiological value, if $\varepsilon_{\min} < \varepsilon < \varepsilon_{\mathrm{cr,w}}$ all the two-spike trajectories potentially have the ability to generate a triggered action potential. Moreover, if α is less than a critical value that makes the DAD amplitude able to be compared with the physiological activation threshold, all the secondary oscillations, whose amplitude is less than $v_{\mathrm{thr,cr}}$, necessarily generate a traveling pulse which, consequently, affects the contraction process of the myocytes, probably causing extra-systole. This effect is in agreement with the so called *all or none* response (see chapter 1) typical of the cardiac electrical activation. Indeed the upstroke initiation is not related to the amplitude of the stimulus, but rather to the fact that the activation threshold is

reached or not. Then if the potential depolarization approaches $v_{\text{thr,phy}}$, the myocyte is excited and such a stimulation easily activates the surrounding tissue.

This is a fundamental result that, although it is based on data that are not strictly accurate, gives an idea on the capabilities of the model in the prediction of DAD-induced afterpotentials.

4.5 The electromechanically coupled FitzHugh-Nagumo model

On the wake of the previous outcomes, it is clear that looking for spike-solutions in more realistic systems allows to make a more accurate analysis that may yield more precise predictions. Therefore in this section we study the occurrence of extra-spikes in the solutions to system (3.48).

In a very first analysis we assign to the fiber contraction the typical value, $\beta = 0.3$. Figure 4.17 illustrates the values $\alpha(v_{\text{thr}}, \bar{\gamma})$ for $\bar{\gamma} = 0.3, 0.5, 0.8$ so that system (3.48) owns solutions with multiple spikes $\forall \alpha < \alpha(v_{\text{thr}})$.

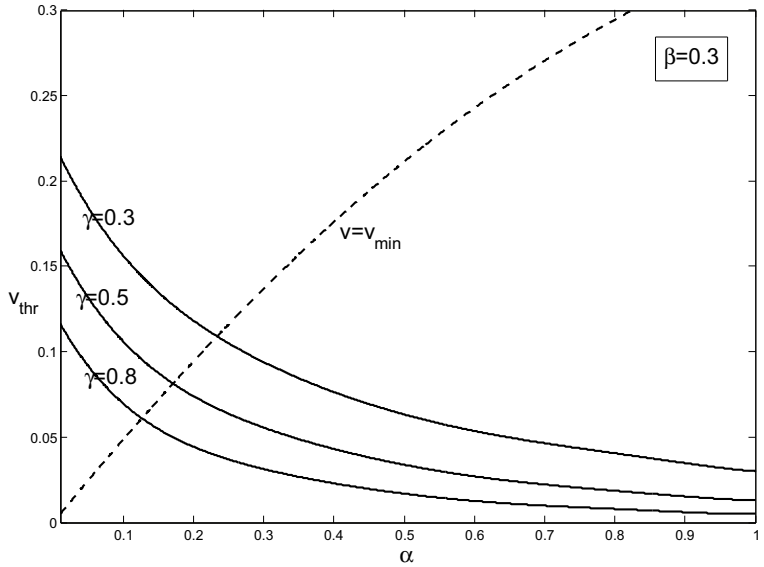

Figure 4.17: Critical values of α for the existence of multi-spike solutions for system (3.48) for different values of the potential threshold and for some values of γ.

Furthermore in Fig. 4.18 we show the values of $\varepsilon_0(v_{\text{thr}}, \alpha)$, with $\gamma = 0.5$. For a fixed $v_{\text{thr}} = \bar{v}_{\text{thr}}$ and $\alpha = \bar{\alpha}$, solutions of system (3.48) perform two spikes if $\varepsilon_{0,\min}(\bar{v}_{\text{thr}}, \bar{\alpha}) < \varepsilon_0 < \varepsilon_{0,\max}(\bar{v}_{\text{thr}}, \bar{\alpha})$, where $\varepsilon_0(\bar{\alpha})$ is the value of ε_0 on the curve associated with $\bar{\alpha}$.

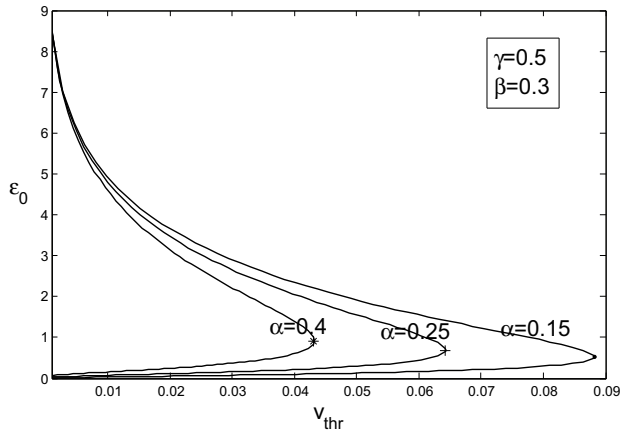

Figure 4.18: Range of values for ε_0 ensuring the existence of multi-spikes solutions for system (3.48) for different values of the potential threshold and for some values of α.

Observe that, for the same α, the values of $v_{\text{thr,cr}}$ for (3.48) are smaller than those for system (3.13) (depicted in Fig. 4.13). This result suggests that increasing the accuracy in the description of the cardiac dynamics limits the choice for the potential threshold further on.

In order to know if the last statement is true for other values of the fiber shortening, we have studied how $v_{\text{thr,cr}}$ changes as a function of the parameter β.

From an analytical point of view, if β increases, the value of $v_{\text{cr}} = (2\beta)^{-1}$ decreases and approaches the null value. This means that the trajectory is more likely to cross the critical line $v = v_{\text{cr}}$ in the phase plane and the region where the solution has a non-singular behavior becomes smaller and smaller. Consequently the maximal value of the threshold for the occurrence of multiple-spike solutions will decrease.

This phenomenon is described in Fig. 4.19, which contains the results clarified in the following. If we fix $\beta \in [0.1, 0.7]$ and $\alpha = 0.15, 0.25, 0.4$, there exist solutions that perform more than one spike and the amplitude of the secondary oscillation is less or equal than $v_{\text{thr,cr}}(\beta, \alpha)$, this value being detected on the corresponding curve in Fig 4.19.

For $\beta = 0.3$, $v_{\text{thr,cr}}(\alpha)$ coincides with the x-coordinate of the points marked with $*$, $+$ and $\bullet$ in Fig. 4.18.

From a physiological point of view, Fig. 4.19 evidences that, as the contractile capacitance of the myocytes decreases, the likelihood for triggered activity induced by delayed after-depolarization is enhanced, since $v_{\text{thr,cr}}$ increases thus approaching the physiological potential threshold $v_{\text{thr,phy}}$.

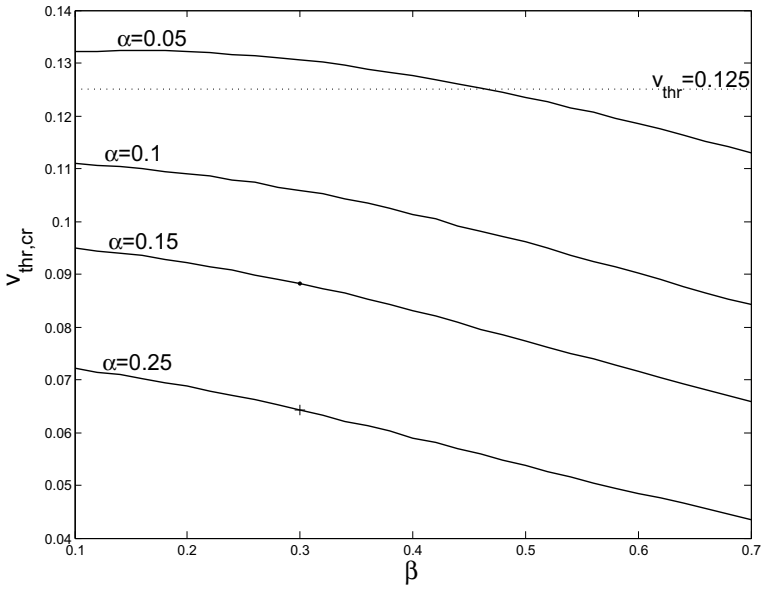

Figure 4.19: Behavior of $v_{\text{thr,cr}}$ as the contraction parameter β varies in $[0.1, 0.7]$ and emergence of supra-threshold DADs.

Real confirmations of this phenomenon can be found in the literature. In [63] it is observed that, while at rapid heart rates the occurrence of DAD is more likely, the contractile force is decreased because in failing hearts the increasing rate of stimulation reduces the shortening capacitance of the myocytes [64, 65].

In [47] it is performed a more detailed analysis. Pogwizd et al. analyze the causes of the contractile dysfunction of the myocyes and then prove that similar mechanisms are involved in the appearance of DAD and then in arrhythmogenesis.

The reduced contraction force of a myocyte is principally due to a decrease in the release of calcium from the sarcoplasmic reticulum (SR). In turn, the decreased SR Ca^{2+} release is caused by a reduction in SR Ca^{2+} content. In [47] it is shown that the unloading of SR Ca^{2+} is due to the increased activity of the Na^{+}-Ca^{2+} exchanger. Indeed it contributes to the efflux of calcium in exchange with sodium ions.

On the other hand, although the load of SR Ca^{2+} is reduced, in heart failure a lower threshold of calcium load in sarcoplasmic reticulum is required to trigger the spontaneous Ca^{2+} release and then DAD. Moreover Pogwizd et al. show that failing heart cells exhibit a residual $\beta-$adrenergic activity that enables the spontaneous SR Ca^{2+} release which may cause arrhythmias.

Fig. 4.19 emphasizes the importance of accounting for the electro-mechanical

coupling in the model, and in particular for the process by which cellular depolarization causes myocytes to contract (excitation-contraction coupling). Indeed, in dependence of the value of the muscle contraction and for some values for α (Fig. 4.19 displays only $\alpha = 0.05$), a secondary spike amplitude may exceed the physiological threshold and trigger a spontaneous upstroke. In other words, there exists a critical value of β that determines, for some fixed α, the onset of supra-threshold DADs.

The importance of considering a contracting domain for the equations had been already detected in [45]. Indeed by integrating the 1-dimensional dynamical system (3.47), Ambrosi et al. found that the pulse propagating in a contracting fiber has a greater speed than if it propagates in a fixed domain. Moreover the width of the stroke is shorter. This means that the solution computed for $\beta = 0$ yields non-negligible errors.

By looking for a traveling front solution for (3.47), thus neglecting the recovery phase, they proved also that a condition on the parameters must be satisfied so that a traveling front exists. To be precise, the condition $\alpha\beta < 1/2$ must hold.

In the framework of the 0-dimensional setting, we have shown here that, by adding the description of the mechanical activity of the contractile units of the cardiac muscle, the DAD-predictive property of the FitzHugh-Nagumo model is enriched with information on the nature of the delayed depolarization, namely its sub-threshold or supra-threshold feature.

Conclusions and future work

In this Thesis we have analyzed a mathematical model that characterizes and predicts possible distortions in the evolution of the electric signal generated in the cardiac cells. Indeed, the excitation process, responsible for the contraction of the cardiac fibers, can be altered by physiological factors and, in particular, before the cardiomyocytes have recovered the stable configuration, a secondary electrical wave can be generated, thus modifying the equilibrium of the cells and, consequently, the contraction mechanisms. The underlying event that induces this abnormal behavior is a membrane depolarization that perturbs the final stage of the cardiac action potential and is called delayed after-depolarization.

The FitzHugh-Nagumo model provides a well-suited scheme to study these phenomena, since it can easily modified and extended to fit the particular features of the question we deal with. Although it was introduced to reproduce the transmission of the electric signal in the neuronal membrane, it can be easily adapted to the cardiac framework. Indeed many examples where the cardiac action potential is modeled through the FitzHugh-Nagumo scheme can be recovered in the literature.

In the present Thesis we have defined particular solutions of the FitzHugh-Nagumo dynamical system, labeled spike-solutions, characterized by the number of supra-threshold turns they perform around the equilibrium point before the potential approaches the equilibrium configuration. We have considered here a set of parameter values which ensures that the dynamical system has only one steady state, and we have proved that, for all the values of the constitutive parameters ensuring the existence of one stable configuration, limit cycle solutions and unbounded orbits are absent in the phase plane. However our analysis can be easily generalized, provided that there exists a stable attractor in the phase plane and the basin of attraction of this equilibrium includes only trajectories approaching the rest state as $t \to +\infty$.

A deep examination of the spike-solutions may yield a quantitative description of the DAD event, since they exactly reproduce the oscillations the potential evolution may undergo at the final phase of the process.

A crucial property defining such orbits is the amplitude of the first spike, called v_{thr} since it plays the rule of a potential threshold. Indeed this parameter, compared with the physiological activation threshold, can give useful information on the nature of the spike, and in particular it can distinguish between supra-threshold and sub-threshold DADs.

In a first analysis we assigned $v_{\text{thr}} = v_{\min}(\alpha)$, $v_{\min}(\alpha)$ being the minimum point of the nullcline corresponding to the variable that describes the fast dynamics of the signal propagation. Nevertheless this proved to be an inappropriate choice since, in correspondence with the decreasing of α, the amplitude of the first spike considerably decreases and several-spikes solutions occur. This happens because v_{thr} is moving away from its physiological value and the resulting oscillations are exclusively due to the spiral attraction from the equilibrium point. Indeed the threshold should not depend on the physiological properties of the cardiac membrane, since it must represent an objective parameter denoting the typical physiological condition of a healthy individual.

Therefore we focused on a fixed value of v_{thr}, trying to calibrate its magnitude on the basis of the data found in the literature. This analysis has produced interesting results. First of all, we found that if α is large enough, the secondary spike does not occur, whatever the choice of v_{thr} (Fig. 4.11), so that once the electrical impulse is triggered, the potential immediately stabilizes around the rest state. Moreover, even if the value for α guarantees the existence of a secondary spike, the parameter ε has to vary in a suitable range and there exists an upper limit for the DAD amplitude, beyond which the depolarization can be neglected.

Once we have identified the correct values of the parameters ensuring the existence of DADs, we wondered under which conditions the depolarization could generate a traveling pulse perturbing, in such a way, the evolution of the action potential. In practice we investigated the occurrence of a DAD-induced traveling wave that excites again the cardiac muscle and leads to after-contractions of the fibers. Such a possibility needs the fulfilment of other parameter requirements, and, specifically, the parameter ε must not exceed a critical value (Fig. 4.6). This means that we have to restrict the admissible range of values of the constitutive parameters further on. A peculiar threshold is associated with the critical value of ε, limiting the choice of the magnitude of the secondary spike. More interestingly, contrary to what we would have expected, in order to induce a propagating pulse, the depolarization occurring after the repolarization phase can not exceed a critical value of the potential, that we have called $v_{\text{thr,cr,w}}$. However Fig. 4.16 shows that, if α assumes small values, every time an extra-spike occurs, it generates a traveling wave, since in this case, $v_{\text{thr,cr,w}}$ is comparable with the physiological

values.

Obviously, the analysis of traveling pulse solutions involves the spatial dimension of the problem and, more particularly, we must account for a diffusion of the potential through the tissue, that necessarily yields a dispersion of the initial impulse. Consequently, the occurrence of two-spike solutions will be subjected to slightly different criterions that will account for the scattering potential. On the basis of this observations, it is clear that the FitzHugh-Nagumo dynamical system must be refined and extended in order to obtain more precise results. There are several models which improve the FitzHugh-Nagumo scheme. One of the simplest generalizations is provided by the Aliev-Panfilov model [25], which simulates the restitution property of cardiac tissue and fits the shape of the action potential. This model is almost as simple as the FitzHugh-Nagumo model since, more specifically, it preserves the shape of the cubic function $f(v)$, the character of the equilibrium configuration and the information contained in the parameters definition. However, we showed that the Aliev-Panfilov model can not predict the emergence of DAD, since the phase plane structure of this dynamical system does not allow the potential to perform turns around the equilibrium configuration. For this reason we studied other refinements of the FitzHugh-Nagumo model that are predisposed to be DAD-predictive schemes.

A possible choice aimed at making the model more realistic requires to consider the dependence of the parameter ε on the potential v itself [45]. In this way we may simulate properly the dependence of the activation of the contraction of the cardiac muscle on the potential field. The analysis of the spike-solutions for this dynamical system produces fundamental outcomes. Indeed we have shown that, by modeling the mechanical activity of the cardiac fibers, the DAD-predictive feature of the FitzHugh-Nagumo model contains also information on the nature of the extra-spike, namely its sub-threshold or supra-threshold property. In dependence of the magnitude of the shortening, the secondary oscillation can exceed the physiological threshold and then trigger an action potential. More particularly if the contraction of the fibers is sufficiently strong, no supra-threshold DAD are generated, whereas, if it is less than a critical value, the extra-spike amplitude reaches the activation threshold and gives rise to a secondary wave.

Such a result provides a relation between the contraction ability of the myocytes and the possible occurrence of arrhythmias. This connection is also proved at a molecular level, since some authors studied the consequences of a contractile dysfunction on the ionic environment that could establish the generation of DAD. Nevertheless, since the model itself can predict the cardiac triggered activity on the basis of the contraction magnitude, it represents a powerful tool that enables to design and predict decisive interventions in

prevention of arrhythmical episodes.

By collecting all the outcomes summarized here we can conclude that the onset of a delayed after-depolarization that generates triggered arrhythmias depends on the contemporary occurrence of many factors. First of all the physiological parameters should assume certain critical values both for the generation of the DAD and for its propagation. Moreover the DAD amplitude must satisfy some requirements. In particular, it has to be at the same time smaller that the critical values found by the numerical analysis presented here and greater, or at least equal, to the physiological value of the potential activation threshold. This confirms the common opinion that DAD triggered arrhythmia represents an abnormal evolution of the cardiac dynamic which occurs only in the case of altered physiological conditions.

As we have already noted, a natural development of the research is the extension of the DAD-predictive model presented in this work to a multidimensional setting. Indeed, a spatial-dependent model allows the study of the diffusion of the electric wave through the cardiac domain, and, in particular, the possible propagation of a secondary action potential, triggered by a supra-threshold DAD, that may cause the onset of abnormal heart contractions.

Moreover, once we have verified that under suitable conditions an action potential can propagate in a multi-dimensional domain, and in particular a supra-threshold spike may generate a secondary electric wave, the FitzHugh-Nagumo dynamical system must be enriched with an appropriate artifice that models in the correct way the threshold phenomenon. That is we need some device that triggers an action potential whenever the potential v exceeds the value v_{thr}. With this approach, we could check if the triggered action potential propagates along the cardiomyocyte or it burns out immediately, thus not compromising the heart functioning.

This last topic requires the introduction of substantial changes in the dynamical system and will be a remarkable subject for a future work. Indeed such a study can allow an outstanding employment of the DAD predictive model for practical purposes.

Aknowledgments

I would like to thank my advisor, Prof. Paolo Biscari, for having suggested the topic of this Thesis and for his clear advices and ideas which have always stimulated me during the project. I am also grateful to Prof. Riccardo Sacco since he has made available his support and encouragement in many occasions.

Bibliography

[1] M. P. Nash and A. V. Panfilov, "Electromechanical model of excitable tissue to study reentrant cardiac arrhythmias," *Progress in Biophysics and Molecular Biology*, vol. 85, pp. 501–522, 2004.

[2] J. S. Meyer, A. Mehdirad, B. I. Salem, W. A. Jamry, A. Kulikowska, and P. Kulikowski, "Sudden arrhythmia death syndrome: importance of the long QT syndrome," *Americal Familiy Physician*, vol. 68, pp. 483–488, 2003.

[3] A. Kalin, J. Usher-Smith, V. J. Jones, C. L.-H. Huang, and I. N. Sabir, "Cardiac arrhythmia: a simple conceptual framework," *Trends in Cardiovascular Medicine*, vol. 20, pp. 103–107, 2010.

[4] R. FitzHugh, "Thresholds and plateaus in the HodgkinHuxley nerve equations," *The Journal of General Physiology*, vol. 43, pp. 867–896, 1960.

[5] R. FitzHugh, "Impulses and physiological states in theoretical models of nerve membrane," *Biophysical Journal*, vol. 1, pp. 445–465, 1961.

[6] J. S. Nagumo, S. Arimoto, and S. Yoshizawa, "An active pulse transmission line simulating nerve axon," *Proceedings of the IRE*, vol. 50, pp. 2061–2071, 1962.

[7] P. A. Iaizzo, *Handbook of cardiac anatomy, physiology and devices*. Springer, 2009.

[8] Z. F. Issa, J. M. Miller, and D. P. Zipes, *Clinical arrhythmology and electrophysiology: a companion to Braunwald's heart disease*. Saunders Elsevier, 2009.

[9] H. T. Shih, "Anatomy of the action potential in the heart," *Texas Heart Institute Journal*, vol. 21, pp. 30–41, 1994.

[10] J. Malmivuo and R. Plonsey, *Bioelectromagnetism*. Oxford University Press, 1995.

[11] B. C. Knollmann and D. M. Roden, "A genetic framework for improving arrhythmia therapy," *Nature*, vol. 451, pp. 929–936, 2008.

[12] H. Cheng and W. J. Lederer, "Calcium sparks," *Physiological Reviews*, vol. 88, pp. 1491–1545, 2008.

[13] D. D. Friel, "$[Ca^{2+}]_i$ oscillations in symphathetic neurons: an experimental test of a theoretical model," *Biophysical Journal*, vol. 68, pp. 1752–1766, 1995.

[14] J. M. Nerbonne and R. Kass, "Molecular physiology of cardiac repolarization," *Physiological Reviews*, vol. 85, pp. 1205–1253, 2005.

[15] H. Hibino, A. Inanobe, K. Furutani, S. Murakami, I. Findlay, and Y. Kurachi, "Inwardly rectifying potassium channels: their structure, function, and physiological roles," *Physiological Reviews*, vol. 90, pp. 291–366, 2010.

[16] C. H. Luo and Y. Rudy, "A dynamic model of the cardiac ventricular action potential. II. Afterdepolarization, triggered activity, and potentiation," *Circulation Research*, vol. 74, pp. 1097–1113, 1994.

[17] K. Schlotthauer and D. M. Bers, "Sarcoplasmic reticulum Ca^{2+} release causes myocyte depolarization: underlying mechanism and threshold for triggered action potentials," *Circulation Research*, vol. 87, pp. 774–780, 2000.

[18] Y. Xie, D. Sato, A. Garfinkel, Z. Qu, and J. Weiss, "So little source, so much sink: requirements for afterdepolarizations to propagate in tissue," *Biophysical Journal*, vol. 99, pp. 1408–1415, 2010.

[19] I. Weiss, A. Urbaszek, and M. Schaldach, "Ionic mechanisms of cardiac arrhythmia," *Progress in Biomedical Research*, 2000.

[20] C. Antzelevitch and S. Sicouri, "Clinical relevance of cardiac arrhythmias generated by afterdepolarization. Role of M cells in the generation of U waves, triggered activity and torsade de pointes," *Journal of the American College of Cardiology*, vol. 23, pp. 259–277, 1994.

[21] C. Antzelevitch, "M cells in the human heart," *Circulation Research*, vol. 106, pp. 815–817, 2010.

[22] R. H. Clayton, O. Bernus, E. M. Cherry, H. Dierckx, F. H. Fenton, L. Mirabella, A. V. Panfilov, F. B. Sachse, G. Seemann, and H. Zhang, "Models of cardiac tissue electrophysiology: Progress, challenges and open questions," *Progress in Biophysics and Molecular Biology*, vol. 3, pp. 1–27, 2010.

[23] R. H. Clayton and A. V. Panfilov, "A guide to modelling cardiac electrical activity in anatomically detailed ventricles," *Progress in Biophysics and Molecular Biology*, vol. 96, pp. 19–43, 2008.

[24] M. E. Belik, T. P. Usyk, and A. D. McCulloch, "Computational methods for cardiac electrophysiology," in *Computational models for the human body, Special Volume of Handbook of Numerical Analysis, Volume XII.*, pp. 129–188, Elsevier B.V., 2004.

[25] R. R. Aliev and A. V. Panfilov, "A simple two-variable model of cardiac excitation," *Chaos Solitons and Fractals*, vol. 7, pp. 293–301, 1996.

[26] A. L. Hodgkin, "A note on conduction velocity," *Journal of Physiology*, vol. 125, pp. 221–224, 1954.

[27] A. L. Hodgkin and A. F. Huxley, "A quantitative description of membrane current and its application to conduction and excitation in nerve," *Journal of Physiology*, vol. 117, pp. 500–544, 1952.

[28] D. Noble, "A modification of the HodgkinHuxley equations applicable to Purkinje fibre action and pace-maker potentials," *Journal of Physiology*, vol. 160, p. 317352, 1962.

[29] G. W. Beeler and H. Reuter, "Reconstruction of the action potential of ventricular myocardial fibres," *Journal of Physiology*, vol. 268, pp. 177–210, 1977.

[30] C. H. Luo and Y. Rudy, "A model of the ventricular cardiac action potential. Depolarization, repolarization and their interaction," *Circulation Research*, vol. 68, pp. 1501–1526, 1991.

[31] D. DiFrancesco and D. Noble, "A model of cardiac electrical activity incorporating ionic pumps and concentration changes," *Philosophical Transactions of the Royal Society B*, vol. 307, pp. 353–398, 1985.

[32] J. Keener and J. Sneyd, *Mathematical physiology.* Springer Verlag, 1998.

[33] B. D. Sleeman, "Fitzhugh's nerve axon equations," *Journal of Mathematical Biology*, vol. 2, pp. 341–349, 1975.

[34] M. W. Green and B. D. Sleeman, "On FitzHugh's nerve axon equations," *Journal of Mathematical Biology*, vol. 1, pp. 153–163, 1974.

[35] J. Rinzel, "Repetitive activity and Hopf bifurcation under point-stimulation for a simple FitzHugh-Nagumo nerve conduction model," *Journal of Mathematical Biology*, vol. 5, pp. 363–382, 1978.

[36] C. Rocsoreanu, A. Georgescu, and N. Giurgiteanu, *The Fitzhugh-Nagumo model. Bifurcation and Dynamics*. Kluwer Academic Publisher, 2000.

[37] M. Ringkvist and Y. Zhou, "On existence and non existence of limit cycles for FitzHugh-Nagumo class models," *Lecture Notes in Control and Information Science*, vol. 321, pp. 337–351, 2005.

[38] T. Kostova, R. Ravindran, and M. Schonbek, "FitzHugh-Nagumo revisited: types of bifurcations, periodical forcing and stability regions by a Lyapunov functional," *International Journal of Bifurcation and Chaos*, vol. 14, pp. 913–925, 2004.

[39] F. Verhulst, *Nonlinear differential equations and dynamical systems*. Springer-Verlag, 2006.

[40] J. Sugie and T. Hara, "Nonexistence of periodic solutions of the Liénard system," *Journal of Mathematical Analysis and Applications*, vol. 159, pp. 224–236, 1991.

[41] J. Sugie, "Nonexistence of periodic solutions for the FitzHugh nerve system," *Quarterly of Applied Mathematics*, vol. 49, pp. 543–554, 1991.

[42] P. Kohl and F. Sachs, "Mechanoelectric feedback in cardiac cells," *Philosophical Transactions of the Royal Society A*, vol. 359, pp. 1173–1185, 2001.

[43] C. Cherubini, S. Filippi, P. Nardinocchi, and L. Teresi, "An electromechanical model of cardiac tissue: constitutive issues and electrophysiological effects," *Progress in Biophysics and Molecular Biology*, vol. 97, pp. 562–573, 2008.

[44] S. Göktepe and E. Kuhl, "Electromechanics of the heart: a unified approach to the strongly coupled excitation-contraction problem," *Computational mechanics*, vol. 45, pp. 227–243, 2010.

[45] D. Ambrosi, G. Arioli, F. Nobile, and A. Quarteroni, "Electromechanical coupling in cardiac dynamics: the active strain approach," *SIAM Journal on Applied Mathematics*, vol. 71, pp. 605–621, 2011.

[46] J. M. Rogers and A. D. McCulloch, "A collocation-Galerkin finite element model of cardiac action potential propagation," *IEEE Transactions on Biomedical Engineering*, vol. 41, pp. 743–757, 1994.

[47] S. M. Pogwizd, K. Schlotthauer, L. Li, W. Yuan, and D. M. Bers, "Arrhythmogenesis and contractile dysfunction in heart failure: roles of sodium-calcium exchange, inward rectifier potassium current, and residual β-adrenergic responsiveness," *Circulation Research*, vol. 88, pp. 1159–1167, 2001.

[48] V. Elharrar and B. Surawicz, "Cycle length effect on restitution of action potential duration in dog cardiac fibers," *American Journal of Physiology*, vol. 244, pp. 782–792, 1983.

[49] J. W. Cain and D. G. Schaeffer, "Shortening of cardiac action potential duration near an insulating boundary," *Mathematical Medicine and Biology*, vol. 25, pp. 21–36, 2008.

[50] M. Courtemanche, R. Ramirez, and S. Nattel, "Ionic mechanisms underlying human atrial action potential properties: insights from a mathematical model," *American Journal of Physiology Heart and Circulatory Physiology*, vol. 275, pp. H301–H321, 1998.

[51] K. H. W. J. ten Tusscher, D. Noble, P. J. Noble, and A. V. Panfilov, "A model for human ventricular tissue," *American Journal of Physiology Heart and Circulatory Physiology*, vol. 286, pp. H1573–H1589, 2004.

[52] R. H. Keldermann, M. P. Nash, and A. V. Panfilov, "Pacemakers in a reaction-diffusion mechanics system," *Journal of Statistical Physics*, vol. 128, pp. 375–392, 2007.

[53] A. Tonnelier, "The McKean's caricature of the FitzHugh-Nagumo model. I. The space-clamped system," *SIAM Journal on Applied Mathematics*, vol. 63, pp. 459–484, 2002.

[54] P. Biscari and C. Lelli, "Spike transitions in the Fitzhugh-Nagumo model," *European Physical Journal Plus*, vol. 126, 2011.

[55] J. Dumas and A. Rondepierre, "Modeling the electrical activity of a neuron by a continuous and piecewise affine hybrid system," *Proceedings pf Hybrid Systems: Computation and Control*, pp. 156–171, 2003.

[56] N. A. Wedge, M. S. Branicky, and M. Cavusoglu, "Computationally efficient cardiac bioelectricity models toward whole-heart simulation," in *Proceedings 26th International Conference IEEE Engineering in Medicine and Biology Society*, pp. 3027–3030, 2004.

[57] N. A. Wedge, *Analysis of cellular cardiac bioelectricity models toward computationally efficient whole-heart simulation*. PhD thesis, Case Western Reserve University, 2004.

[58] D. P. Zipes, H. R. Besch, and A. M. Watanabe, "Role of the slow current in cardiac electrophysiology," *Circulation*, vol. 51, pp. 761–766, 1975.

[59] S. P. Hastings, "Single and multiple pulse waves for the FitzHugh-Nagumo equations," *SIAM Journal on Applied Mathematics*, vol. 42, pp. 247–260, 1982.

[60] J. A. Feroe, "Existence and stability of multiple solutions of a nerve equation," *SIAM Journal on Applied Mathematics*, vol. 42, pp. 235–246, 1982.

[61] J. Rinzel and J. B. Keller, "Traveling wave solutions of a nerve conduction equation," *Biophysical Journal*, vol. 13, pp. 1313–1337, 1973.

[62] J. Rinzel and D. Terman, "Propagation phenomena in a bistable reaction-diffusion system," *SIAM Journal on Applied Mathematics*, vol. 42, pp. 1111–1137, 1982.

[63] M. J. Janse, "Electrophysiological changes in heart failure and their relationship to arrhythmogenesis," *Cardiovascular Research*, vol. 61, pp. 208–217, 2004.

[64] G. Hasenfuss, H. Reinecke, R. Studer, B. Pieske, M. Meyer, H. Drexler, and H. Just, "Calcium cycle proteins and force-frequency relationship in heart failure," *Basic Research in Cardiology*, vol. 91 (Suppl. 2), pp. 17–22, 1996.

[65] L. A. Mulieri, G. Hasenfuss, B. J. Leavitt, P. D. Allen, and N. R. Alpert, "Altered myocardial force-frequency relation in human heart failure," *Circulation*, vol. 85, pp. 1743–1750, 1992.

[66] A. P. M. Gorgels, M. A. Vos, J. L. R. M. Smeets, E. Kriek, P. Brugada, and H. J. J. Wellens, "Delayed afterdepolarizations and atrial and ventricular arrbythmias," in *Cardiac Electrophysiology: A Text Book.*, Mount Kisco (NY): Futura.

[67] D. M. Bers, "Calcium fluxes involved in control of cardiac myocyte contraction," *Circulation Research*, vol. 87, pp. 275–281, 2000.

[68] G. Berecki, R. Wilders, B. de Jonge, A. C. G. van Ginneken, and A. O. Verkerk, "Re-evaluation of the action potential upstroke velocity as a measure of the Na^+ current in cardiac myocytes at physiological conditions," *PLoS ONE*, vol. 5, p. e15772, 2010.